BEHAVIOR OF CHANNEL-SHAPED

REINFORCED CONCRETE COLUMNS

UNDER COMBINED BIAXIAL BENDING AND COMPRESSION

by
Dureseti Chidambarrao

Thesis submitted to the Faculty of the Graduate School of
the New Jersey Institute of Technology in partial fulfillment of
the requirements for the degree of
Master of Science in Civil Engineering
1983

APPROVAL SHEET

Title of Thesis: Behavior of Channel-Shaped Reinforced Concrete Columns under Combined Biaxial Bending and Compression

Name of Candidate: Dureseti Chidambarrao
Master of Science in Civil Engineering

Thesis and Abstract Approved:

	C.T. Thomas Hsu, PhD. Associate Professor, Department of Civil and Environmental Engineering	Date

Signatures of other members of the thesis committee.		Date
		Date

VITA

Name: Dureseti Chidambarrao.

Degree and date to be conferred: MSCE, 1983.

Secondary education: Timpany School, Visakhapatnam, India, December 1975.

Collegiate institutions attended	Dates	Degree	Date of Degree
Indian Institute of Technology, Madras, India	6/76-6/81	Bachelor of Technology	Aug.12, 1981
New Jersey Institute of Technology, Newark, N.J., U.S.A.	9/81-8/83	Master of Science in Civil Engineering	Oct. 1983

Major: Civil Engineering.

ABSTRACT

Title of Thesis: Behavior of Channel-Shaped Reinforced Concrete Columns under Combined Biaxial Bending and Axial Compression

Dureseti Chidambarrao, Master of Science in Civil Engineering, 1983

Thesis directed by: Dr. C.T. Thomas Hsu, Associate Professor of Civil Engineering

The inelastic behavior of irregular shaped reinforced concrete columns has been a constant concern for a structural engineer, to design a safe and economic structure in modern buildings and bridge piers. The shape of the elements in a reinforced concrete structure may be used to optimize its structural strength, to make better use of the available space, to improve the aesthetic appearance of the structure, or to facilitate construction. Due to the locations of the columns, the shapes of the buildings and the nature of the applied loads, many columns are subject to combined biaxial bending and axial load.

Seven 1/4 scale direct models of the short, tied columns with channel-shaped cross sections were constructed for the present investigation. All the specimens were tested and studied for their complete strength and deformation behavior under combined biaxial bending moments and axial compression, and were used to examine some of the variables involved such as relative eccentricities and loading variations. The end conditions are assumed to be pinned-ended. The experimental load-strain and biaxial moment-curvature curves have been compared with the

analytical results of the strength and deformation for biaxially loaded channel-shaped column members, and a satisfactory agreement was obtained from zero up to the ultimate load condition.

The above inelastic behavior of channel-shaped reinforced concrete columns has formed the basis of the redistribution of the moments and forces in a statically indeterminate structure, and these characteristics can also be found useful for the limit analysis and design of reinforced concrete structures.

PREFACE

The topic for this investigation was suggested by Dr. C.T. Thomas Hsu, whose guidance and assistance is deeply appreciated.

This study is part of a continuing investigation of the behavior of columns under combined biaxial bending and compression. Studies have already taken place for L-shapes. The present study is based on channel-shapes, and later on T- and then walled-channel shaped columns will be studied.

A group of students originally cast the specimens in early 1982 which were used in this study. Being inadequate in bracket design, two of the sample specimens failed in the brackets. This called for an increase in bracket size. It was achieved by surrounding the bracket with steel tubes and grouting the gap between the steel tube and bracket with 5,000 psi concrete.

Five specimens were tested and the data analyzed and compared with the analytical results, achieved through use of the computer program written by Dr. C.T. Thomas Hsu.

to my parents and brothers

ACKNOWLEDGEMENTS

I wish to thank Dr. C.T. Thomas Hsu and Dr. C.F. Peck, Jr. for the valuable assistance and guidance throughout the entire project.

The special skills of Mr. Daniel Diserio and Mr. Eric Skurbe of the Institute staff are gratefully appreciated.

The participation of Mr. Ali Kermani, Mr. Saeed Naeni, Mr. Tony Nader and Mr. Amar Shah during the testing is gratefully acknowledged. Further, the assistance of the people who helped in the casting is gratefully appreciated.

I thank Dr. Methi Wecheratana and Dr. R. J. Craig as well as my friends Mr. Avijit Mookerjee and Mr. Sitaram Mahadev for their suggestions and help throughout the project.

Finally I thank Mrs. Joan Schroeder whose patience when typing this manuscript is greatly appreciated.

TABLE OF CONTENTS

TABLE OF CONTENTS (Continued)

LIST OF TABLES

Note: Tables in each chapter are at the end of the respective chapter.

LIST OF FIGURES

Note: Figures in each chapter are at the end of the respective chapter.

LIST OF FIGURES (Continued)

LIST OF FIGURES (Continued)

LIST OF NOTATIONS

a_k - area of element k

e_x - eccentricity along x axis

e_y - eccentricity along y axis

E_c - maximum compressive concrete strain

E_k - strain in element k

E_p - uniform direct strain due to an axial load p

$(E_t)_k$ - tangent modulus of elasticity for steel or concrete element k

f_c' - ultimate strength of concrete

f_k - stress across element k

f_y - yield strength of steel reinforcement

f_{y2}, f_{y3}, f_{y4}, and f_{y5} - steel tensile strength shown in Figure 4.3.b.

f'_{y2}, f'_{y3}, f'_{y4} and f'_{y5} - steel compressive strength shown in Figure 4.3.b.

k - element number

kd - distance from maximum compressive concrete strain to the neutral axis

l - total length of column

M_{nx} - $P_n e_y$

M_{ny} - $P_n e_x$

M_{ox} - M_{nx} capacity at axial load P_n when M_{ny} is zero

M_{oy} - M_{ny} capacity at axial load P_n when M_{nx} is zero

M_{ult} - moment at failure

M_x - bending moment about x axis

M_y - bending moment about y axis

P - axial load

s - spacing of lateral reinforcement

u' - allowable compatibility for P

v' - allowable compatibility for M_x

w' - allowable compatibility for M_y

x_k - x coordinate of element k w.r.t. axis of symmetry

y_k - y coordinate of element k w.r.t. axis of symmetry

- non-dimensional constant in equation 6.1.

ϵ_{y2}, ϵ_{y3}, ϵ_{y4} and ϵ_{y5} - steel tensile strain in Figure 4.3.b.

ϵ'_{y2}, ϵ'_{y3}, ϵ'_{y4} and ϵ'_{y5} - steel compressive strain in Figure 4.3.b.

ϕ - curvature

ϕ_x - the curvature produced by the bending moment component M_x and is considered positive when it causes compressure strain in the positive y direction (refer Figure 4.2.).

ϕ_y - the curvature produced by the bending moment component M_y and is considered positive when it causes compressive strain in the positive x direction (refer Figure 4.2.).

δ_x - deflection in the x-direction

δ_y - deflection in the y-direction

subscript (c) - indicates values calculated in an iteration cycle (refer Chapter V).

subscript (M) and (M+1) - indicate the "M" and "M+1" iteration cycles (refer Chapter V).

subscript n - denotes a stage of constant value

subscript (s) - indicates the value at the beginning of each iteration cycle (refer Chapter V).

CHAPTER I. GENERAL INTRODUCTION AND SCOPE OF RESEARCH

A. General Introduction

There is little known about the analytical and experimental behavior of irregularly shaped columns subjected to combined biaxial bending and axial compression; further, almost all investigations of columns under combined biaxial bending and axial compression have emphasized the ultimate strengths and resulting interaction diagrams.

Current code provisions do not provide guidelines for determination of strength and ductility of biaxially loaded reinforced concrete columns. Therefore this investigation is aimed at an experimental and analytical study of the behavior of reinforced concrete channel-shaped short columns as the applied load is increased monotonically from zero until failure.

This study has special emphasis on channel-shaped columns as the use of such columns, which include T-shapes, L-shapes, etc., can be expected to increase in the future. To design such structural members the following provisions are needed:

1. Design aids such as interaction diagrams or modified load contour design equations for cross sections other than rectangular or circular, from which computer models can be developed.

2. Verification of mathematical modelling transcribed into computer programs by experimental testing and, if

necessary, to incorporate any changes from the findings in the models.

3. The stress-strain relationship of concrete and reinforcing steel must be reexamined in its application to columns other than rectangular and circular.

4. Even though experimental work may to some extent clarify the behavior of structural members, it would greatly enhance behavioral study of structural members if members were instrumental so that behavior could be monitored at full-size scale.

This study does not presume to encompass all that is required to recommend provisions to the ACI, but it does render a better understanding of the strength and deformation behavior of channel-shaped columns and the possible use of the analytical study proposed by Hsu (1). The experimental results are compared to the analytical model to assess the accuracy of the computer method developed by Hsu (1).

B. Research Objective

The primary objective of this project is to study the strength and deformation behavior of channel-shaped columns under combined biaxial bending and axial compression experimentally, and to assess the accuracy of a computer analytical model.

The results will form a basis for a recommended analysis and design technique which will be developed for use by the practicing engineer. The proposed design recommendation of examining the load contour equation, developed only for rectangular and circular shaped columns, could be gleaned from this research work and extended to include the effect of a shape function for this column. In evaluating the collected experimental and analytical data design aids and interaction diagrams may be arrived at specifically for channel-shaped columns. Nevertheless, the procedure of developing and using charts as design aids for columns is inherently limited to very simple geometrics when only a few loading cases are to be handled. Therefore the mathematical models and optimizations of computer design times must be kept in mind.

C. State of the Art

There is extensive use of different shapes as structural members. In the case of reinforced concrete columns and shear walls, wide flange cross sections have been used to improve the structural strength of the member, L-shaped cross sections are usually located at building corners, S- and X-shapes have been used for purely architectural reasons, C-shaped columns are commonly used as columns and enclosures of the elevator shafts, and other irregular shapes are used in the pre-cast concrete industry. In concrete bridge pier construction, the hollow box or round columns are frequently used. Hollow round cross sections are also used in piling and pole construction.

The behavior of these members is not well known. They are usually overdesigned and this causes the structure to be stiffer, which is questionable when applied to seismic regions. Ductility plays an important role when designing columns in seismic regions. Inelastic behavior study is required to have a better understanding of columns in the seismic regions.

Up to circa 1975 there was very little work done in analyzing the behavior of irregularly shaped columns under biaxial bending and compression. Not only were there no design aids or computer analytical models, but very little experimental work was done. Channel-shaped columns are the primary concern of this project, but before getting to the crux of the matter a brief historical review of irregularly shaped columns other than channel-shaped is appropriate.

The methods of analysis are similar to channel-shaped columns and will be covered in great detail later.

Experimental work in column research has been limited almost exclusively to rectangular, circular and octagonal cross sections.

I-shaped sections have been tested under cyclic loading by Fiorato, Oesterle and Corley (2).

Some sections which have published design charts are:

1. Hollow circular sections. A collection of interaction diagrams for hollow circular columns has been developed by Grasser (3), covering a wide range of thickness ratios and steel distribution. Jiménez Montoya et al. (4) have developed interaction diagrams for three section types

for CEB criteria.

Anderson and Moustafa (5) have developed interaction diagrams for hollow circular and octagional columns in accordance with ACI criteria.

2. Hollow rectangular sections. Jiménez Montoya et al. (4) have developed interaction diagrams for six symmetrical hollow sections loaded in one axis of symmetry in accordance with CEB criteria. The shape of these interaction diagrams is similar to the interaction diagrams of solid rectangular sections.

Brettle (6) developed 12 charts for designing single and triple cell hollow box bridge piers using eccentricities as abscissas, which results in open surfaces that lose precision near pure bending.

3. X-sections. Marín (7) has developed 32 interaction diagrams for types of symmetrical cruciform sections loaded on one axis of symmetry or on the diagonal.

4. L-sections. Marín (8) has developed a collection of 50 isoload charts for 5 different types of L-sections. These charts are similar in shape to the charts developed by Chen and Atsuta (9) for steel angles.

5. T-sections. Jalil et al. (10) have developed interaction diagrams for T-sections.

6. Other sections. Marín has developed interaction diagrams for off-shore structures. The field of developing design aids for the design of columns with cross-sections other than the circle or the rectangle is still open.

Jiménez Montoya et al. (4) have pointed out that it is possible to transfer results from square cross section to any other affine section such as rectangle, rhombus or parallelogram derived from it, or from a circular to an ellipse, provided appropriate dimensionless variables are used.

Having looked at other irregularly shaped cross-sections, the state of research progress made in channel-shaped columns is under examination in this project.

To determine the strength of a rectangular cross-section, the procedure outlined here is the same for any shape as mentioned earlier; subject to biaxial bending and compression the equilibrium of parallel forces represented by the combination of the concrete compressive stress block, seen in Figure 1.1, and the reinforcement, which depends on the material strength properties and the geometry of cross-section and reinforcement, should be established.

The concrete stress distribution's volume and centroid may be defined by integration over the areas of the contour where stresses act. The reinforcement forces may be treated as discrete point forces. Further, since the strength of the section depends on the location of the neutral axis, the resultant of the forces should be obtained for each neutral axis location. For a few cross-sections, mainly retangular and circular, a set of particular equations has been obtained to evaluate the concrete stress volume for different locations of the neutral axis.

There are different methods of calculating stress block volumes and these methods of analysis are listed below:

1. Discrete element method. In order to avoid the above mentioned integration, a common simplication of concentrating concrete elements into such grids as square, rectangular or triangular is used.

Since the normal strain distribution is planar, the corresponding stresses are unidimensional because they depend only on the distance to the neutral axis. Therefore the compression zone can be discretized into bands parallel to the neutral axis and the resultant band concentrated to its center of gravity.

2. Triangular superposition methods. These methods consist in describing the compression section by triangles and superposing the axial load and moment resultants, which are evaluated for a given stress block. Since any polygonal section can be systematically described using triangular components, and the principle of superposition of forces and moments is valid while a planar strain distribution occurs, this method can be easily programmed. Using the Newton-Raphson method, Gurfinkel (11) applied the triangular superposition principle to footings, which can be extended to reinforced concrete columns of arbitrary cross-sections as Menegotto and Pinto (12) did.

3. Line integrals. If the concrete stress block can be represented by a polynomial function, it is possible to

obtain the corresponding stress integrals by converting them to line integrals, which are then evaluated directly from the vertex coordinate by straight integration or using the Gaussian quadrative technique.

Hsu (1) presented a computer program using the extended Newton-Raphson method and the discrete element method.

The material properties of the concrete and reinforcing steel and the section geometry are the input features. The idealization of the stress-strain curves of the concrete and steel was done by piece-wise linear approximation. The output features of the program include moment-curvature behavior of a structural member under biaxial bending and compression. It can be modified to accommodate tension instead of compression. This program was compared with rectangular column tests by Anderson and Lee, Bresler, Ramamurthy and Hsu (1). Excellent agreement was obtained between the experimental and analytical results according to Hsu (1).

Design aids for C-sections have been developed by Marín (13) and Park and Paulay (14). Figure 1.2. shows a set of interaction diagrams for a C-section developed by Marín and Martin (15) and Park and Paulay (14) which may be applied to a shear wall in an elevator core. In this figure, the balance failure occurs in pure flexure at a steel percentage of 2.6. These charts are very sensitive to the distribution of the steel reinforcement.

There are very few test results of channel-shaped columns since most experimental work in column research for biaxial bending and compression was limited primarily to rectangular, circular and octagonal cross sections.

Herrera and Ochoa (16) tested five C-shaped columns under monotonic loading with relative eccentricities of 0.25 and 0.375. Although limited in scope these tests showed a lineal strain distribution and concrete strains up to 0.007.

The state of the art in the inelastic behavior of irregularly shaped columns is gaining momentum, as it is foreseeable that in the future there will be an increased use of irregularly shaped columns. There is greater need of design aids and computer models under bending and compression.

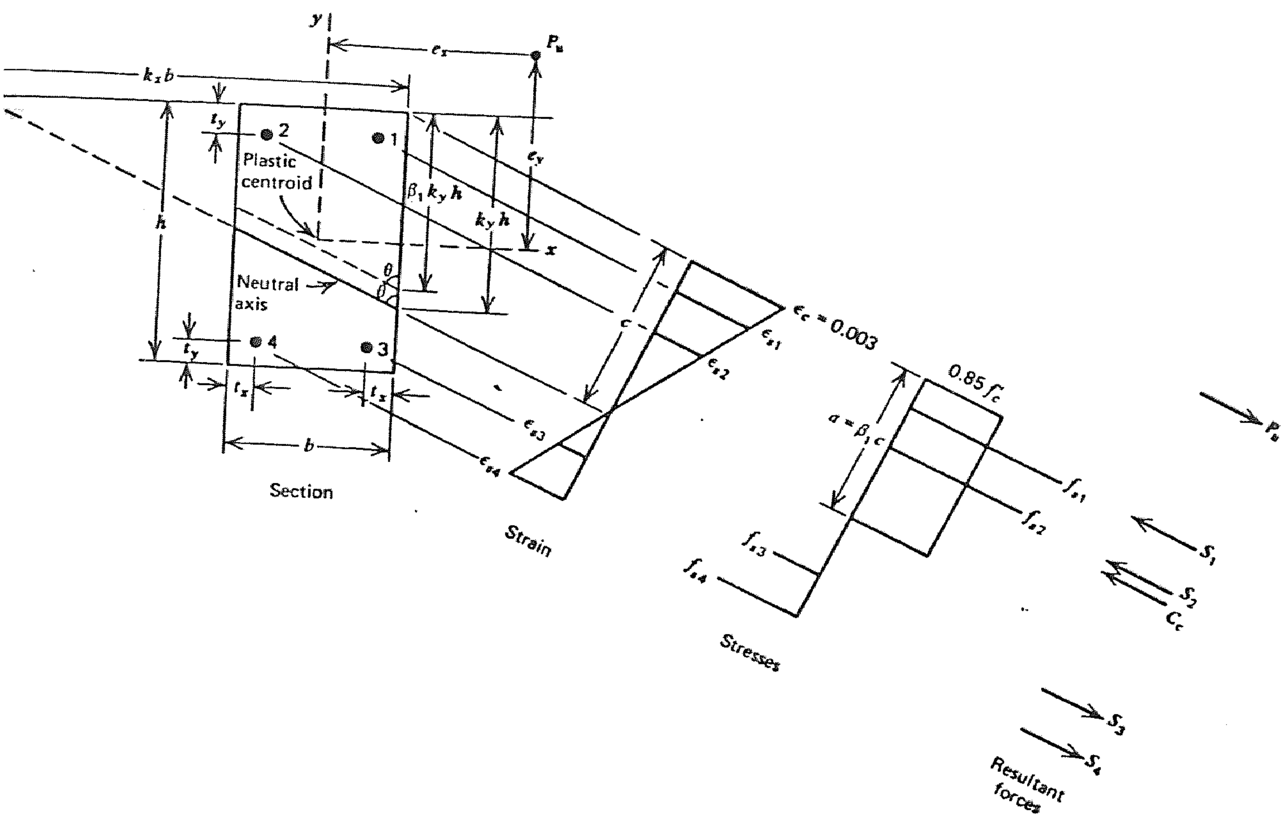

FIGURE 1.1 COLUMN SECTION WITH BIAXIAL BENDING AT THE ULTIMATE LOAD

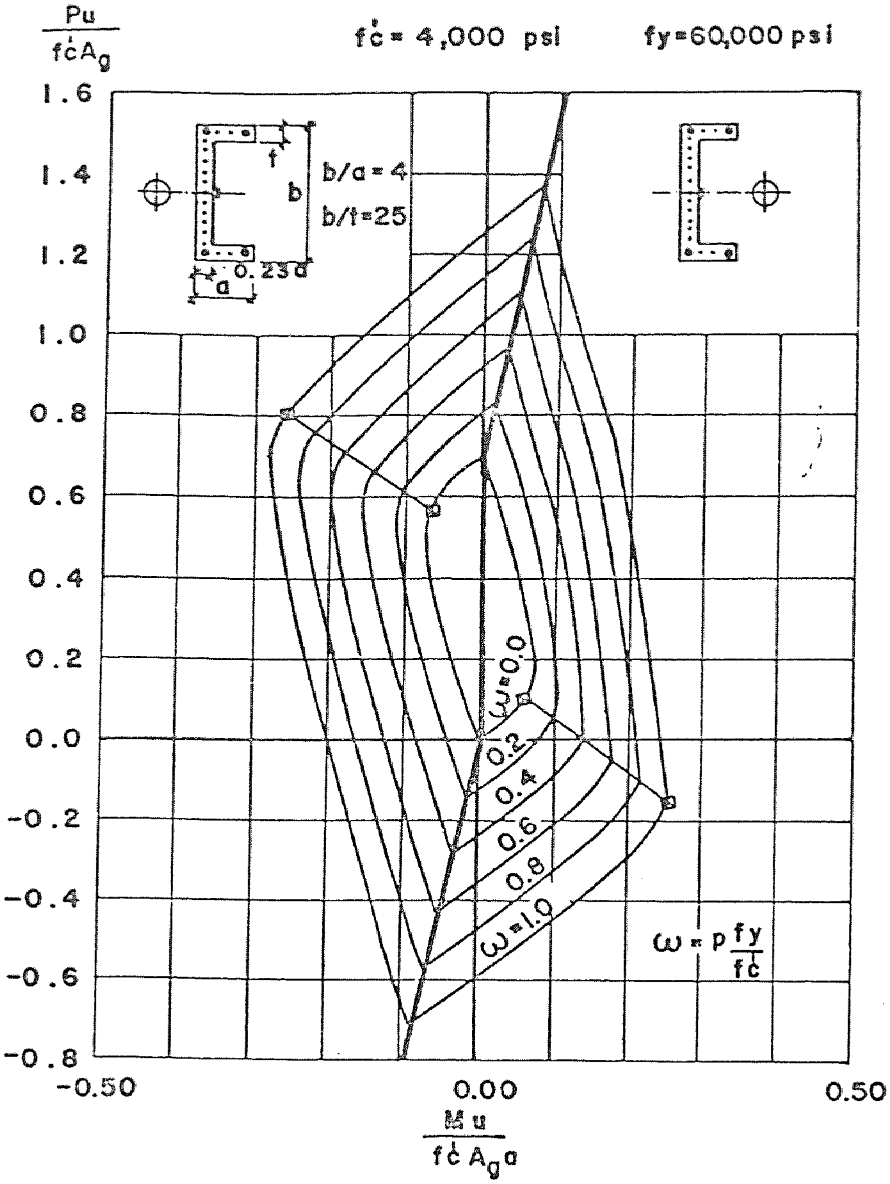

FIG 1.2 INTERACTION DIAGRAM FOR "C" CROSS SECTION

CHAPTER II. TEST PROGRAM

A. Description of Test Specimens

The test specimen series cross section and loading arrangements are shown in Figure 2.1. All columns were designed as short columns and were each 6 feet long.

The brackets were heavily reinforced to prevent local failures, seen in Figure 2.2.a. Nevertheless, though thick plates were used to distribute the load evenly on the bracket face on the first two specimens, seen in Figure 2.2.a., they failed by shear failures at the brackets. So the remaining five specimens were redesigned for their brackets. The brackets were confined within foot long steel tubes on each end and the gap between the steel tubes and original brackets was grouted with 5,000 psi concrete, as shown in Figure 2.2.b.

Each column was reinforced longitudinally by 22 Grade 60 #3 bars, as seen in Figure 2.1. These longitudinal bars in the column were held together by ties -- Grade 60 bars at spacings of 4 inches center to center. (Specific spacings of stirrups for each specimen are given along with the calculations and test results.) The stirrups were connected to the main reinforcing bars by binding wires. Two additional bars were bent and positioned at ends of specimens to facilitate moving from the casting area into the testing apparatus by means of an overhead joist.

At least six 4x8 inch and six 3x6 inch standard concrete test cylinders were cast with each batch of concrete mix.

B. Materials and Fabrication

1. Cement. High early strength type III Portland cement was used for all concrete mixes. The cement was purchased from a local supplier and was properly stored in a dry area.

2. Sand. Crushed quartz sand was used as fine aggregate. It was purchased from a local supplier and stored in bins in a dry area. A mixture of crushed quartz sand in the proportions listed in Table 2.1. was used. Figure 2.8. gives the Grain Size Analysis.

3. Concrete. The concrete mixed was of the following proportions, specified by weight: The water-cement ratio was 0.8, and the cement-sand ratio was 3.2 for all columns. Coarse aggregate was not used. Six 4x8 inch and 3x6 inch cylinders were cast with each batch. The cylinders were cast and cured under conditions identical to those of the column test specimens and were tested at the same age.

4. Steel Reinforcement. The steel reinforcement was obtained from a local supplier as straight bars. ASTM A615 Grade 60 #3 bars (diameter = 0.375 in., area = 0.11 in.^{2}) were used in all columns for main reinforcing steel. Grade 60 (diameter =.0087 in., area = 0.0086 in.^{2}) were used for stirrups.

The main reinforcements and the stirrups were carefully bent to the required sizes with standard bar benders. Ordinary steel binding wire was used to hold the main reinforcement and stirrups together.

To test the quality and strength properties of the reinforcing steel bars used, and the stirrups used, random samples of the bars were taken and tested in a mechanical testing machine in tension (see Fig. 3.2.).

C. Formwork, Proportioning, Mixing, Casting and Curing

1. Formwork. The test specimens were cast in a horizontal position in 5/8" thick plywood formwork. The form was built in sections which were connected together by screws to ensure ease of removal of the cast specimens and to allow repeated use of the same form. The plywood was braced with 2x4 inch lumber. After the formwork was cleaned, connected together and oiled with a thin layer of motor oil (to prevent adherence of specimen to formwork), the reinforcing cages were put into the formwork. Chairs were used to provide the cover required between the steel reinforcing cage and the form cover. See Figures 2.3.a. and 2.3.b.

2. Proportioning. Based on a design for an f_c' of 3,500 psi the following mix design was used: one with cement-sand ratio of 3.2 by weight with a water-cement ratio of 0.8. Dry ingredients were used for all mixes.

3. Mixing. Dry ingredients were placed in a 16 cubic foot capacity electric mixer. Mixing time for each batch

was approximately five minutes. After thorough mixing of the concrete the mix was poured into mortar pans and transported to the casting area where it was poured into the formwork.

4. Casting and Curing. The test specimens were cast horizontally. This kind of casting was more practical as compared to the vertical position. While a horizontal casting causes a strength differential across the column section, vertical casting will cause a differential in concrete quality along the column length because of better compaction at the bottom. After the concrete was placed in the form, it was compacted by means of a high frequency vibrator.

The test specimens and the control cylinders were cured in the moulds for one day before being removed from the moulds. The test specimens and the control cylinders were then cured under wet burlap for six days before exposing them. They were then kept in storage until the day before testing.

D. Instrumentation

1. Loading Method. The testing frame was originally designed for testing small columns. But since pinned-ended conditions were required more space, in the form of head room to accommodate the pins, was required. The frame was expanded by a row of bolts and was checked for maximum loads. The columns were tested in the horizontal position, as seen in Figure 2.4.

The columns were axially loaded using the Enerpac 100 ton capacity hydraulic cylinder ram (effective area = 20.63 in.^{2}). Manual Enerpac Pump Model PEM 2042 with a maximum pressure of 10,000 psi was used to push the ram.

The stress of the load being applied was directly read by a pressure gauge connected in the hose linking the pump and the ram. Valves were provided in line with the pressure hose to control the loading and also reverse the loading direction. These values were operated manually and were also set up in such a way so as to be able to hold the load at any particular stage as necessary. From the pressure reading the load can be calculated easily as the pressure times the effective area of the ram.

2. Strain and Curvature Measurements. The measurements of strain and curvature were done by the demec gauge method. The strain was calculated from measured deformation, between a pair of demec points, divided by the distance between the two points; see Figure 2.4.a. The curvature can be calculated from these strain values from the four or five pairs of demec gauges as seen in Figure 2.4.a. The instrument used to measure the strain value between a pair of demec points is the 6 in. range demec mechanical gauge with a least count of 0.0001 inch.

The demec gauges were glued to the column surface using epoxy. The surface was first sandpapered and then a thin layer of epoxy was applied. Once this layer dried the demec gauges were glued to the column at the appropriate points.

The strains looked at have so far been only concrete strains. Steel strains were measured too for some bars. The standard procedure of installing strain gauges was used. Protection for the gauges was used, as seen in Figure 2.6.

3. Deflection Measurements. The measurements of the mid-span deflections were made using Ames dial gauges (range = 2 inches, least count = 0.001 inch). There were four gauges placed two on the top to measure vertical deflection and two on the side to measure horizontal deflection, seen in Figure 2.7. The average deflection of the two gauges on the top gives the deflection at mid-span in the y-direction, while the average of the two gauges on the side gives the deflection at mid-span in the x-direction.

Table 2.1.

PROPORTION OF SIEVE SIZE IN CRUSHED QUARTZ SAND

SIEVE ANALYSIS

Sieve No.	10	40	70	200	pan
Sieve Opening (mm)	2.00 mm	.420 mm	212 mm	.074 mm	-
Mass Sieve (gm)	665 g	561.0 g	338 g	507 g	490
Mass Sieve + Soil (gm)	755 g	1756 g	600 g	693 g	510
Mass Soil Retained (gm)	90	1195	262	186	20
% Retained	5.1%	68.2%	14.95%	10.6%	1.15%
Cumulative % Retained	5.1%	73.3%	88.25%	98.85%	100%
% Finer Than	94.9%	26.7%	11.75%	1.15%	0

Soil Sample Mass	
Mass Container + Dry Soil (gm)	2097 g
Mass Container (gm)	344 g
Mass Dry Soil (gm)	1753 g

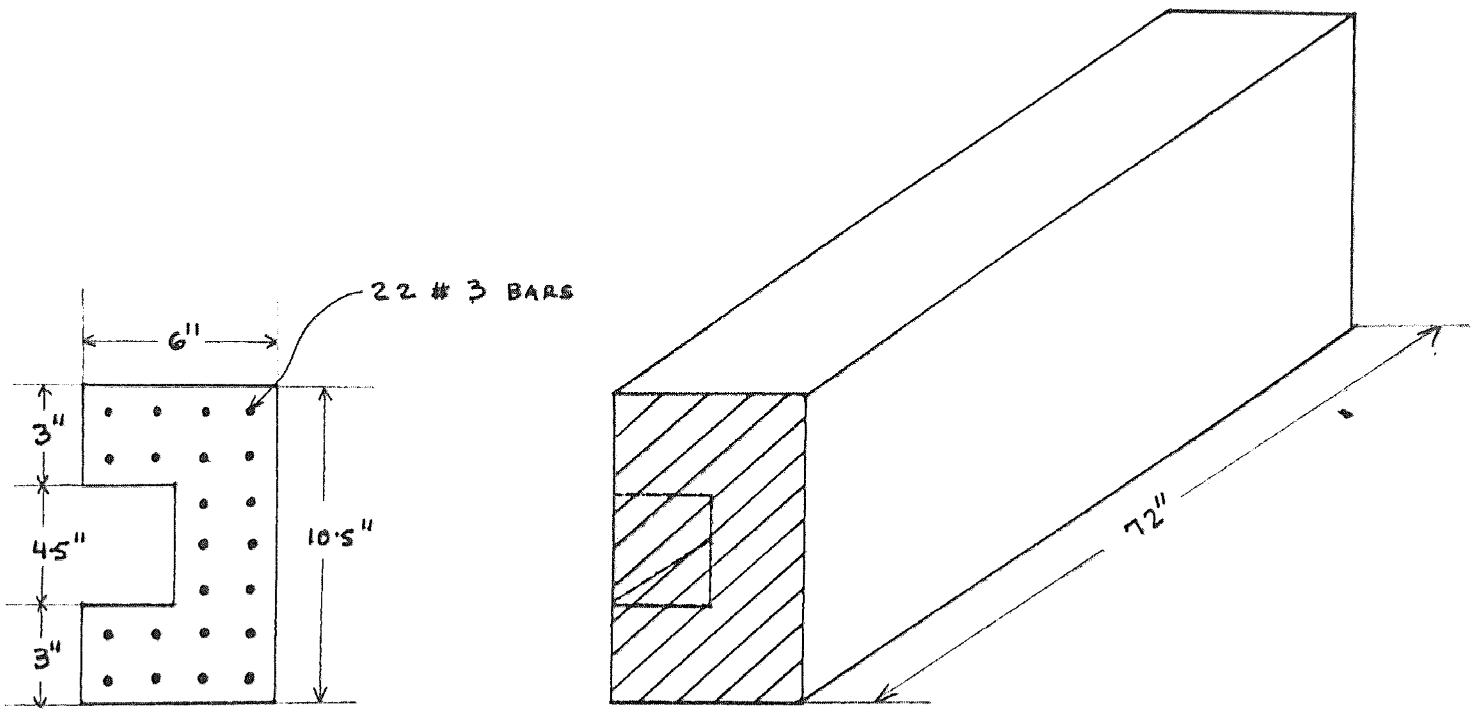

FIGURE 2.1 TEST SPECIMEN DETAILS

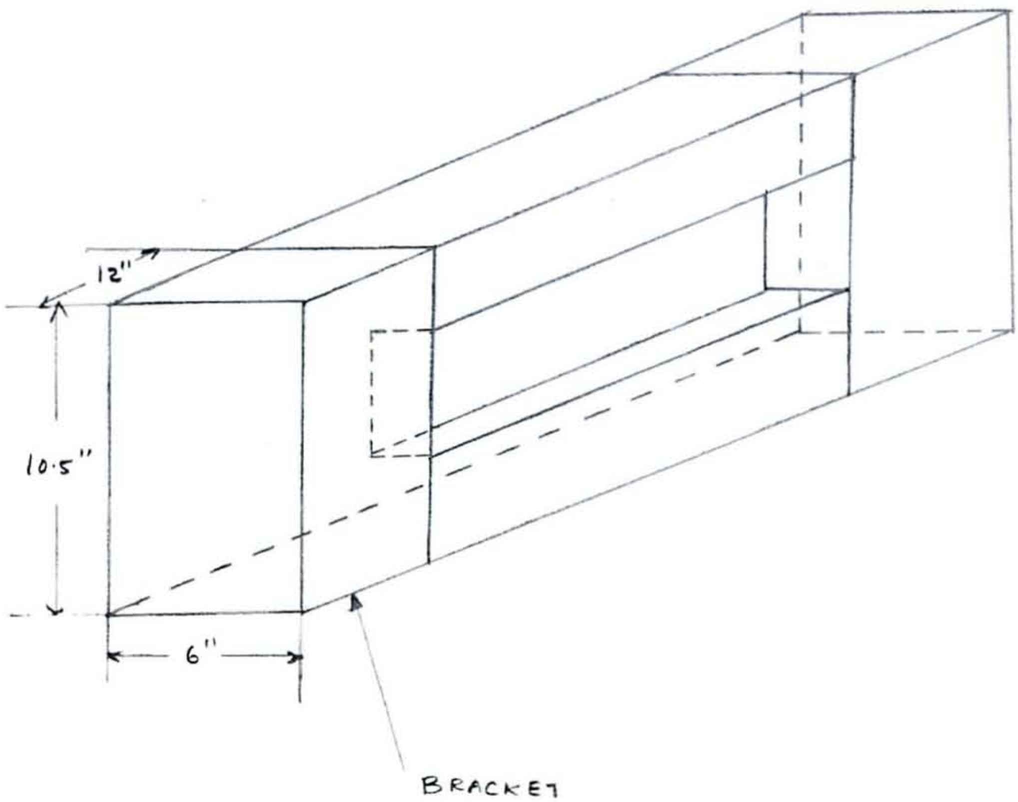

FIGURE 2.2.a ORIGINAL BRACKET USED IN FIRST TWO TESTS

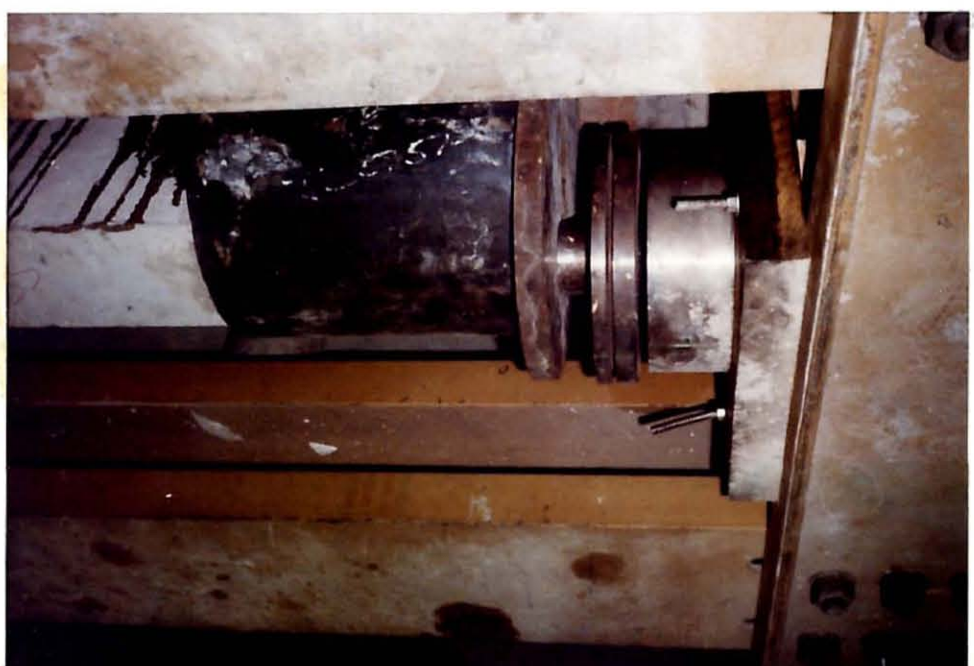

FIGURE 2.2.b REDESIGNED BRACKET WITH STEEL TUBE GROUTED WITH CONCRETE

FIGURE 2.3a FORMWORK DETAILS - SHOWING THEM UNFILLED

FIGURE 2.3.b FORMWORK DETAILS - SHOWING THEM FILLED

FIGURE 2.4 TEST FRAME AND SET UP

FIGURE 2.5 DEMEC GAUGE LOCATIONS

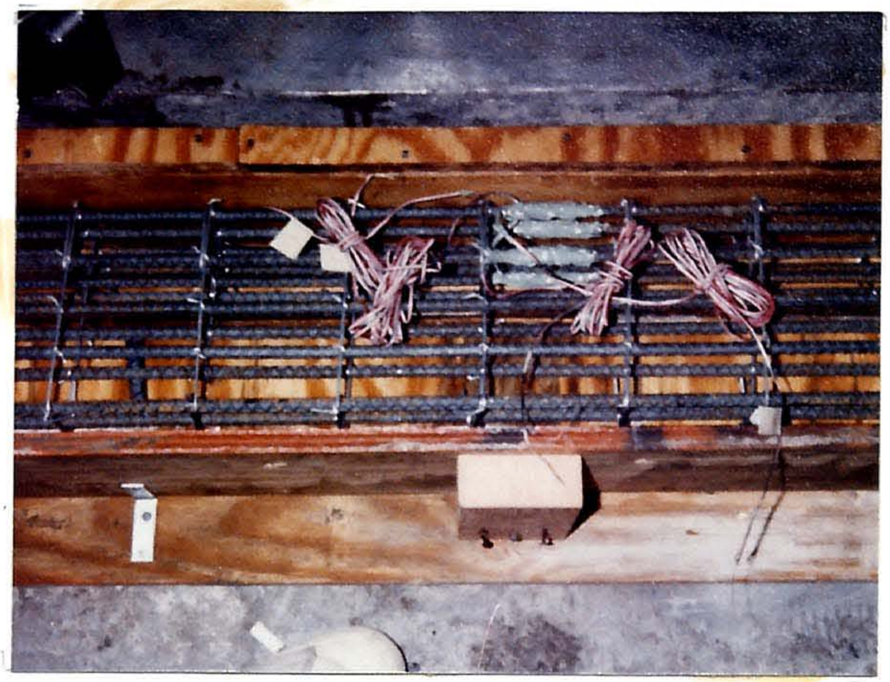

FIGURE 2.6.a STRAIN GAUGE INSTALLATION

FIGURE 2.6.b STRAIN GAUGE INDICATOR

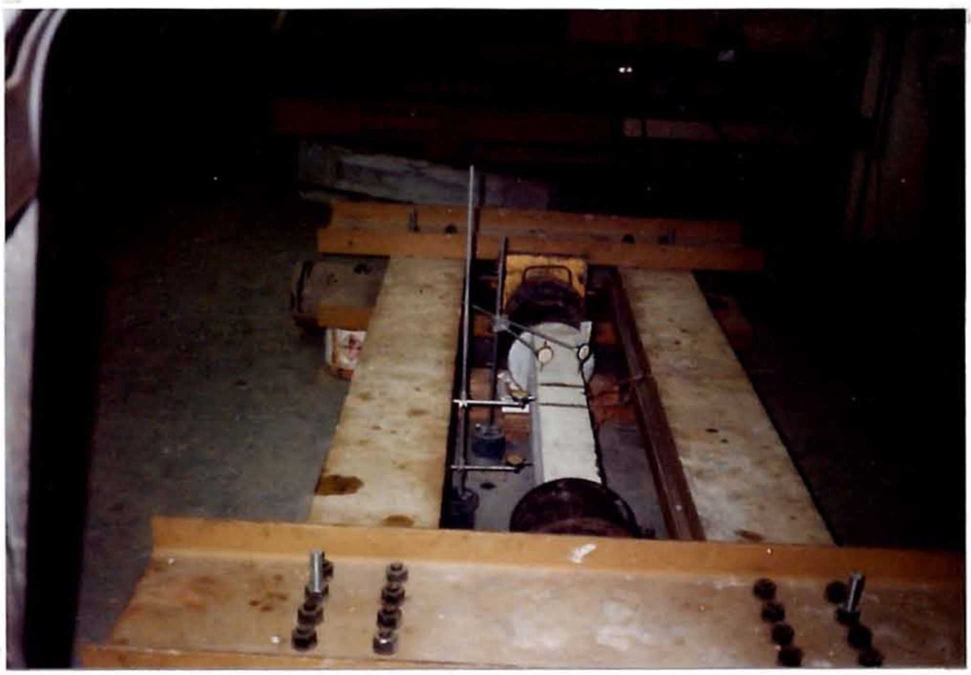

FIGURE 2.7 ARRANGEMENT OF DEFLECTION GAUGES

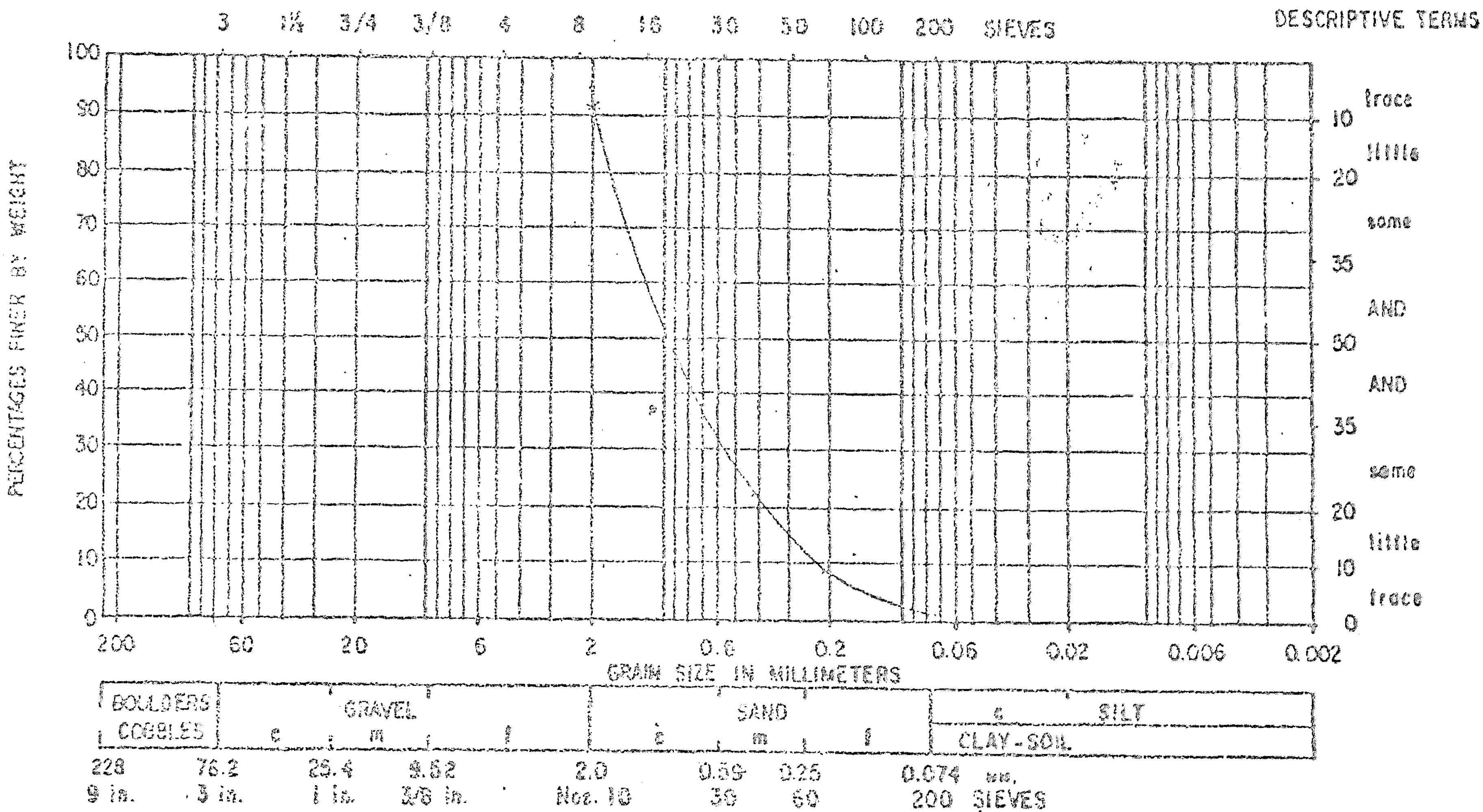

FIGURE 2.8 GRAIN SIZE ANALYSIS

CHAPTER III. TEST PROCEDURE

A. Column Tests

The specimen was hoisted into the frame and supported on roller supports built up to the required heights by the use of pieces of styrofoam and plates of steel.

The load points were marked on the bracket face. The height of the specimen from the floor was adjusted so that the load points were coincident with the hydraulic ram center on one end and the swivel head center on the other end. The column was then aligned by moving the rollers sideways so that the load goes through in a straight line from one end to the other with the exact required eccentricities.

The steel plates were placed flat against the bracket faces on each end. The pins were placed against the center of the ram on one end and the center of the swivel head on the other end. A small load was applied so that the plates and pins would stay in place.

The strain gauge wires were then connected to the strain gauge indicator and the Ames dial gauges were then placed. The demec gauges had been connected earlier.

The column was then ready for testing. The initial readings were taken for all the instruments. The load was then increased in increments of 500 psi. When the pressure read 1,500 psi the roller supports or shims were taken out. The loads were held steady using the valves. Once the dial gauges came to rest the readings for each load were taken.

The load was then incremented by 500 psi and the readings taken again. This continued until the failure of the specimen. On an average, each set of measurements took about 5 minutes. The complete test duration excluding the experiment setup was about 2 hours. Peak loads were recorded. Notes were taken periodically for future reference and analysis. Pictures were taken during the progress of the test.

B. Cylinder Tests

Standard 4x8 inch and 3x6 inch cylinders had been cast for each batch of concrete. The cylinders were capped using a sulphur compound the day before the test. Then following the test the cylinders were tested on the same day. A soil test 400,000 pound capacity hydraulic testing machine was used. Two Linear Voltage Direct Transducers (one on each side) were connected to a compressometer which was attached to the cylinders. The voltages were measured for each load. Post peak behavior was also recorded because the load control could be very delicately handled. The stress-strain curves including post peak behavior were obtained along with the ultimate strength as seen in Figure 3.1. The calculations of fc'-ultimate strength are seen in Table 3.2.

C. Steel Reinforcement Tests

Random samples of the bars were taken and tested in a mechanical testing machine in tension.

Twenty-one inch test specimens were cut from the #3 bars and punch marks were marked 50 mm apart. The strain measurements were taken using a strain gauge with a gauge factor of 2.03. Also a 50 mm gauge length was marked out at the center of the specimen. The experiment was load controlled until the yielding of the steel bar. Past the yield point it was strain controlled, the load readings being taken at regular intervals of strain. The resulting stress-strain curve for the reinforcing steel is shown in Figure 3.2.

Stirrups were also tested and stress-strain curves plotted as seen in Figure 3.3. Only here, strain gauges could not be attached and the entire experiment was deformation controlled.

Table 3.1.

CALCULATIONS FOR STRESS-STRAIN CURVES OF CONCRETE

The Roman capital represents a specimen cylinder.

	I.			II.			III.	
Load (pounds)	Stress (ksi)	Strain (in/in)	Load (pounds)	Stress (ksi)	Strain (in/in)	Load (pounds)	Stress (ksi)	Strain (in/in)
0	0	0	0	0	0	0	0	0
5000	0.707	$17.3\text{x}10^{-5}$	5000	0.707	$24.5\text{x}10^{-5}$	5000	0.707	$24.5\text{x}10^{-5}$
10000	1.415	$38.2\text{x}10^{-5}$	10000	1.415	$49\text{x}10^{-5}$	10000	1.415	$49\text{x}10^{-5}$
15000	2.122	$58.1\text{x}10^{-5}$	15000	2.122	$70.8\text{x}10^{-5}$	15000	2.122	$75.4\text{x}10^{-5}$
20000	2.829	$85.4\text{x}10^{-5}$	20000	2.829	$99.9\text{x}10^{-5}$	20000	2.821	$109\text{x}10^{-5}$
24000	3.395	$112.6\text{x}10^{-5}$	24000	3.395	$130.7\text{x}10^{-5}$	22000	3.112	$126.2\text{x}10^{-5}$
26000	3.678	$131.7\text{x}10^{-5}$	26000	3.678	$148.9\text{x}10^{-5}$	24000	3.395	$147.1\text{x}10^{-5}$
28000	3.961	$174.3\text{x}10^{-5}$	28000	3.961	$179.8\text{x}10^{-5}$	26000	3.678	$180.7\text{x}10^{-5}$
24000	3.395	$278.7\text{x}10^{-5}$	28400	4.018	$213.4\text{x}10^{-5}$	26500	3.749	$228.8\text{x}10^{-5}$
20000	2.829	$344.1\text{x}10^{-5}$	26000	3.678	$268.7\text{x}10^{-5}$	24000	3.395	$270.5\text{x}10^{-5}$
16000	2.264	$404.9\text{x}10^{-5}$	24000	3.395	$288.7\text{x}10^{-5}$	20000	2.829	$305\text{x}10^{-5}$
12000	1.698	$488.4\text{x}10^{-5}$	20000	2.829	$372.2\text{x}10^{-5}$	15000	2.122	$389.5\text{x}10^{-5}$
10000	1.415	$542.9\text{x}10^{-5}$	15000	2.122	$428.5\text{x}10^{-5}$	10000	1.415	$450.3\text{x}10^{-5}$
			10000	1.415	$524.7\text{x}10^{-5}$			

Table 3.2.

CALCULATIONS FOR f_c' - ULTIMATE STRENGTH OF CONCRETE

Specimen No.	Ultimate Load (pounds)	Area (inches squared)	Ultimate Stress (psi)	Date of Casting	Average for each Date of Casting (psi)
1	22000	7.069	3112	Nov. 7, 81	
2	28400	7.069	4018	Nov. 7, 81	f_c'
3	26500	7.069	3749	Oct. 15, 81	Average Nov. 7, 1981 = 3662 psi
4	28000	7.069	3961	Oct. 15, 81	Average Oct. 15, 1981 = 3899 psi
5	54000	12.566	4297	Oct. 11, 81	Average Oct. 11, 1981 = 4237 psi
6	53000	12.566	4218	Oct. 11, 81	
7	48000	12.566	3820	Oct. 11, 81	
8	48000	12.566	3820	Nov. 7, 81	
9	51000	12.566	4059	Oct. 15, 81	
10	48500	12.566	3859	Nov. 7, 81	
11	51000	12.566	4059	Oct. 15, 81	
12	58000	12.566	4616	Oct. 11, 81	
13	44000	12.566	3502	Nov. 7, 81	
14	46000	12.566	3661	Oct. 15, 81	
15	28000	7.069	3901	Oct. 11, 81	
16	32600	7.069	4527	Oct. 11, 81	

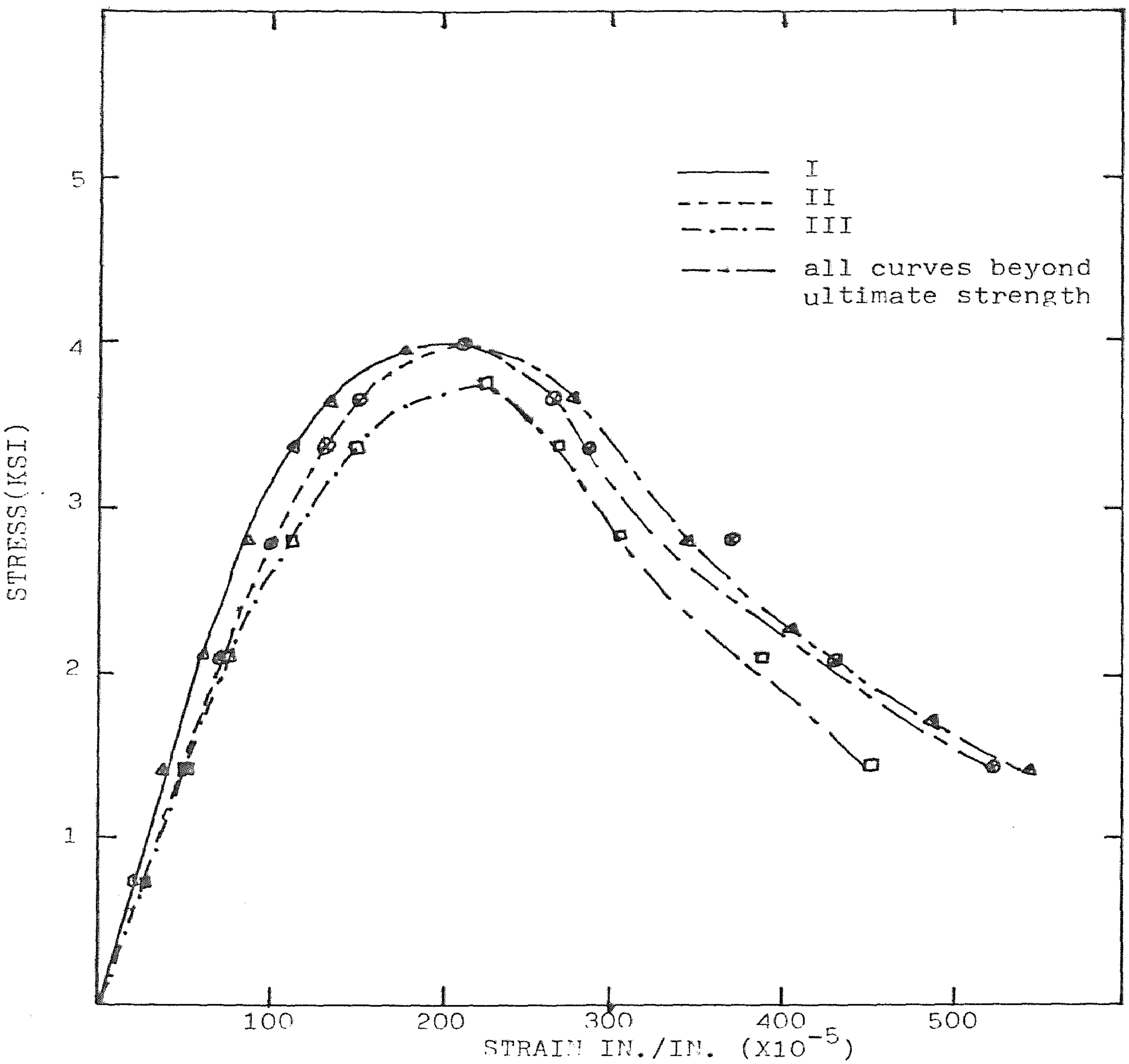

FIGURE 3.1 STRESS STRAIN CURVES FOR CONCRETE

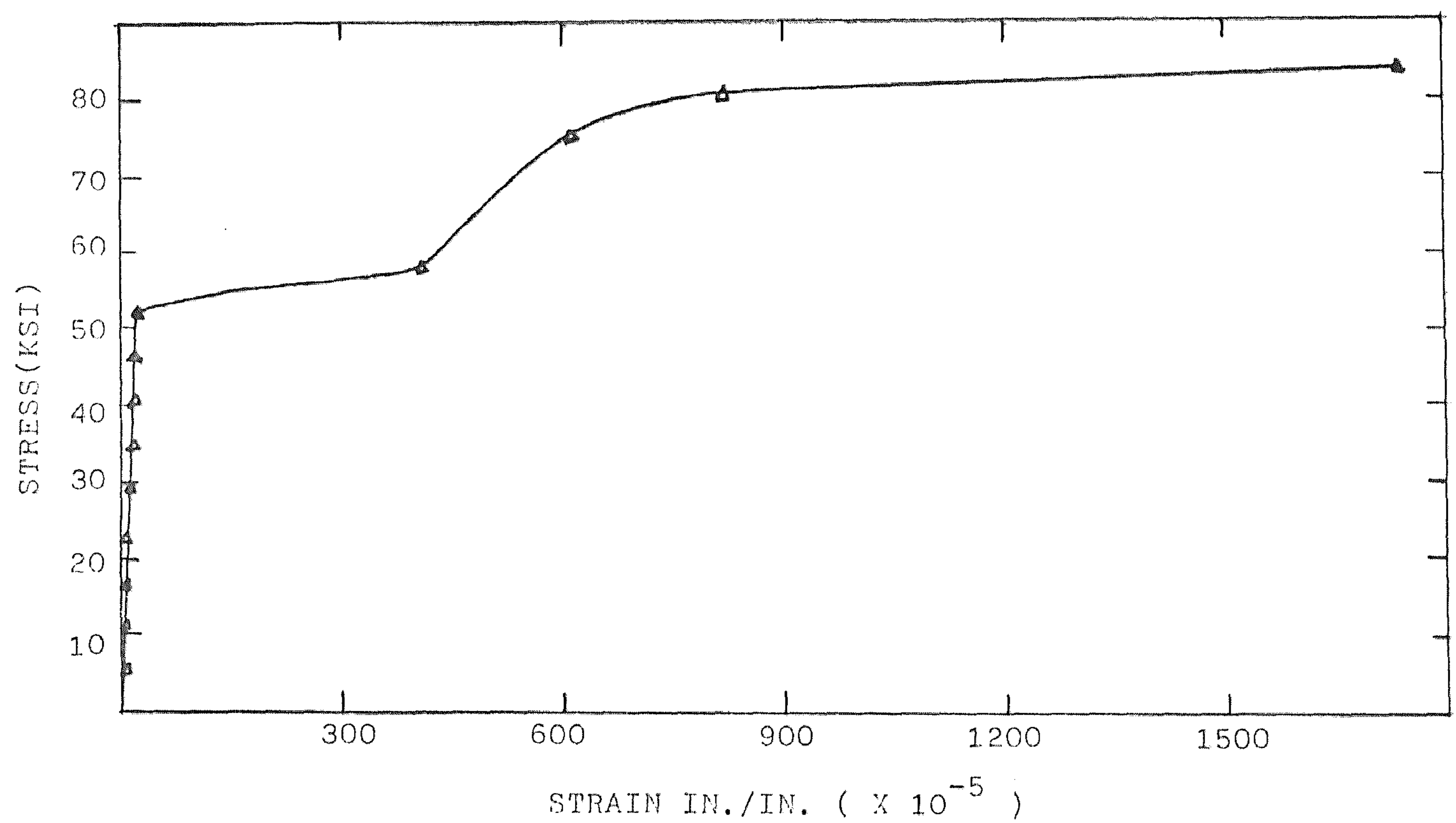

FIGURE 3.2 STRESS STRAIN CURVE FOR STEEL REINFORCEMENT

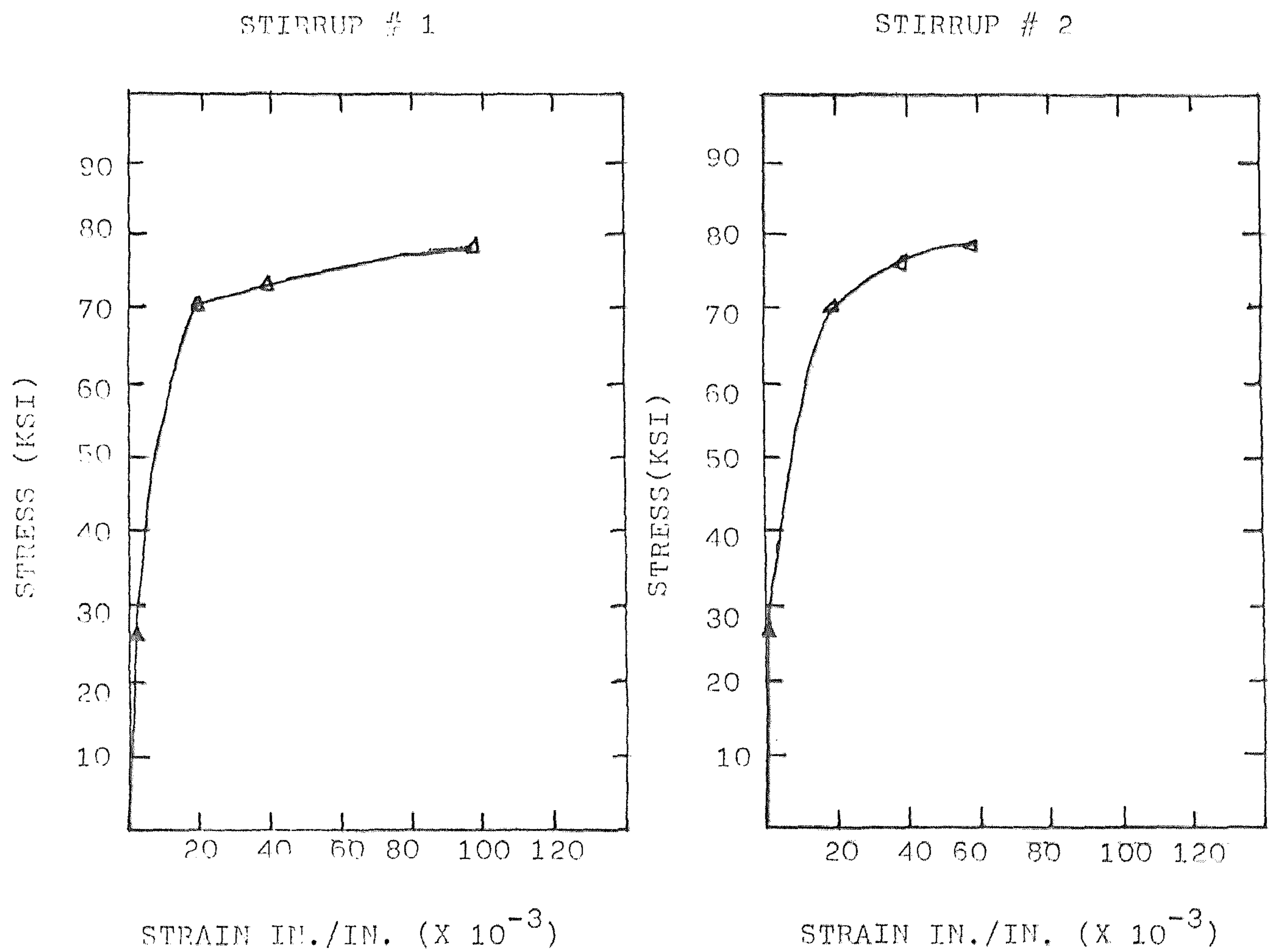

FIGURE 3.3 STRESS STRAIN CURVES FOR STIRRUPS

CHAPTER IV. THEORETICAL ANALYSIS AND COMPUTER PROGRAM

A. Introduction and Assumptions

The theory used in analyzing columns under combined biaxial bending and axial cone pressure is mathematical once the cross section properties and material properties are known. Therefore a set of mathematical equations has been developed and a computer program model proposed by Hsu (1).

Before going into any detail about the theoretical background, however, the basic assumptions must be clearly stated; they are:

1. The bending moments are applied around the principal axes.

2. Plane sections remain plane after bending.

3. The effect of creep and shrinkage are ignored, which means that the longitudinal stress at a point is a function only of the longitudinal strain of that point.

4. The stress-strain curves for the materials used are known.

5. Strain reversal does not occur.

6. The effect of deformation due to shear, torsion and impact effects are neglected.

7. Perfect bond exists between the concrete and the reinforcing steel.

8. The section does not buckle before the ultimate load is obtained.

B. Theoretical Development

The theory and computer program are based on the same principle, and hence looking at the theory gives a good idea of the computer program.

Typical moment curvature and load deflection curves are shown in Figure 4.1.; they indicate that close to the peak there can be two equilibrium positions corresponding to the same load. For convenience it is best to find solutions corresponding to specified deflections. Shown below are the calculations for bending moments and curvatures, and strain distribution corresponding to a specific load.

The cross section of the structural member is divided into smaller elements. Considering element k with its centroid at (X_k, Y_k) with reference to the axis of symmetry, seen in Figure 4.2.: The strain E_x along the element k can be assumed to be uniform and, since plane sections remain plane during bending,

$$E_k = E_p + \phi_x Y_k + \phi_y X_k \qquad - \quad 4.1.$$

Where

E_p = uniform direct strain due to an axial load P, and

ϕ_x = curvature produced by M_x considered positive when compressive strain is produced in positive Y direction, and

ϕ_y = curvature produced by M_y considered positive when compressive strain is produced in positive X direction.

Hsu (1) modified Cranston's and Chatterji's (17) stress-strain curves for concrete, Figure 4.3.a., and the stress-strain curve for steel has been idealized using piece-wise linear approximation to the curve in the strain hardening region shown in Figure 4.3.b. Therefore $(E_t)_k$ can be obtained for a steel or concrete element.

Once the strain distribution across a section has been identified, the following equations apply:

$$P_{(c)} = \sum_{k=1}^{n} f_k a_k$$

$$M_{x(c)} = \sum_{k=1}^{n} f_k a_k y_k \qquad - \quad 4.2.$$

$$M_{y(c)} = \sum_{k=1}^{n} f_k a_k x_k$$

The subscript (c) indicates an iterative cycle and a_k the area of the element.

For a given section P, M_x and M_y can be expressed as functions of ϕ_x, ϕ_y and E_p.

If $P_{(s)}$ is the final value of P for which the equilibrium and compatibility conditions are satisfied, the convergence of $P_{(c)}$ to $P_{(s)}$ is accelerated using a modification of the extended Newton-Raphson method.

$$M_{x(s)} = P_{(s)} e_y \qquad - \quad 4.3.$$

$$M_{y(s)} = P_{(s)} e_x$$

Using Taylor's expansion retaining linear terms $P_{(s)}$, $M_{x(s)}$ and $M_{y(s)}$ can be expressed in terms of their respective iterative values:

$$P_{(s)} = P_{(c)} + \frac{\partial P_{(c)}}{\partial \phi_x} \delta\phi_x + \frac{\partial P_{(c)}}{\partial \phi_y} \delta\phi_y + \frac{\partial P_{(c)}}{\partial E_p} \delta E_p$$

$$M_{x(s)} = M_{x(c)} + \frac{\partial M_{x(c)}}{\phi_x} \delta\phi_x + \frac{M_{x(c)}}{\phi_y} \delta\phi_y + \frac{M_{x(c)}}{E_p} \delta E_p \qquad - 4.4.$$

$$M_{y(s)} = M_{y(c)} + \frac{\partial M_{y(c)}}{\partial \phi_x} \delta\phi_x + \frac{\partial M_{y(c)}}{\partial \phi_y} \delta\phi_y + \frac{\partial M_{y(c)}}{\partial E_p} \delta E_p$$

Let

$$u' = P_{(c)} - P_{(s)}$$

$$v' = M_{x(c)} - M_{x(s)} \qquad - 4.5.$$

$$w' = M_{y(c)} - M_{y(s)}$$

Substituting 4.5. in 4.4.

$$-u' = \frac{\partial P_{(c)}}{\partial \phi_x} \delta\phi_x + \frac{\partial P_{(c)}}{\partial \phi_y} \delta\phi_y + \frac{\partial P_{(c)}}{\partial E_p} \delta E_p$$

$$-v' = \frac{\partial M_{x(c)}}{\partial \phi_x} \delta\phi_x + \frac{\partial M_{x(c)}}{\partial \phi_y} \delta\phi_y + \frac{\partial M_{x(c)}}{\partial E_p} \delta E_p \qquad - 4.6.$$

$$-w' = \frac{\partial M_{y(c)}}{\partial \phi_x} \delta\phi_x + \frac{\partial M_{y(c)}}{\partial \phi_y} \delta\phi_y + \frac{\partial M_{y(c)}}{\partial E_p} \delta E_p$$

An increment in axial load $\delta P_{(c)}$ produces an increment of strain δE_p, at each element in the section. The corresponding stress change at element k is therefore $\delta E_p \; (E_t)_k$.

Therefore the change $\delta P_{(c)}$ in $P_{(c)}$ is:

$$\delta P_{(c)} = \sum_{k=1}^{n} (E_t)_k \, a_k \, E_p$$

Therefore:

$$\frac{\delta P_{(c)}}{\delta E_p} = \sum_{k=1}^{n} (E_t)_k \, a_k \qquad - 4.7.$$

Similarly $\partial M_{x(c)}$ and $\partial M_{y(c)}$ are expressed in terms of δE_p and generate these equations:

$$\frac{\partial M_{x(c)}}{\partial E_p} = \sum_{k=1}^{n} (E_t)_k a_k y_k$$

$$\frac{\partial M_{y(c)}}{\partial E_p} = \sum_{k=1}^{n} (E_t)_k a_k y_k$$

Similarly $\delta P_{(c)}$, $\delta M_{x(c)}$ and $\delta M_{y(c)}$ can be differentiated with respect to $\delta\phi_x$ and $\delta\phi_y$,

and the equations are:

$$\frac{\partial P_{(c)}}{\partial \phi_x} = \sum_{k=1}^{n} (E_t)_k a_k y_k$$

$$\frac{\partial M_{x(c)}}{\partial \phi_x} = \sum_{k=1}^{n} (E_t)_k a_k y_k^2$$

$$\frac{\partial M_{y(c)}}{\partial \phi_x} = \sum_{k=1}^{n} (E_t)_k a_k x_k y_k$$

$$\frac{\partial P_{(c)}}{\partial \phi_y} = \sum_{k=1}^{n} (E_t)_k a_k x_k$$

$$\frac{\partial M_{x(c)}}{\partial \phi_y} = \sum_{k=1}^{n} (E_t)_k a_k y_k x_k$$

$$\frac{\partial M_{y(c)}}{\partial \phi_y} = \sum_{k=1}^{n} (E_t)_k a_k y_k x_k^2$$

In matrix form equations 4.6 and 4.7 give:

$$\begin{pmatrix} \sum_{k=1}^{n} (E_t)_k a_k & \sum_{k=1}^{n} (E_t)_k a_k y_k & \sum_{k=1}^{n} (E_t)_k a_k x_k \\ & \sum_{k=1}^{n} (E_t)_k a_k y_k^2 & \sum_{k=1}^{n} (E_t)_k a_k x_k y_k \\ \text{Symmetric} & & \sum_{k=1}^{n} (E_t)_k a_k x_k^2 \end{pmatrix} \begin{pmatrix} \delta E_p \\ \delta\phi_x \\ \delta\phi_y \end{pmatrix} = -\begin{pmatrix} u' \\ v' \\ w' \end{pmatrix} \qquad - 4.8.$$

or:

$$[k]\begin{pmatrix}\delta E_p\\ \delta\phi_x\\ \delta\phi_y\end{pmatrix} = -\begin{pmatrix}u'\\ v'\\ w'\end{pmatrix} \qquad - \quad 4.9.$$

or:

$$\begin{pmatrix}\delta E_p\\ \delta\phi_x\\ \delta\phi_y\end{pmatrix} = -[k]^{-1}\begin{pmatrix}u'\\ v'\\ w'\end{pmatrix} \qquad - \quad 4.10.$$

u', v' and w' are selected to suit the accuracy required and their substitution in equation 4.10 at the end of the M^{th} iteration cycle yields the values of $\delta E_p, \delta\phi_x$ and $\delta\phi_y$ which lead to values of E_p, ϕ_x and ϕ_y for the $(M+1)^{th}$ iteration cycle as follows:

$$E_p(M+1) = E_p(M) + \delta E_p$$

$$\phi_x(M+1) = \phi_x(M) + \delta\phi_x$$

$$\phi_y(M+1) = \phi_y(M) + \delta\phi_y$$

Once convergence is obtained within specified tolerances the computer program takes up the next load level and repeats the entire procedure.

C. Discussion of Accuracy and Convergence

Errors can arise due to one or more of the following:

1. The assumption of uniform strain and hence a strain distribution within a small element makes the accuracy dependent on the number of elements the section has been divided into. A particular error noticed is that the program cannot deal with plastic hinges. The reason is that

the tangent moduli are zero for all elements causing [k], the stiffness matrix, to be singular.

2. Due to incompatibilities u'_{all}, v'_{all} and w'_{all} need to be at least 10^{-5} to 10^{-6} times the values of P, M_x and M_y respectively since curvatures become extremely sensitive to small changes in loads in the inelastic ranges.

3. Errors may arise due to the assumptions for the stress-strain curves in concrete and steel.

Convergence of the procedures to calculate the curvatures and the axial strain corresponding to a given axial load and moment is dependent upon the validity of equations 4.1 and 4.8. If the stiffness becomes very small, the procedure does not converge occasionally. Therefore the program incorporates a factor which requires a maximum number of iterations to be specified. If loads beyond the ultimate load are proposed the procedure will be unable to reach a solution.

D. The Computer Program

The program follows the outline specified in the theory. It is listed in Hsu (1).

The input features are:

(i) The stress-strain curve for steel.

(ii) The cross section dimensions.

(iii) The elements it has been divided into and the x distance, y distance w.r.t. the centroid and also the area of each element.

(iv) The initial load and curvature can be adjusted with the main program.

(v) The time safety factor to stop the program if divergence occurs.

(vi) The e_x and e_y of the applied load w.r.t. the centroid.

The cross section with all the elements is seen in Figure 4.4. The elements with x, y and area are listed in Table 4.1. This table shows centroid calculations too.

The output features are:

(i) Load with the respective M_x, ϕ_x, M_y and ϕ_y.

(ii) The element x, y, area, stress, tangent modulus of elasticity and strain.

The program has to have the initial loads and curvatures to start it. This is within the main program. Then the load, M_x, ϕ_x, M_y and ϕ_y are calculated. Then the load is incremented by an amount that can be adjusted within the main program. Again the M_x, ϕ_x, M_y and ϕ_y are calculated. This occurs until either the subroutine which calculates inverses fails or divergence occurs. In this fashion the complete behavior of the columns can be obtained.

Table 4.1.

ELEMENT X-COORDINATE, Y-COORDINATE
AND AREA FOR INPUT IN COMPUTER PROGRAM

Member	Area	X-Coordinate	Y-Coordinate
1	0.11	2.66	3.00
2	0.11	2.66	4.5
3	0.11	1.16	4.5
4	0.11	-0.34	4.5
5	0.11	-1.84	4.5
6	0.11	-1.84	3.09
7	0.11	-1.84	1.50
8	0.11	-1.84	0.00
9	0.11	-1.84	-1.5
10	0.11	-1.84	-3.00
11	0.11	-1.84	-4.50
12	0.11	-0.34	-4.50
13	0.11	1.16	-4.50
14	0.11	2.66	-4.50
15	0.11	2.66	-3.00
16	0.11	1.16	-3.00
17	0.11	-0.34	-3.00
18	0.11	-0.34	-1.5
19	0.11	-0.34	0.00
20	0.11	-0.34	1.50
21	0.11	-0.34	3.00
22	0.11	1.16	3.00

Table 4.1.
(Continued)

Member	Area	X-Coordinate	Y-Coordinate
23	0.316	3.129	2.531
24	0.211	3.129	3.00
25	0.316	3.129	3.369
26	0.316	3.129	4.031
27	0.211	3.129	4.5
28	0.316	3.129	4.969
29	0.211	2.66	4.969
30	0.316	2.191	4.969
31	0.316	1.629	4.969
32	0.211	1.160	4.969
33	0.316	0.691	4.969
34	0.316	0.316	4.969
35	0.211	-0.34	4.969
36	0.316	-0.809	4.969
37	0.316	-1.371	4.969
38	0.211	-1.84	4.969
39	0.316	-2.309	4.969
40	0.211	-2.309	4.50
41	0.316	-2.309	4.031
42	0.316	-2.309	3.369
43	0.211	-2.309	3.00
44	0.316	-2.309	2.531
45	0.316	-2.309	1.969
46	0.211	-2.309	1.50

Table 4.1.
(Continued)

Member	Area	X-Coordinate	Y-Coordinate
47	0.316	-2.309	1.031
48	0.316	-2.309	0.469
49	0.211	-2.309	0.000
50	0.316	-2.309	-0.469
51	0.316	-2.309	-1.031
52	0.211	-2.309	-1.50
53	0.316	-2.309	-1.969
54	0.316	-2.309	-2.531
55	0.211	-2.309	-3.00
56	0.316	-2.309	-3.369
57	0.316	-2.309	-4.031
58	0.211	-2.309	-4.50
59	0.316	-2.309	-4.969
60	0.311	-1.84	-4.969
61	0.316	-1.371	-4.969
62	0.316	-0.809	-4.969
63	0.211	-0.34	-4.969
64	0.316	0.129	-4.969
65	0.316	0.691	-4.969
66	0.211	1.160	-4.969
67	0.316	1.629	-4.969
68	0.316	2.191	-4.969
69	0.211	2.66	-4.969
70	0.316	3.129	-4.969

Table 4.1.
(Continued)

Member	Area	X-Coordinate	Y-Coordinate
71	0.211	3.129	-4.50
72	0.316	3.129	-4.031
73	0.316	3.129	-3.369
74	0.211	3.129	-3.00
75	0.316	3.129	-2.531
76	0.211	2.66	-2.531
77	0.316	2.191	-2.531
78	0.316	1.629	-2.531
79	0.211	1.160	-2.531
80	0.316	0.691	-2.531
81	0.316	0.129	-2.531
82	0.316	0.129	-1.969
83	0.211	0.129	-1.50
84	0.316	0.129	-1.031
85	0.316	0.129	-0.469
86	0.211	0.129	0.000
87	0.316	0.129	0.469
88	0.316	0.129	1.031
89	0.211	0.129	1.50
90	0.316	0.129	1.969
91	0.316	0.129	2.531
92	0.316	0.691	2.531
93	0.211	1.160	2.531
94	0.316	1.629	2.531

Table 4.1.
(Continued)

Member	Area	X-Coordinate	Y-Coordinate
95	0.316	2.191	2.531
96	0.211	2.66	2.531
97	0.211	2.66	3.469
98	0.211	2.66	4.031
99	0.211	2.191	4.5
100	0.211	1.629	4.5
101	0.211	0.691	4.5
102	0.211	0.316	4.5
103	0.211	-0.809	4.5
104	0.211	-1.371	4.5
105	0.211	-1.84	4.031
106	0.211	-1.84	3.469
107	0.211	-1.84	2.531
108	0.211	-1.84	1.969
109	0.211	-1.84	1.031
110	0.211	-1.84	0.469
111	0.211	-1.84	-0.469
112	0.211	-1.84	-1.031
113	0.211	-1.84	-1.969
114	0.211	-1.84	-2.531
115	0.211	-1.84	-3.369
116	0.211	-1.84	-4.031
117	0.211	-1.371	-4.50
118	0.211	-0.809	-4.50

Table 4.1.
(Continued)

Member	Area	X-Coordinate	Y-Coordinate
119	0.211	0.129	-4.50
120	0.211	0.691	-4.50
121	0.211	1.629	-4.50
122	0.211	2.191	-4.50
123	0.211	2.66	-4.031
124	0.211	2.66	-3.369
125	0.211	2.191	-3.00
126	0.211	1.629	-3.00
127	0.211	0.691	-3.00
128	0.211	0.129	-3.00
129	0.211	-0.34	-2.531
130	0.211	-0.34	-1.969
131	0.211	-0.34	-1.031
132	0.211	-0.34	-0.469
133	0.211	-0.34	0.469
134	0.211	-0.34	1.031
135	0.211	-0.34	1.969
136	0.211	-0.34	2.531
137	0.211	0.316	3.00
138	0.211	0.691	3.00
139	0.211	1.629	3.00
140	0.211	2.191	3.00
141	0.316	2.191	3.469
142	0.316	2.191	4.031
143	0.316	1.629	4.031

Table 4.1.
(Continued)

Member	Area	X-Coordinate	Y-Coordinate
144	0.211	1.16	4.031
145	0.316	0.691	4.031
146	0.316	0.129	4.031
147	0.211	-0.34	4.031
148	0.316	-0.809	4.031
149	0.316	-1.371	4.031
150	0.316	-1.371	3.469
151	0.211	-1.371	3.00
152	0.316	-1.371	2.531
153	0.316	-1.371	1.969
154	0.211	-1.371	1.500
155	0.316	-1.371	1.031
156	0.316	-1.371	0.469
157	0.211	-1.371	0.000
158	0.316	-1.371	-0.469
159	0.316	-1.371	-1.031
160	0.211	-1.371	-1.500
161	0.316	-1.371	-1.696
162	0.316	-1.371	-2.531
163	0.211	-1.371	-3.00
164	0.316	-1.371	-3.369
165	0.316	-1.371	-4.031
166	0.316	-0.809	-4.031
167	0.211	-0.34	-4.031

Table 4.1.
(Continued)

Member	Area	X-Coordinate	Y-Coordinate
168	0.316	0.129	-4.031
169	0.316	0.691	-4.031
170	0.211	1.160	-4.031
171	0.316	1.629	-4.031
172	0.316	2.191	-4.031
173	0.316	2.191	-3.369
174	0.316	1.629	-3.369
175	0.211	1.160	-3.369
176	0.316	0.691	-3.369
177	0.316	0.129	-3.369
178	0.211	-0.340	-3.369
179	0.316	-0.809	-3.369
180	0.211	-0.809	-3.00
181	0.316	-0.809	-2.531
182	0.316	-0.809	-1.969
183	0.211	-0.809	-1.500
184	0.316	-0.809	-1.031
185	0.316	-0.809	-0.469
186	0.211	-0.809	0.000
187	0.316	-0.809	0.469
188	0.316	-0.809	1.031
189	0.211	-0.809	1.50
190	0.316	-0.809	1.969
191	0.316	-0.809	2.531

Table 4.1.
(Continued)

Member	Area	X-Coordinate	Y-Coordinate
192	0.211	-0.809	3.00
193	0.316	-0.809	3.469
194	0.211	-0.34	3.469
195	0.316	0.316	3.469
196	0.316	0.691	3.469
197	0.211	1.160	3.469
198	0.316	1.679	3.469

N.A. about "Y" Axis

$$Y = \frac{(3.0 \times 6.0)(6.0/2)(2) + (4.5 \times 3.0)(1.5)}{(3.0 \times 6.0)(2) + (4.5 \times 3.0)} = 2.59''$$

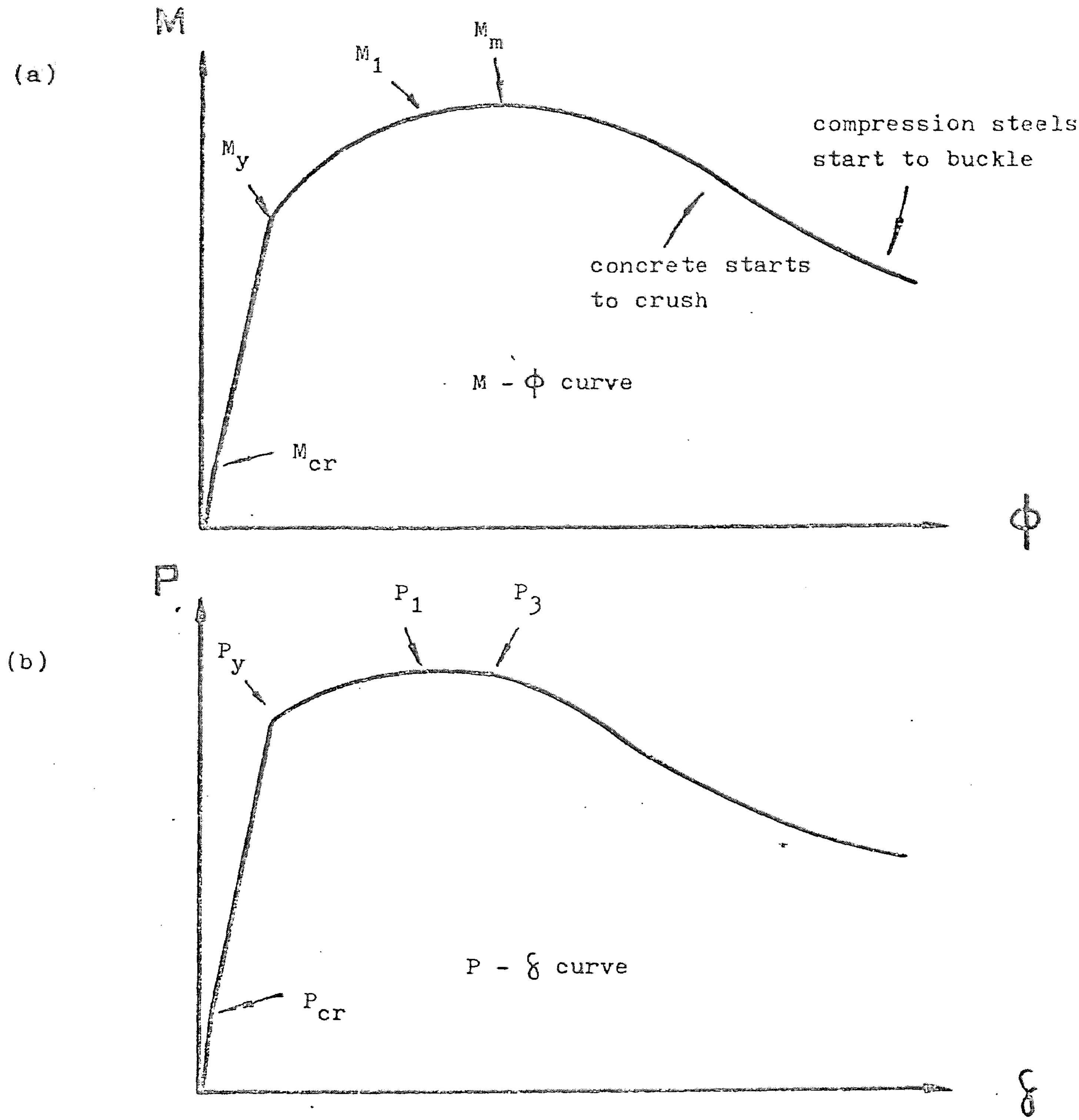

FIG. 4.1 TYPICAL RELATIONSHIP BETWEEN MOMENT-CURVATURE AND LOAD-DEFLECTION CURVES FOR SHORT COLUMNS

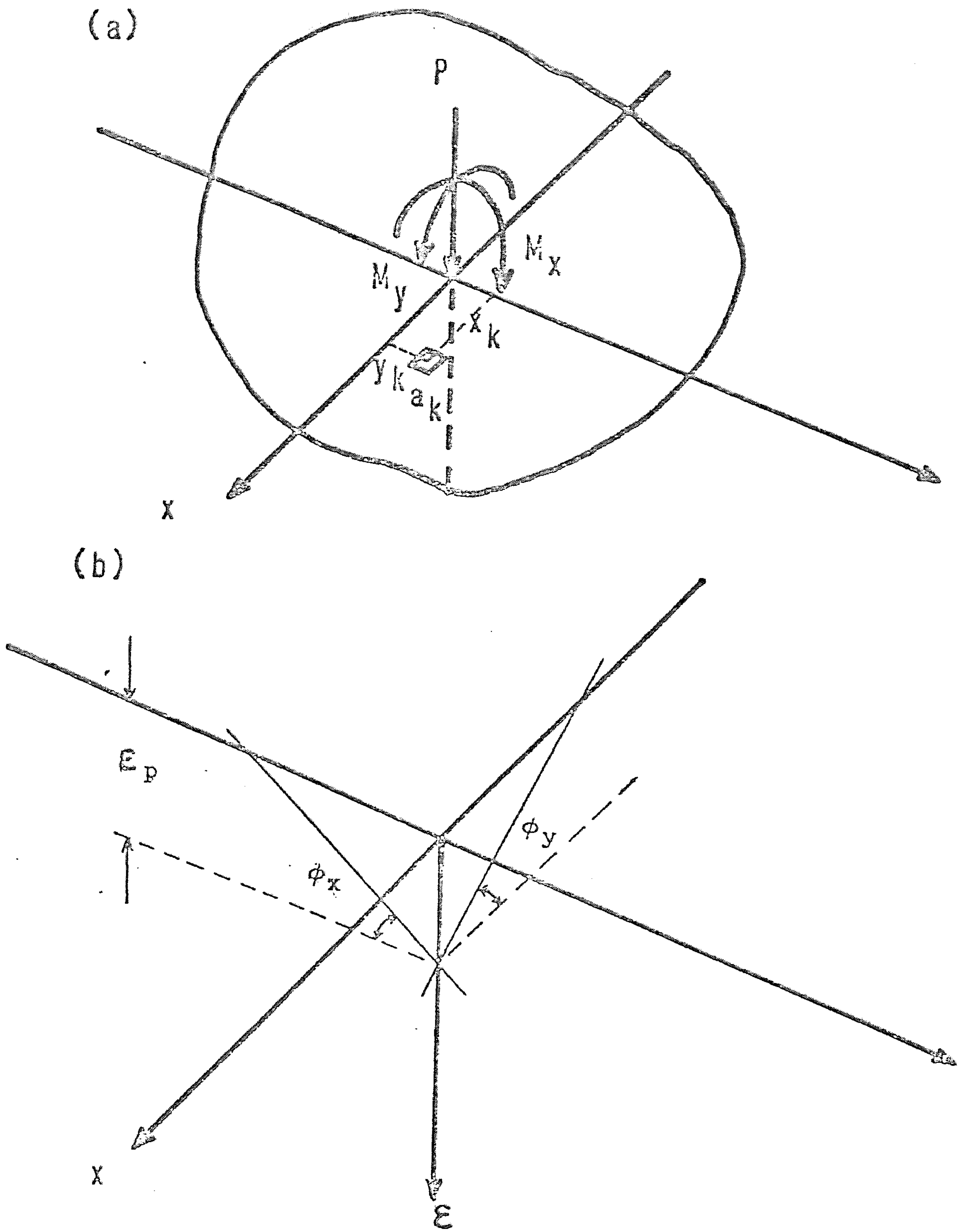

FIG 4.2 IDEALIZATION OF A CROSS-SECTION SUBJECTED TO BIAXIAL BENDING AND AXIAL LOAD

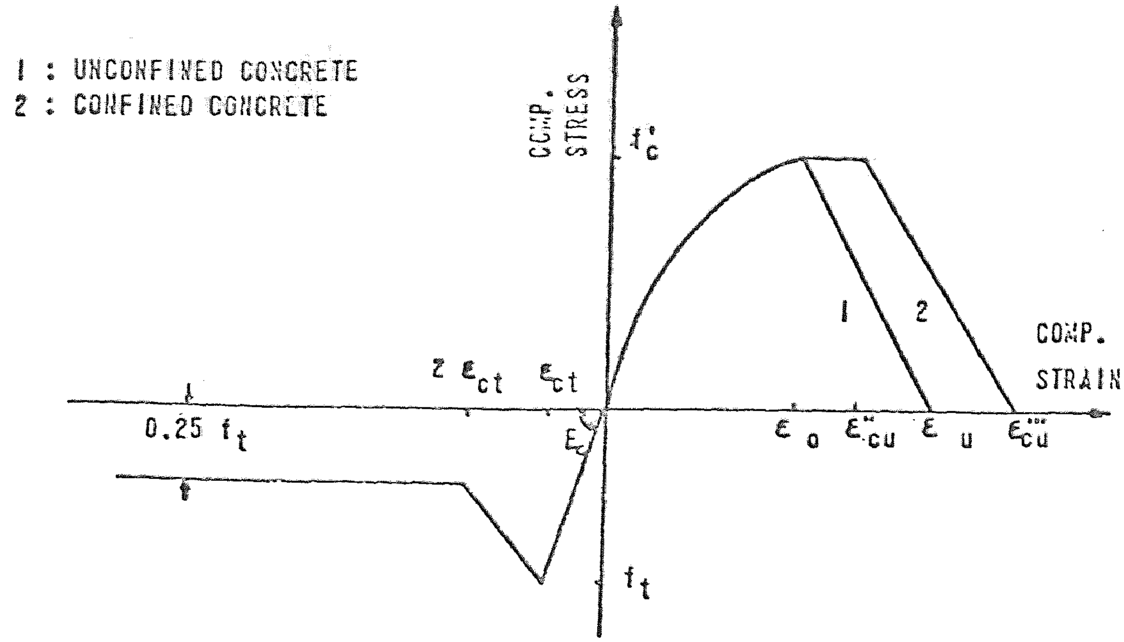

FIG. 4.3.a IDEALIZED STRESS-STRAIN CURVES FOR CONCRETE

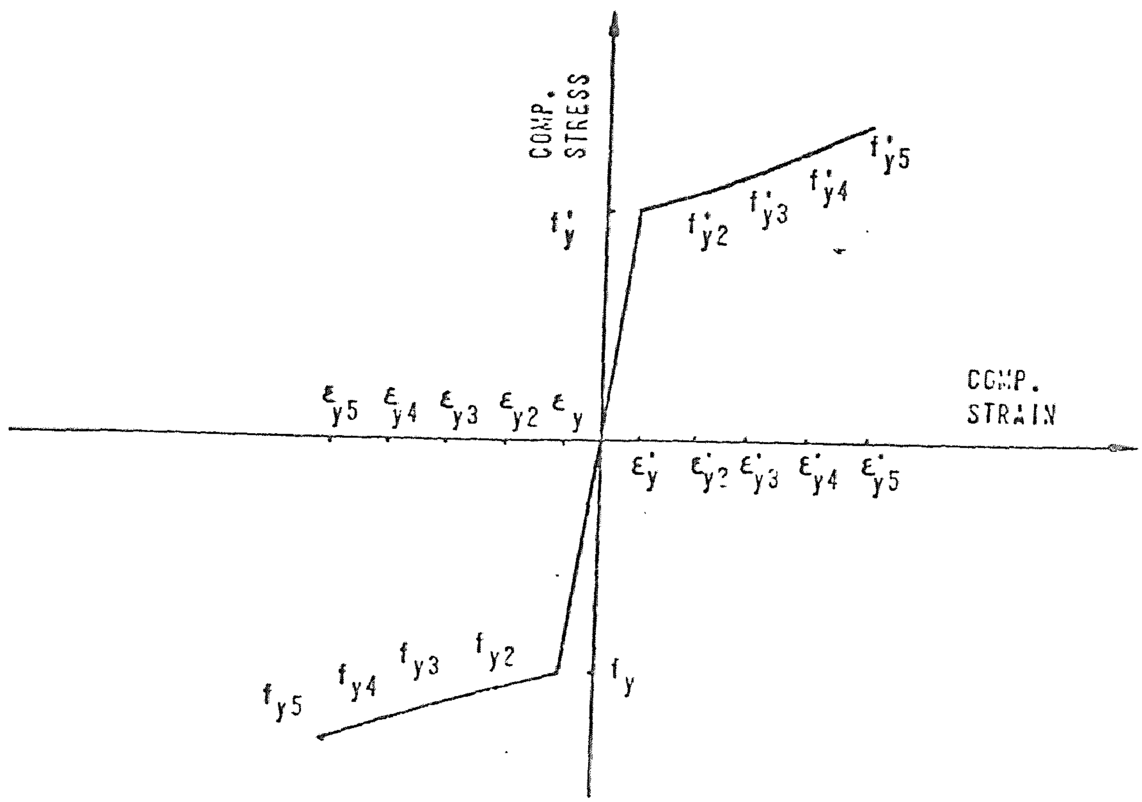

FIG 4.3.b IDEALIZED STRESS-STRAIN CURVE FOR STEEL

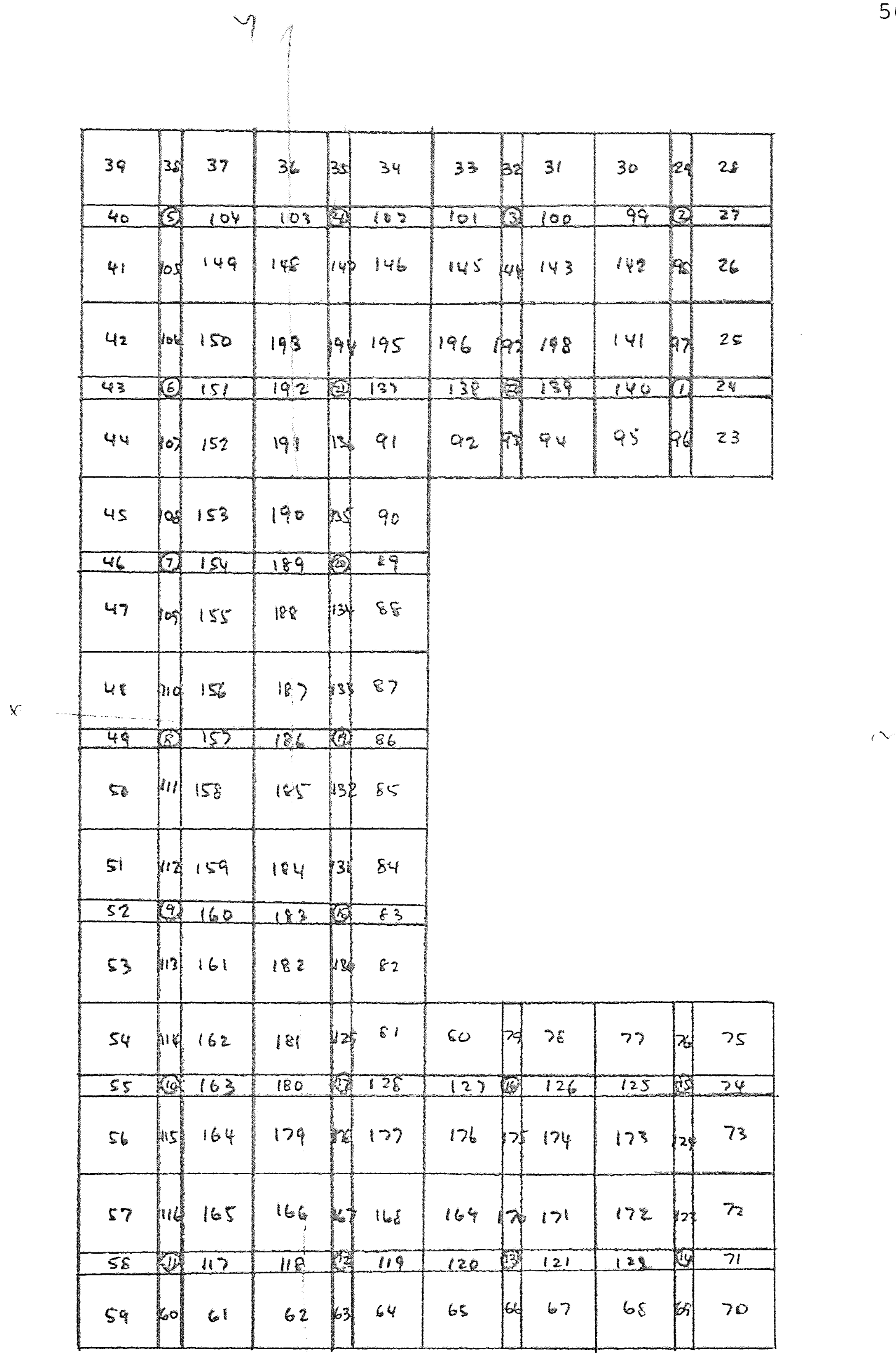

FIGURE 4.4 CROSS SECTION OF COLUMNS SHOWING ALL ELEMENTS

CHAPTER V. TEST AND COMPUTER RESULTS

A. Introduction

There were seven specimens tested. The first two trial specimens failed at the brackets which necessitated confining the brackets for the remaining five specimens. The specimen details are shown in Table 5.1 and the arrangement of demec gauge points are seen in Figure 5.1. The arrangement of the demec gauges was the same in all cases. The strain gauges at mid-span steel are arranged differently in different columns as seen in Figure 5.2.

The computer program results and test results were plotted on the same graphs. Therefore first an analysis of experimental data is shown, and then an interpretation of the computer data. The primary results of interest are the ultimate loads, the M_x-ϕ_x curves and the M_y-ϕ_y curves.

B. Analysis of Test Results

The measurements of all instruments and readings could not be taken at failure because of the danger of sudden failure and possible harm to instrumentation (which is why all the four Ames dial gauges are removed when failure is imminent). For this reason extrapolation is necessary.

A complete set of calculations is seen for Column #3 showing the interpretation of the data. At each stage of explanation the complete data for all columns is analyzed and only the strain distributions, M_x-ϕ_x curves, M_y-ϕ_y curves, load-deflection curves and load strain curves, are plotted. The analysis for only Column #3 is explained at each stage. Also, along with the M_x-ϕ_x, M_y-ϕ_y curves, the computer program M_x-ϕ_x, M_y-ϕ_y curves are plotted on the same graphs.

1. Load-Deflection Curves. The load-deflection curves are a plot of load on the y-axis and deflection on the x-axis. Both the deflections in the x and y direction have been plotted on the same graph for each specimen.

The calculations and tables listed here are for Column #3. The complete calculations for the load-deflection curves for Column #3 are seen in Tables 5.2.a and 5.2.b. The figure 5.3.a gives the load-deflection curves for both the x and y directions. Figures 5.3.b, 5.3.c, 5.3.d and 5.3.e show the load-deflection curves, for both the x and y directions, for Columns 4, 5, 6 and 7 respectively.

2. Moment Curvature Relationships. The first step in determining the in M-ϕ relationship by the demec gauge method is in calculating the strains of the concrete surface between the demec gauge points. Consider pair 1 in Figure 5.1, for example. The strain would be $\Delta l/\ell$, where Δl is the change in length between the original length of 6" and the final reading, and ℓ would be 6". It is assumed to be exactly 6", since the demec gauges were placed as accurately as possible within ± 0.05 inches, which is very little error.

Once the strains of all demec pairs have been obtained the plot of strain vs. distance is drawn. The strain distribution across the section, both in the x and y direction, is calculated for each load. Then for each load the average curvature is found. In view of the fact that not many strain gauges were used for each section which would have enabled the strain gauge method of calculating curvature, the demec gauge method is used as follows:

$$\phi = \frac{E_c}{kd} \qquad - \quad 5.1.$$

Where ϕ = curvature, and

E_c = maximum compressive concrete strain,

and kd = distance from this maximum compressive concrete strain to the point of zero strain (or neutral axis)

The strain gauge method is similar to the demec gauge method.

The calculations for Column #3 are again complete. The calculations are seen here. Reference is made to Figure 5.1 in these explanations. Table 5.3.a gives the measured values of changes in length between the pair of demec gauges. Table 5.3.b is obtained from Table 5.3.a thus: The difference between the reading at a particular load and the original reading divided by 6" gives the strain. Therefore Table 5.3.b consists of the strains for each pair of demec gauges for each load.

The strain distribution across the section is plotted as seen in Figure 5.4.1.a and Figure 5.4.1.b for Column #3. Here a. represents the strain distribution in the y direction giving ϕ_y, and b. represents the strain distribution in the x direction giving ϕ_x. The ϕ_y and ϕ_x are obtained as mentioned before from E_c/kd.

kd is obtained by drawing lines through the maximum concrete strain and the other strains until the neutral axis is bisected. This is seen in Figures 5.4.1.a and 5.4.1.b for Column #3.

M_x and M_y are calculated thus:

$M_x = P(e_y+\delta_y)$

$M_y = P(e_x+\delta_x)$

The table 5.4.1 shows the calculation of M_x, ϕ_x, M_y and ϕ_y for Column #3. kd for both are included. Computer calculations with loads are shown too. Explanations for the computer analysis are included in Chapter IV.D.

Figures 5.4.2.a and 5.4.2.b are the strain distributions in the y and x direction respectively for Column #4. Similarly, the following figures represent other column strain distributions:

Figure 5.4.3.a - Column #5 - y direction

Figure 5.4.3.b - Column #5 - x direction

Figure 5.4.4.a - Column #6 - y direction

Figure 5.4.4.b - Column #6 - x direction

Figure 5.4.5.a - Column #7 - y direction

Figure 5.4.5.b - Column #7 - x direction

Tables listed below give calculations of M_x, ϕ_x, M_y and ϕ_y for other columns. kd for both x and y directions is included. Here computer P, M_x, ϕ_x, M_y and ϕ_y also are included.

Table 5.4.2 - Column #4

Table 5.4.3 - Column #5

Table 5.4.4 - Column #6

Table 5.4.5 - Column #7

The curves of M_x-ϕ_x and M_y-ϕ_y are plotted for all columns listed below. These figures also include plots of M_x-ϕ_x and M_y-ϕ_y from the computer analysis.

Figure 5.5.1.a - Column #3 - x direction

Figure 5.5.1.b - Column #3 - y direction

Figure 5.5.2.a - Column #4 - x direction

Figure 5.5.2.b - Column #4 - y direction

Figure 5.5.3.a - Column #5 - x direction

Figure 5.5.3.b - Column #5 - y direction

Figure 5.5.4.a - Column #6 - x direction

Figure 5.5.4.b - Column #6 - y direction

Figure 5.5.5.a - Column #7 - x direction

Figure 5.5.5.b - Column #7 - y direction

A comparative study is discussed in Chapter V.D. and in the Conclusions.

3. Load Strain Curves. In view of the fact that very few strain gauges are installed as seen in Figure 5.2, these values cannot be used as an alternative method to the demec gauge method. The load strain curves are included in Appendix 1. These give an idea of the yield points in the M-ϕ curves, especially if the failure was due to tension. Beyond yield point the strain gauges are generally damaged.

4. Failure and Crack Patterns. Failure was sudden in all cases and it occurred primarily because of the buckling of compression reinforcement.

Cracks occurred on the tension face in straight lines and progressed from this tension face to the neutral axis as the load increased.

C. Comparative Study of Experiment and Computer Results

The ultimate loads, M_x-ϕ_x and M_y-ϕ_y curves are of primary interest. Table 5.5 gives the comparison between maximum values. The M-ϕ curves are seen in all Figures 5.5.

Table 5.1.

SPECIMEN DETAILS

Column Specimen No.	Size	No. and Size of Bars	f_y (ksi)	A_s. (#1 bar) (in.squared)	S (in.)	f_c' (psi)	e_x (in.)	e_y (in.)	l (in.)
3	Refer Figure 2.1.	22 #3	52	0.01227	4"	3662	1.8"	3"	72"
4		22 #3	52	0.01227	4"	3662	1.8"	2.75"	72"
5		22 #3	52	0.01227	4"	3662	1.8"	3"	72"
6		22 #3	52	0.01227	4"	4237	1.8"	3.5"	72"
7		22 #3	52	0.01227	4"	3899	1.5"	2.5"	72"

Table 5.2.a.

LOAD vs. VERTICAL DEFLECTION CALCULATIONS FOR COLUMN #3

Load (psi)	Load (kips)	Vertical Gauge #1 (inch)	Vertical Gauge #2 (inch)	Vertical Deflection Gauge #1 (inch)	Vertical Deflection Gauge #2 (inch)	δy Average Vertical Deflection at Mid-Span (inch)
0	0	0.988	0.716	0	0	0
500	10.31	0.972	0.699	0.016	0.017	0.0165
1000	20.63	0.959	0.676	0.029	0.040	0.0345
1500	30.95	0.938	0.654	0.050	0.062	0.0560
2000	41.26	0.930	0.626	0.058	0.090	0.0740
2500	51.58	0.907	0.602	0.081	0.114	0.0975
3000	61.89	0.884	0.579	0.104	0.137	0.1205
3500	72.21	0.862	0.556	0.126	0.160	0.1430
4000	82.52	0.830	0.524	0.158	0.192	0.1750
4500	92.84	0.804	0.496	0.184	0.220	0.2020
4750	98.00	0.773	0.458	0.215	0.258	0.2305
5000	103.15	0.761	0.440	0.227	0.276	0.2515
5250	108.31	Failure	-	-	-	-

Table 5.2.b.

LOAD vs. HORIZONTAL DEFLECTION CALCULATIONS FOR COLUMN #3

Load (psi)	Load (kips)	Horizontal Gauge #1 (inch)	Horizontal Gauge #2 (inch)	Horizontal Deflection Gauge #1 (inch)	Horizontal Deflection Gauge #2 (inch)	δ_x Average Horizontal Deflection at Mid-Span (inch)
0	0	0.569	0.489	0	0	0
500	10.31	0.569	0.486	0	0.003	0.0015
1000	20.63	0.567	0.470	0.002	0.019	0.0105
1500	30.95	0.565	0.454	0.004	0.035	0.0195
2000	41.26	0.562	0.434	0.007	0.055	0.0310
2500	51.58	0.523	0.397	0.046	0.092	0.0690
3000	61.89	0.509	0.376	0.060	0.113	0.0865
3500	72.21	0.482	0.348	0.087	0.141	0.1140
4000	82.52	0.419	0.288	0.150	0.201	0.1775
4500	92.84	0.383	0.253	0.186	0.236	0.2110
4750	98.00	0.320	0.194	0.249	0.295	0.2720
5000	103.15	0.298	0.171	0.271	0.318	0.2945
5250	108.31	Failure.				

Table 5.3.a.

MEASURED VALUES OF CHANGES IN LENGTH BETWEEN PAIRS OF DEMEC GAUGES FOR COLUMMN #3

Load (psi)	Demec Gauge Pairs 1	2	3	4	5	6	7	8	9
0	0.0431	0.0160	0.2475	0.2298	0.2442	0.0447	0.0224	0.0684	0.0410
500	0.0444	0.0170	0.2482	0.2301	0.2443	0.0446	0.0220	0.0680	0.0405
1000	0.0462	0.0188	0.2491	0.2307	0.2444	0.0444	0.0215	0.0675	0.0397
1500	0.0475	0.0200	0.2497	0.2312	0.2445	0.0443	0.0211	0.0668	0.0388
2000	0.0486	0.0210	0.2503	0.2316	0.2446	0.0442	0.0202	0.0664	0.0380
2500	0.0499	0.0216	0.2510	0.2320	0.2447	0.0441	0.0204	0.0657	0.0343
3000	0.0516	0.0230	0.2519	0.2324	0.2448	0.0439	0.0196	0.0624	0.0313
3500	0.0537	0.0240	0.2530	0.2332	0.2449	0.0438	0.0163	0.0604	0.0283
4000	0.0562	0.0266	0.2543	0.2344	0.2450	0.0434	0.0142	0.0572	0.0250
4500	0.0613	0.0290	0.2575	0.2357	0.2451	0.0427	0.0118	0.0542	0.0223
4750	0.0691	0.0357	0.2602	0.2366	0.2453	0.0417	0.090	0.0512	0.0175
5000	0.0772	0.0437	0.2645	0.2401	0.2458	0.0404	0.061	0.0484	0.0130
5250	- T	- T	Failure T	- T	- Ten	- C	- C	- C	- C

Table 5.3.b.

STRAINS OF CONCRETE SURFACE BETWEEN DEMEC GAUGE PAIRS - FOR COLUMN #3

All units are multiplied by a factor of ($x10^{-6}$).

Load (psi)	1	2	3	4	5	6	7	8	9
0	0	0	0	0	0	0	0	0	0
500	216.7	166.7	116.7	66.7	16.7	-16.7	-66.7	-66.7	-83.3
1000	516.7	466.7	266.7	150	33.3	-50	-150	-150	-216.7
1500	733.3	666.7	366.7	233.3	50	-66.7	-216.7	-266.7	-366.7
2000	916.7	833.3	466.7	300	66.7	-83.3	-366.7	-333.3	-500
2500	1133.3	933.3	583.3	366.7	83.3	-100	-333.3	-450	-1116.7
3000	1416.7	1166.7	733.3	433.3	100	-133.3	-466.7	-1000	-1616.7
3500	1766.7	1333.3	916.7	566.7	116.7	-150	-1016.7	-1333.3	-2116.7
4000	2183.3	1766.7	1133.3	766.7	133.3	-216.7	-1366.7	-1866.7	-2666.7
4500	3033.3	2166.7	1666.7	983.3	150	-333.3	-1766.7	-2366.7	-3116.7
4750	4333.3	3283.3	2116.7	1133.3	200	-500	-2233.3	-2866.7	-3916.7
5000	5683.3	4616.7	2833.3	1716.7	266.7	-716.7	-2716.7	-3333.3	-4777.7
5250	-	-	Failure	-	-	-	-	-	-

Table 5.4.1.

CALCULATIONS OF EXPERIMENTAL AND COMPUTER M_x, ϕ_x, M_y, ϕ_y - COLUMN #3

Experiment							Computer				
Load (kips)	M_x (kip in.)	kd (inch)	ϕ_x 1/inch	M_y (kip in.)	kd (in.)	ϕ_y 1/inch	Load (kips)	M_x (kip in.)	ϕ_x 1/inch	M_y (kip in.)	ϕ_y 1/inch
0	0	-	0	0	-	0	0	0	0	0	0
10.31	31	.1	1.7×10^{-5}	18.6	6.5"	3.3×10^{-5}	50.09	150.3	8×10^{-5}	90.2	18.9×10^{-5}
20.62	62.6	0.85	4.1×10^{-5}	37.4	6 "	8.6×10^{-5}	51.59	154.8	8.3×10^{-5}	92.9	19.6×10^{-5}
30.95	94.6	0.86	5.5×10^{-5}	56.5	6 "	12.2×10^{-5}	60.09	180.3	10×10^{-5}	108.2	23.9×10^{-5}
41.26	126.8	0.90	7×10^{-5}	75.6	6	15.3×10^{-5}	70.09	210.3	12.4×10^{-5}	126.2	29.5×10^{-5}
51.58	159.8	0.94	9.2×10^{-5}	96.4	6	18.9×10^{-5}	80.09	240.3	15.4×10^{-5}	144.2	36.7×10^{-5}
61.89	193.1	0.84	11.4×10^{-5}	116.9	6	23.6×10^{-5}	90.10	270.3	20.9×10^{-5}	162.2	49.9×10^{-5}
72.21	226.9	0.88	14.6×10^{-5}	138.2	5.9	29.9×10^{-5}	96.37	289.1	26.9×10^{-5}	173.5	59.2×10^{-5}
82.52	262	0.76	17.8×10^{-5}	163.1	5.8	37.6×10^{-5}	100.1	300.3	33.5×10^{-5}	180.2	78.6×10^{-5}
92.84	297.3	0.63	25.5×10^{-5}	186.7	5.8	52.3×10^{-5}	102.4	307.1	45.1×10^{-5}	184.3	105.5×10^{-5}
98.00	317.2	0.57	35.8×10^{-5}	202.9	5.8	74.7×10^{-5}	Failure computer.				
103.15	335.4	0.54	53.5×10^{-5}	216.3	5.7	99.7×10^{-5}					
108.31	356	-	-	231	-	-					

Table 5.4.2.

CALCULATIONS OF EXPERIMENTAL AND COMPUTER M_x, ϕ_x, M_y, ϕ_y - COLUMN #4

Experiment							Computer				
Load (kips)	M_x (kip in.)	kd (inch)	ϕ_x 1/inch	M_y (kip in.)	kd (in.)	ϕ_y 1/inch	Load (kips)	M_x (kip in.)	ϕ_x 1/inch	M_y (kip in.)	ϕ_y 1/inch
0	0	-	0	0	-	0	0	0	0	0	0
10.31	28.37	0.91	1.8×10^{-5}	18.62	7	2.8×10^{-5}	50.09	137.8	7.2×10^{-5}	90.2	18.5×10^{-5}
20.63	56.84	-	-	37.74	6.35	5.9×10^{-5}	60.09	165.3	9.1×10^{-5}	108.2	23.4×10^{-5}
30.95	85.75	0.89	4.4×10^{-5}	57.61		-	70.09	192.8	11.2×10^{-5}	126.2	28.8×10^{-5}
41.26	114.56	0.78	6.3×10^{-5}	77.78		-	80.09	220.3	13.7×10^{-5}	144.2	35.2×10^{-5}
51.58	143.63	-	-	98.47	5.9	16.3×10^{-5}	90.1	247.8	18.2×10^{-5}	162.2	46.5×10^{-5}
61.89	173.01	0.72	9.3×10^{-5}	119.66	5.75	20.9×10^{-5}	96.37	265.6	22.7×10^{-5}	173.5	57.7×10^{-5}
72.21	203.16	0.65	11.5×10^{-5}	141.82		-	100.1	275.3	26.7×10^{-5}	180.2	67.5×10^{-5}
82.52	233.08	0.59	14.2×10^{-5}	164.63	5.65	31.8×10^{-5}	102.45	281.7	30.7×10^{-5}	184.4	76.8×10^{-5}
92.84	263.25	0.47	20.2×10^{-5}	188.7	5.6	44.5×10^{-5}	103.06	283.4	31.8×10^{-5}	185.5	79.4×10^{-5}
103.15	293.72	0.39	33.1×10^{-5}	214.55	5.65	70.8×10^{-5}					
119.65	345	Failure	-	258	-	-					

Table 5.4.3.

CALCULATIONS OF EXPERIMENTAL AND COMPUTER M_x, ϕ_x, M_y, ϕ_y - COLUMN #5

Experiment							Computer				
Load (kips)	M_x (kip in.)	kd (inch)	ϕ_x 1/inch	M_y (kip in.)	kd (in.)	ϕ_y 1/inch	Load (kips)	M_x (kip in.)	ϕ_x 1/inch	M_y (kip in.)	ϕ_y 1/inch
0	0	-	0	0	-	0	0	0	0	0	0
10.31	30.95	1	1.7×10^{-5}	18.66	-	-	50.09	150.3	8×10^{-5}	90.2	18.9×10^{-5}
20.63	61.96	-	-	38.03	7.3"	5×10^{-5}	51.59	154.8	8.3×10^{-5}	92.9	19.6×10^{-5}
30.95	93.04	1	5×10^{-5}	57.74	-	-	60.09	180.3	10×10^{-5}	108.2	23.9×10^{-5}
41.26	124.34	0.75	6.7×10^{-5}	78.04	6.15	13.6×10^{-5}	70.09	210.3	12.4×10^{-5}	126.2	29.5×10^{-5}
51.58	155.77	-	-	98.62	5.95	17.4×10^{-5}	80.09	240.3	15.4×10^{-5}	144.2	36.7×10^{-5}
61.89	187.34	0.92	10.9×10^{-5}	119.76	5.95	21.9×10^{-5}	90.1	270.3	20.9×10^{-5}	162.2	49.9×10^{-5}
72.21	219.84	0.82	14.2×10^{-5}	143.37	5.8	27.9×10^{-5}	96.37	289.1	26.9×10^{-5}	173.5	59.2×10^{-5}
82.52	252.3	0.73	18.3×10^{-5}	165.82	5.8	34.5×10^{-5}	100.1	300.3	33.5×10^{-5}	180.2	78.6×10^{-5}
92.84	284.83	0.61	27.3×10^{-5}	191.07	5.8	48×10^{-5}	102.4	307.1	45.1×10^{-5}	184.3	105.5×10^{-5}
103.15	318.4	-	Failure	219	-	-					

Table 5.4.4.

CALCULATIONS OF EXPERIMENTAL AND COMPUTER M_x, ϕ_x, M_y, ϕ_y - COLUMN #6

Experiment							Computer				
Load (kips)	M_x (kip in.)	kd (inch)	ϕ_x 1/inch	M_y (kip in.)	kd (in.)	ϕ_y 1/inch	Load (kips)	M_x (kip in.)	ϕ_x 1/inch	M_y (kip in.)	ϕ_y 1/inch
0	0	-	0	0	-	0	0	0	0	0	0
10.31	36.13	-	-	18.69	6"	3.1×10^{-5}	50.09	175.3	8.6×10^{-5}	90.2	17.7×10^{-5}
20.63	72.4	.8"	4.2×10^{-5}	37.89	5.4"	6.5×10^{-5}	60.09	210.3	10.8×10^{-5}	108.2	22.4×10^{-5}
30.95	108.84	-	-	57.3	5.65	9.4×10^{-5}	70.09	245.3	13.3×10^{-5}	126.2	27.7×10^{-5}
41.26	145.48	.86	5.8×10^{-5}	77.14	-	-	80.09	280.3	16.4×10^{-5}	144.2	34.1×10^{-5}
51.58	182.34	0.91	9.2×10^{-5}	97.2	-	-	90.1	315.3	21.4×10^{-5}	162.2	45.4×10^{-5}
61.89	219.77	-	-	118.06	5.85	21.1×10^{-5}	95.37	333.8	25.9×10^{-5}	171.7	55×10^{-5}
72.21	257.57	0.94	14.2×10^{-5}	139.33	6.1	24.6×10^{-5}	98.37	344.3	30.1×10^{-5}	177.1	64×10^{-5}
82.52	296	0.86	17.4×10^{-5}	163.39	6.1	30.1×10^{-5}	100.38	351.3	33.7×10^{-5}	180.7	71.7×10^{-5}
92.84	333.62	0.74	22.5×10^{-5}	185.36	6	40.3×10^{-5}	102.45	358.6	41.1×10^{-5}	184.4	86.6×10^{-5}
103.5	377.53	0.6	47.2×10^{-5}	212.85	5.85	86.1×10^{-5}	103.58	361.8	45.6×10^{-5}	186.1	95.8×10^{-5}
107.28	395.2	-	-	225.9							

Table 5.4.5.

CALCULATIONS OF EXPERIMENTAL AND COMPUTER M_x, ϕ_x, M_y, ϕ_y - COLUMN #7

Experiment							Computer				
Load (kips)	M_x (kip in.)	kd (inch)	ϕ_x 1/inch	M_y (kip in.)	kd (in.)	ϕ_y 1/inch	Load (kips)	M_x (kip in.)	ϕ_x 1/inch	M_y (kip in.)	ϕ_y 1/inch
0	0	-	0	0	-	0	0	0	0	0	0
10.31	25.83	1"	1.7×10^{-5}	15.57	5.4	3.1×10^{-5}	50.09	125.2	5.8×10^{-5}	75.1	13.9×10^{-5}
20.63	51.75	2"	2.5×10^{-5}	31.53	-	-	60.09	150.2	7.3×10^{-5}	90.1	17.4×10^{-5}
30.95	77.96	2"	4.2×10^{-5}	48.93	-	-	70.09	175.2	8.9×10^{-5}	105.1	21.2×10^{-5}
41.26	104.16	-	-	65.81	-	-	80.09	200.2	10.7×10^{-5}	120.1	25.5×10^{-5}
51.58	130.76	1.75	6.7×10^{-5}	83.41	6.3	12.7×10^{-5}	90.1	225.2	12.7×10^{-5}	135.1	30.3×10^{-5}
61.89	157.51	-	-	101.69	6.1	16.1×10^{-5}	100.1	250.2	15.7×10^{-5}	150.1	37.5×10^{-5}
72.21	184.1	1.667	10×10^{-5}	119.76	6.3	19.1×10^{-5}	110.1	275.2	21.2×10^{-5}	165.1	50.6×10^{-5}
82.52	212.04	1.571	11.7×10^{-5}	139.38	6.1	23.5×10^{-5}	115.5	288.7	26.2×10^{-5}	173.2	62.2×10^{-5}
92.84	238.83	1.5	13.3×10^{-5}	158.94	6.2	27.2×10^{-5}	120.	300.2	33.7×10^{-5}	180.2	79.1×10^{-5}
103.15	267.06	1.4	16.7×10^{-5}	180.93	6.2	33.3×10^{-5}					
121.72	326.21			236.75							

Table 5.5.

COMPARATIVE STUDY OF EXPERIMENTAL AND COMPUTER RESULTS

Column Specimen No.	f_c' (psi)	e_x (in.)	e_y (in.)	$P_{ult.}$ expt. (kips)	$P_{ult.}$ comp. (kips)	M_x ult. expt. (kip.in.)	M_x ult. comp. (kip.in.)	M_y ult. expt. (kip.in.)	M_y ult. comp. (kip.in.)
3	3662	1.8	3	108.31	102.4	356	307.1	231	184.3
4	3662	1.8	2,75	119.65	103.06	345	283.4	258	185.5
5	3662	1.8	3	103.15	102.4	318.4	307.1	219	184.3
6	4237	1.8	3.5	107.28	103.58	395.2	361.8	225.9	186.1
7	3899	1.5	2.5	121.72	120	326.2	300.2	236.8	180.2

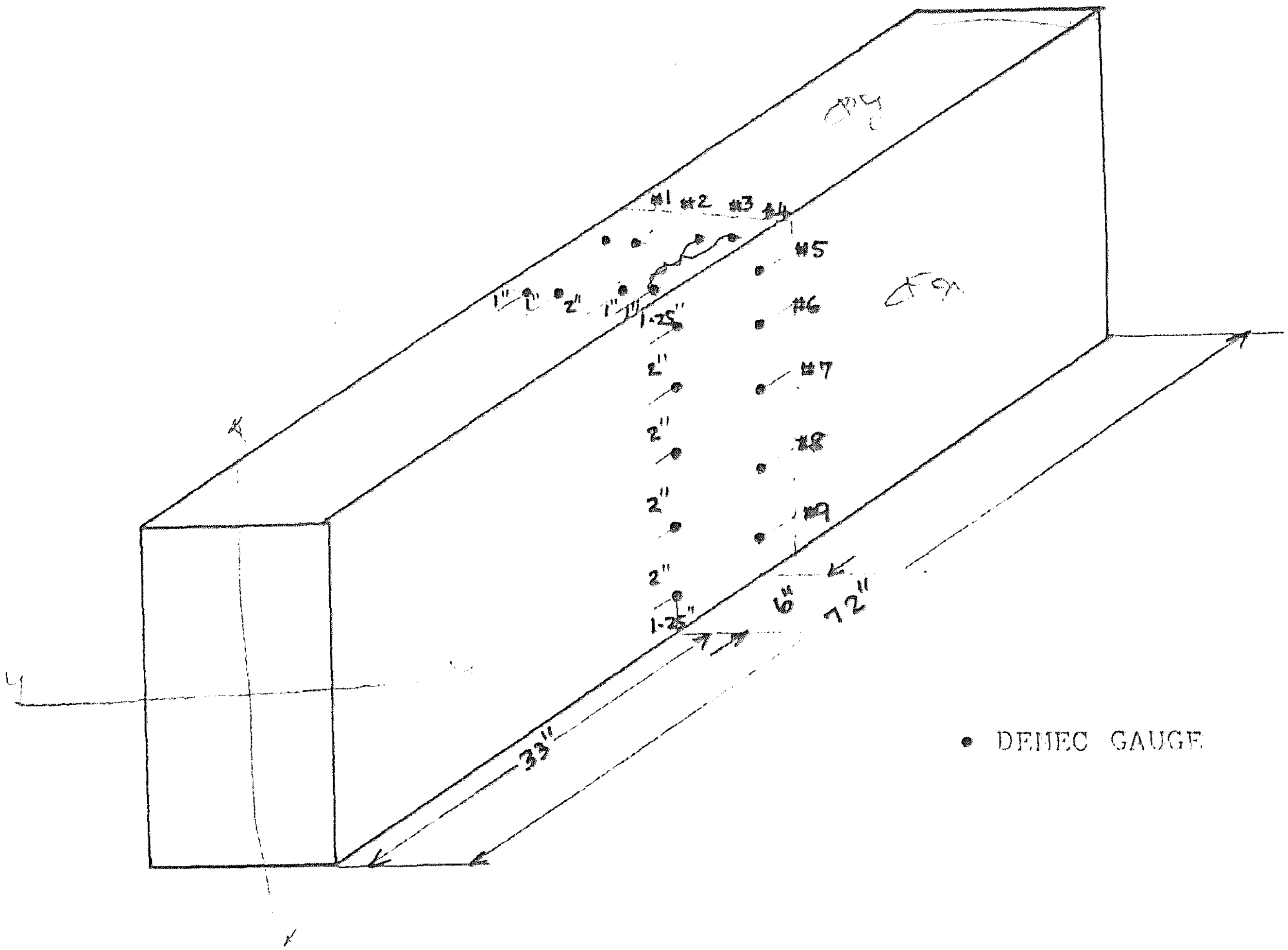

FIGURE 5.1 ARRANGEMENT OF DEMEC GAUGES

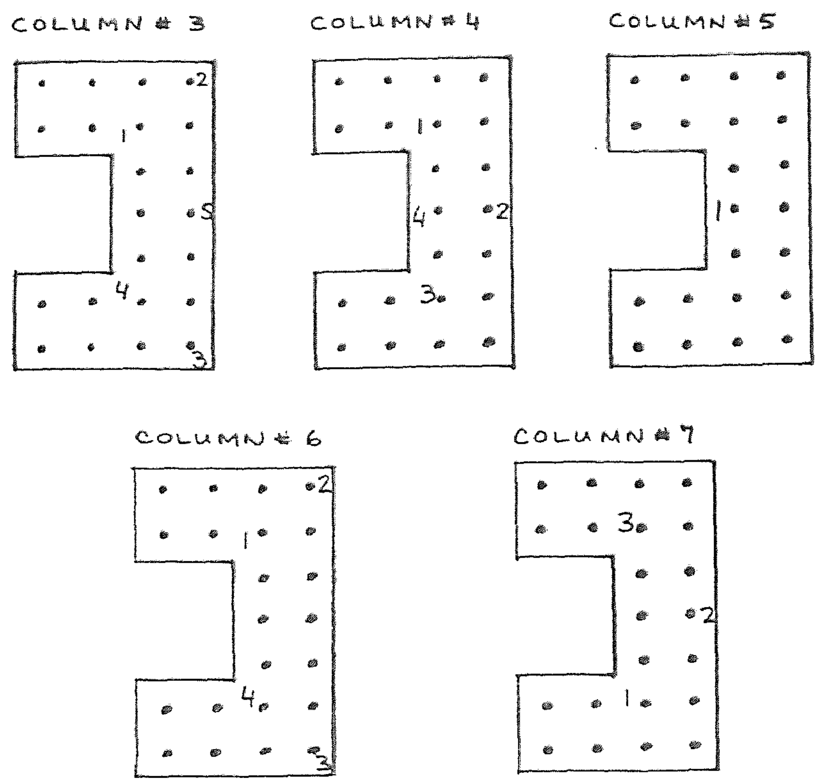

FIGURE 5.2 STRAIN GAUGE ARRANGEMENT IN STEEL REINFORCEMENT AT MID-SECTION FOR ALL SPECIMENS

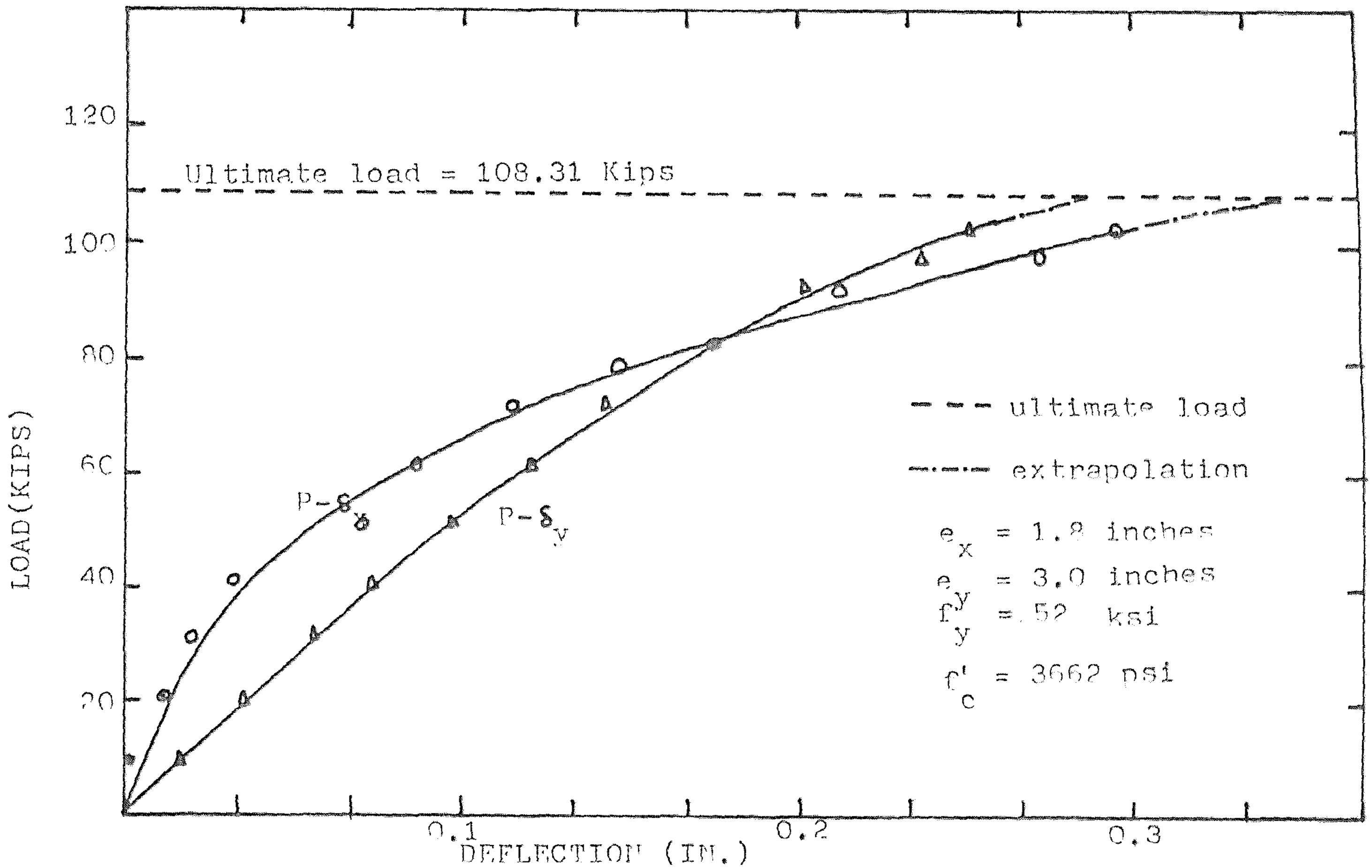

FIGURE 5.3.a EXPERIMENTAL LOAD-DEFLECTION CURVES IN X AND Y DIRECTIONS - COLUMN #3

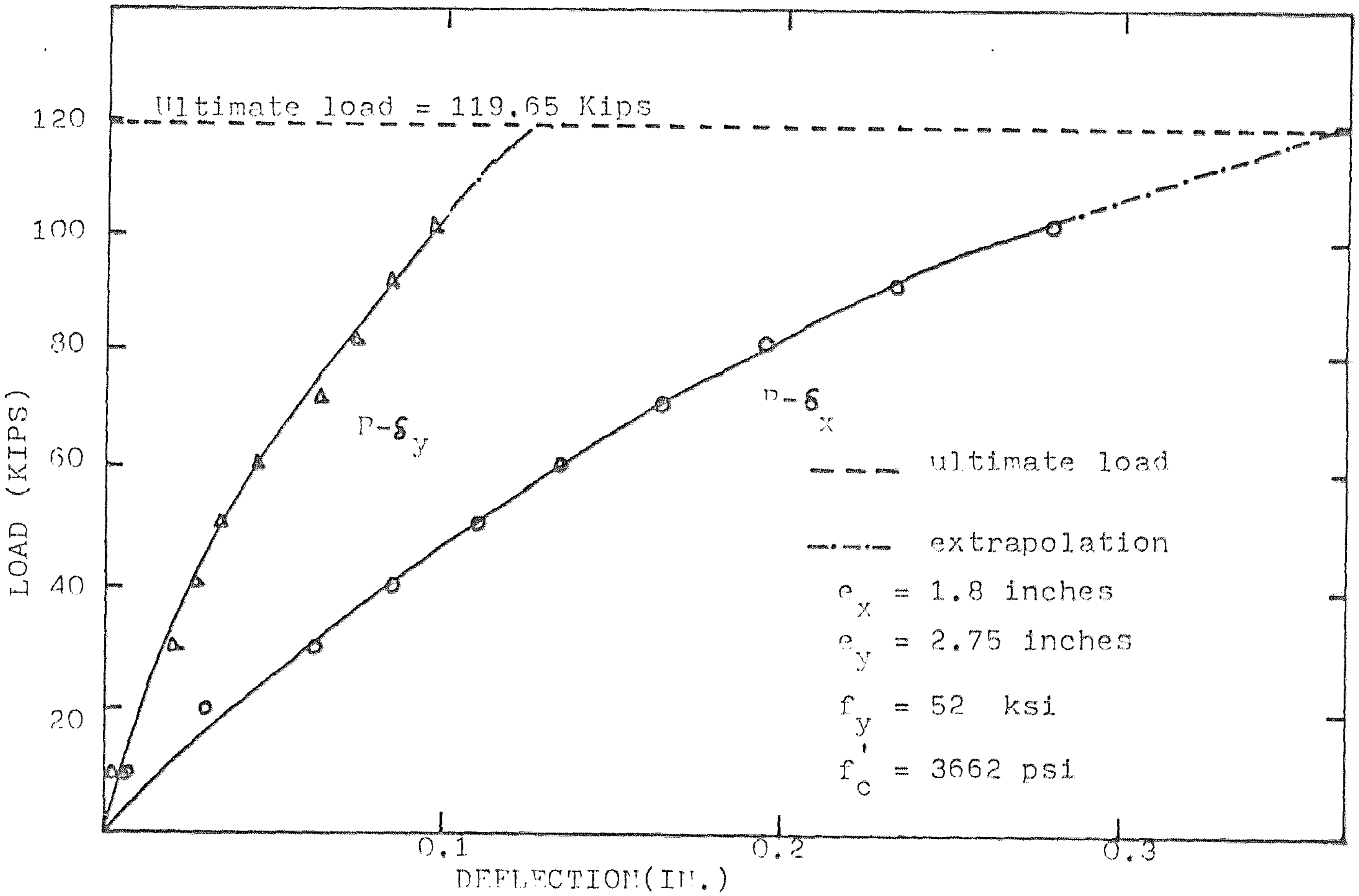

FIGURE 5.3.b EXPERIMENTAL LOAD-DEFLECTION CURVES IN X AND Y DIRECTIONS - COLUMN #4

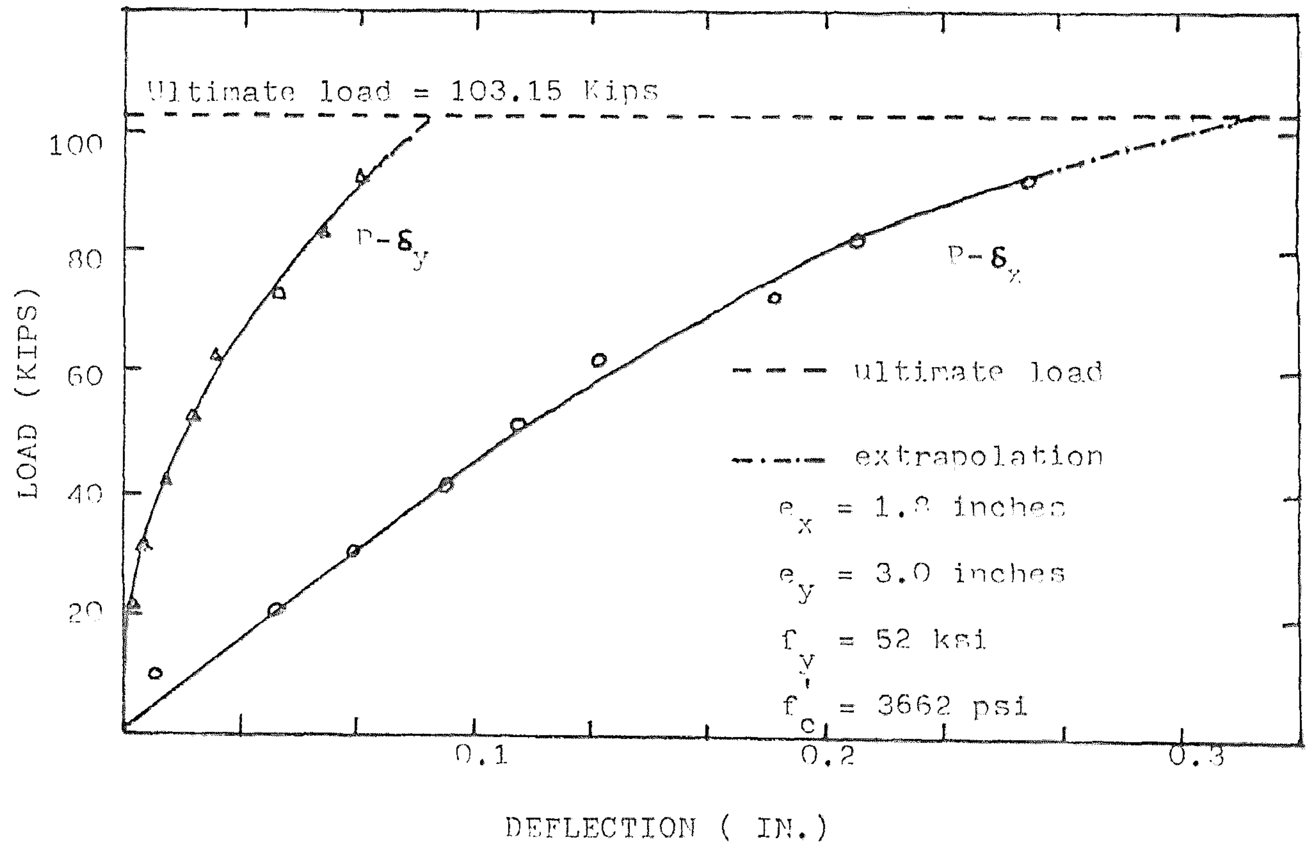

FIGURE 5.3.c EXPERIMENTAL LOAD-DEFLECTION CURVES IN X AND Y DIRECTIONS - COLUMN #5

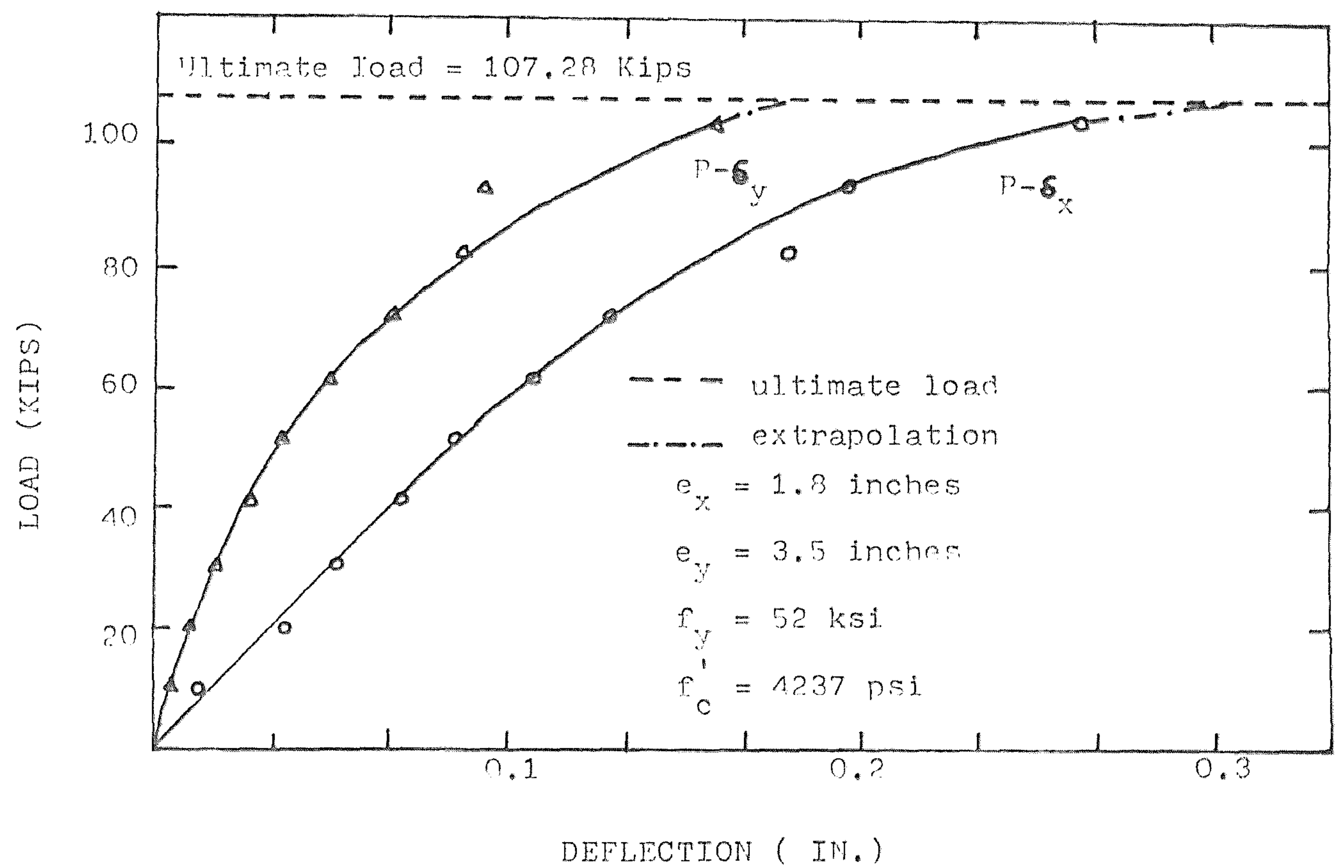

FIGURE 5.3.d EXPERIMENTAL LOAD-DEFLECTION CURVES IN X AND Y DIRECTIONS - COLUMN #6

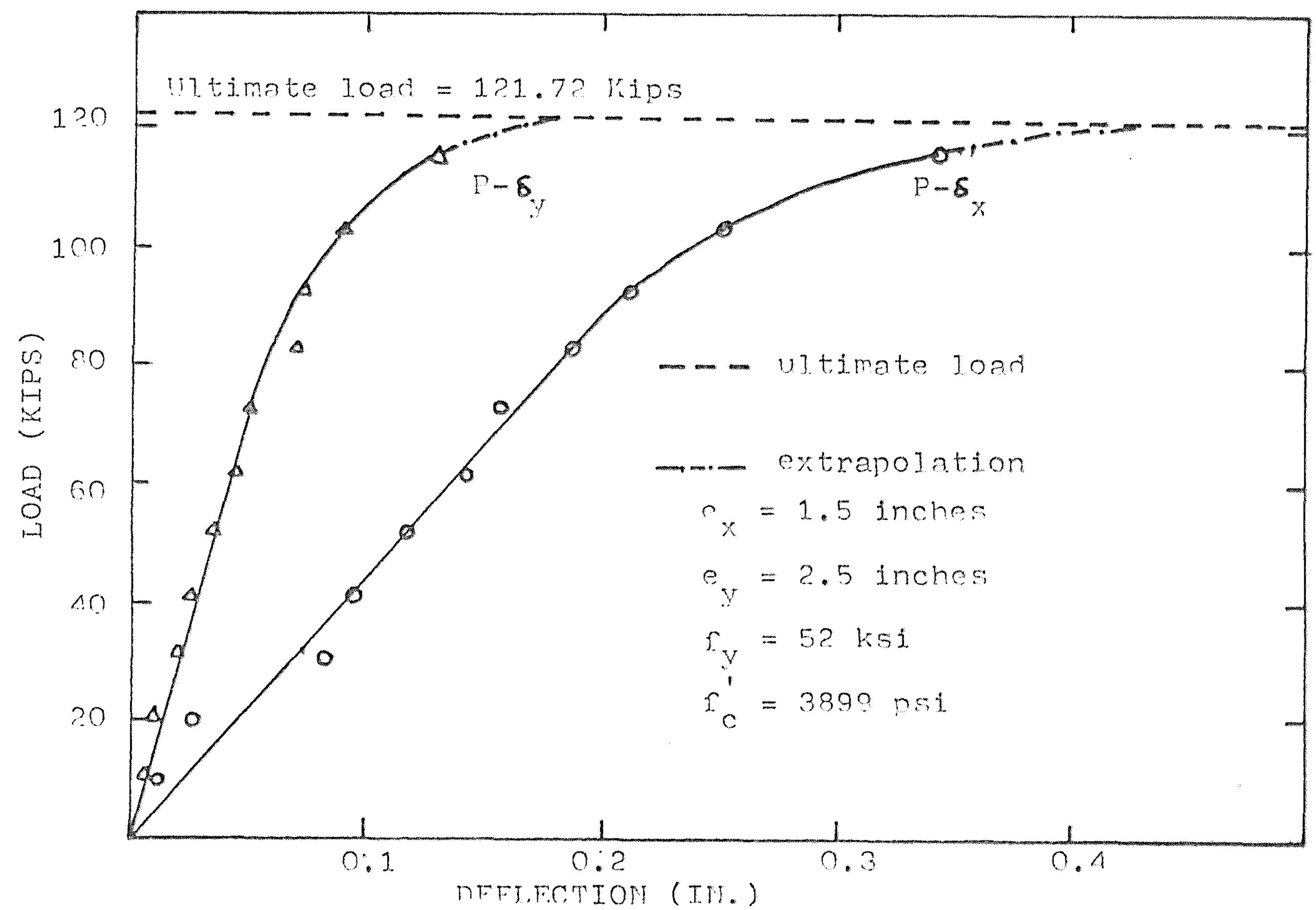

FIGURE 5.3.e EXPERIMENTAL LOAD-DEFLECTION CURVES IN X AND Y DIRECTIONS - COLUMN #7

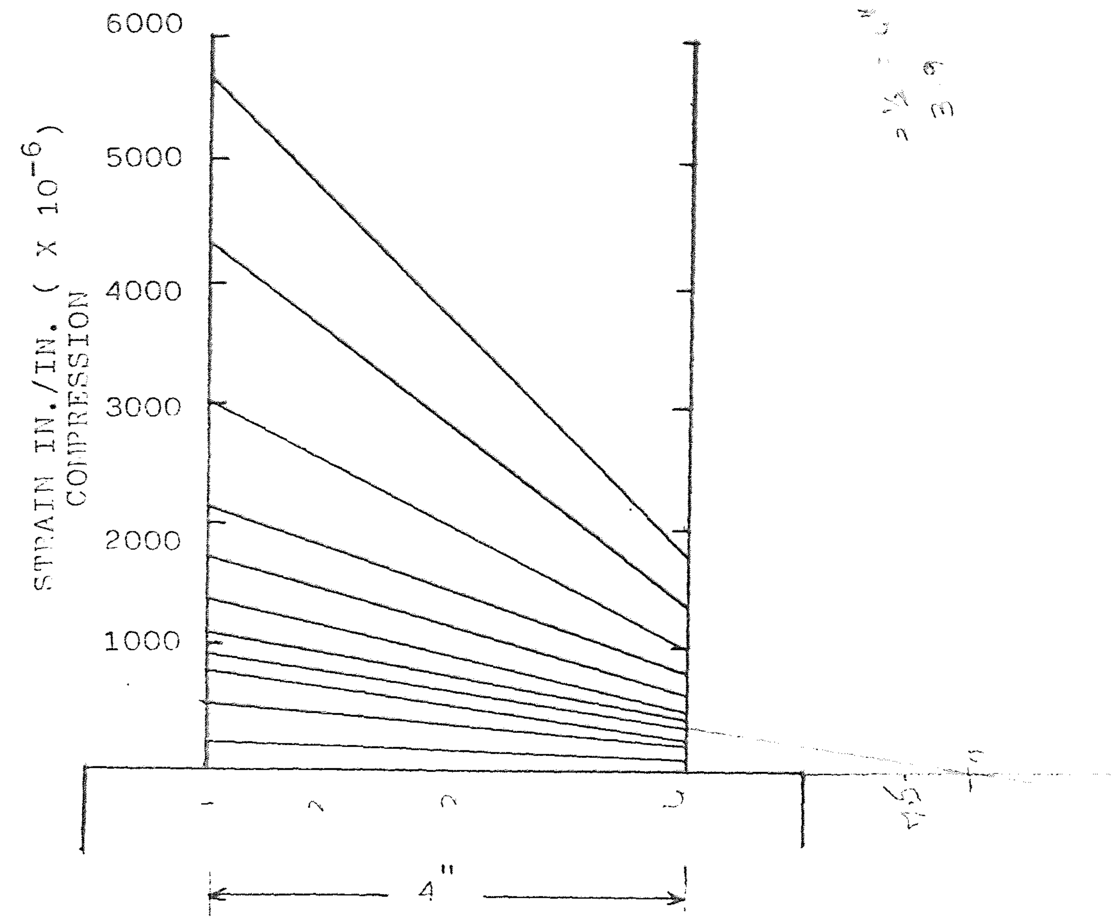

FIGURE 5.4.1.a STRAIN DISTRIBUTION LEADING TO Φ_Y
COLUMN #3

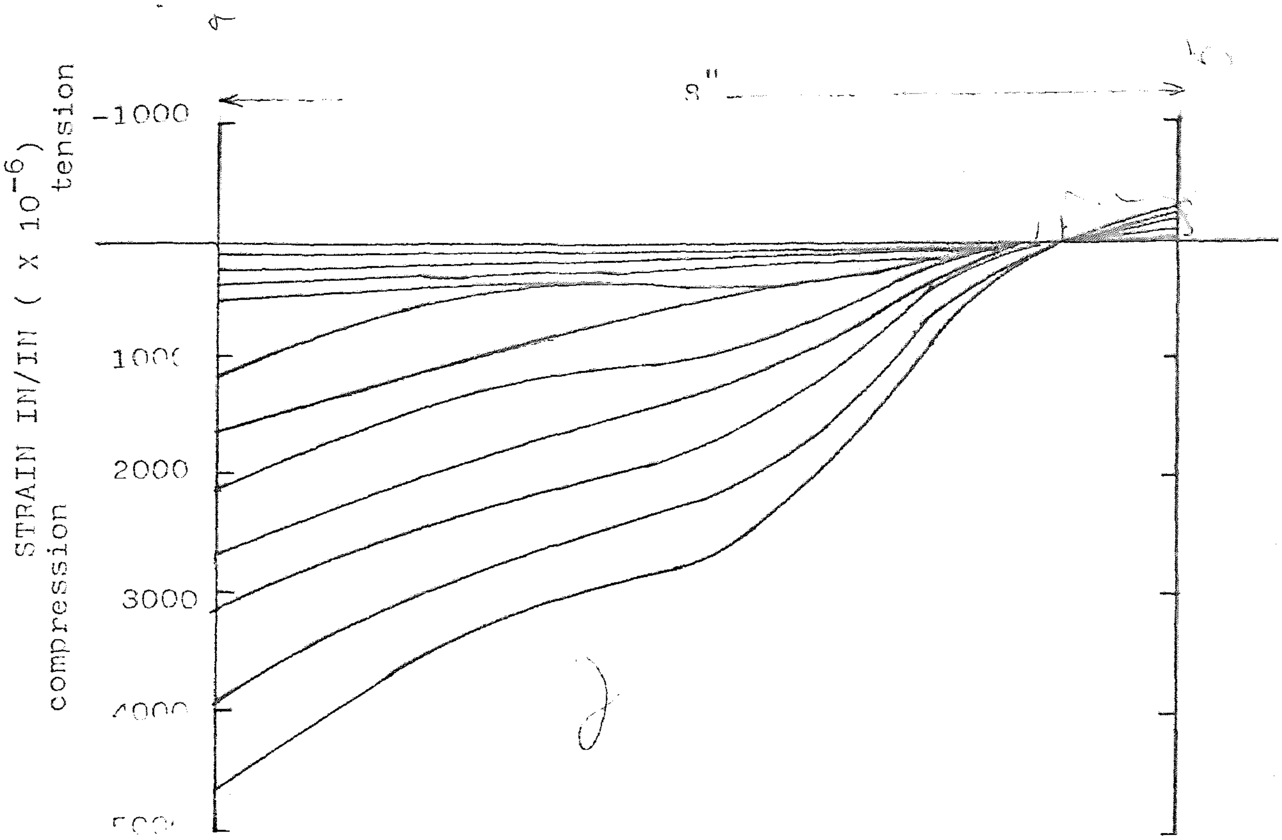

FIGURE 5.4.1.b STRAIN DISTRIBUTION LEADING TO ϕ_X
COLUMN #3

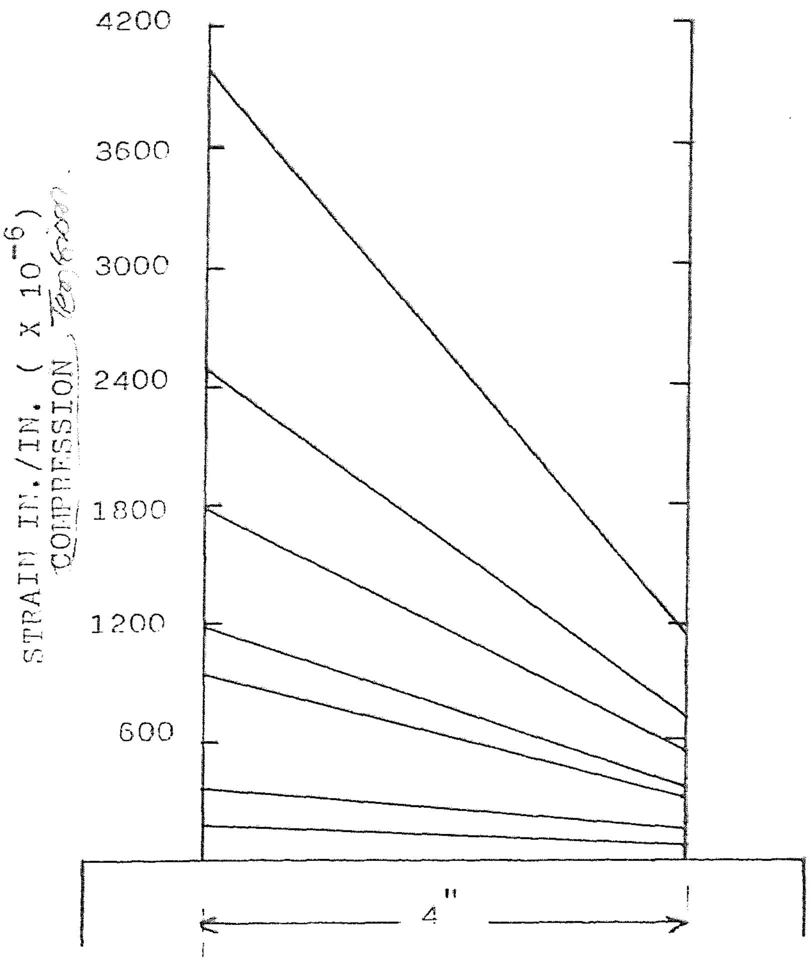

FIGURE 5.4.2.a STRAIN DISTRIBUTION LEADING TO ϕ_Y
COLUMN #4

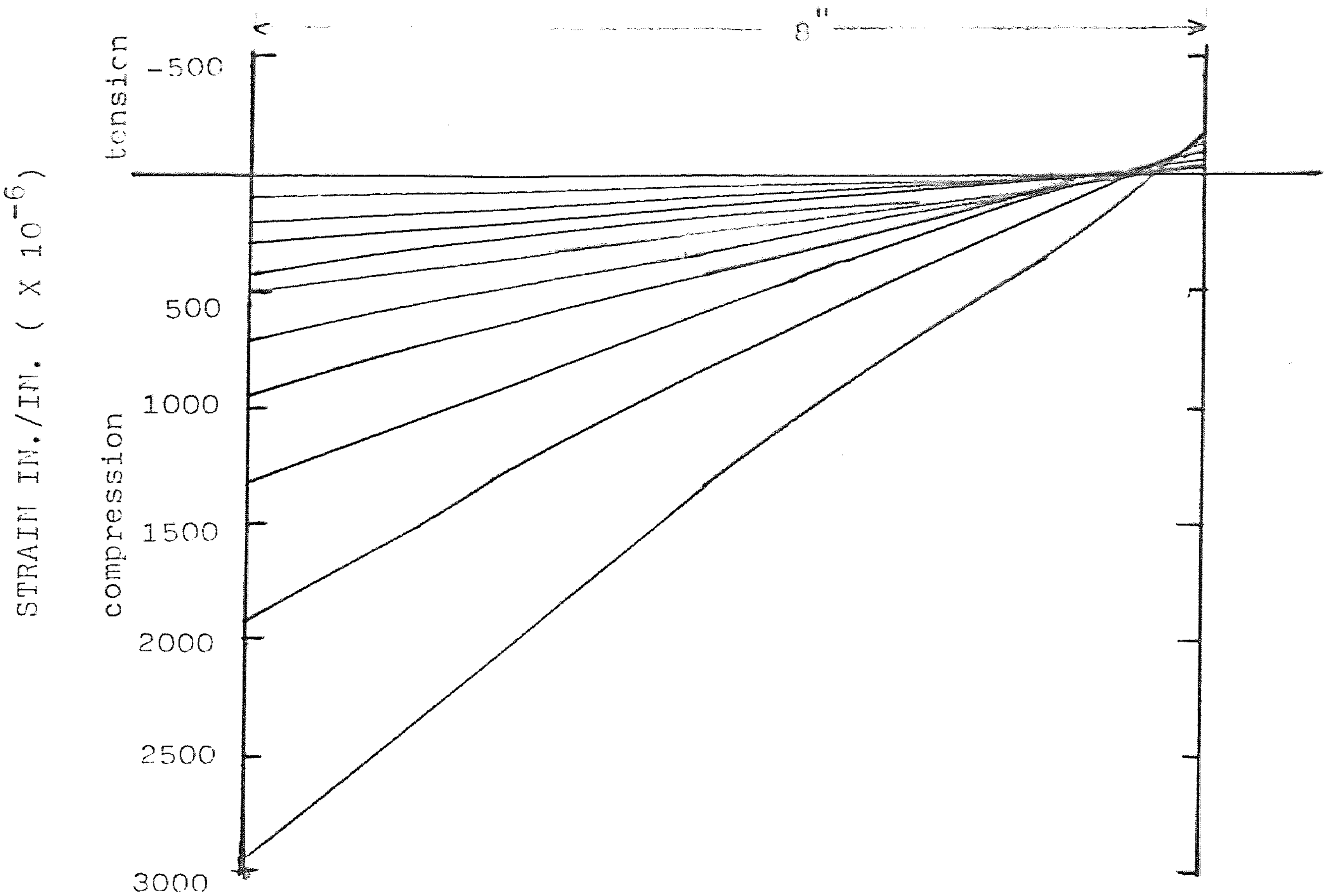

FIGURE 5.4.2.b STRAIN DISTRIBUTION LEADING TO ϕ_X
COLUMN #4

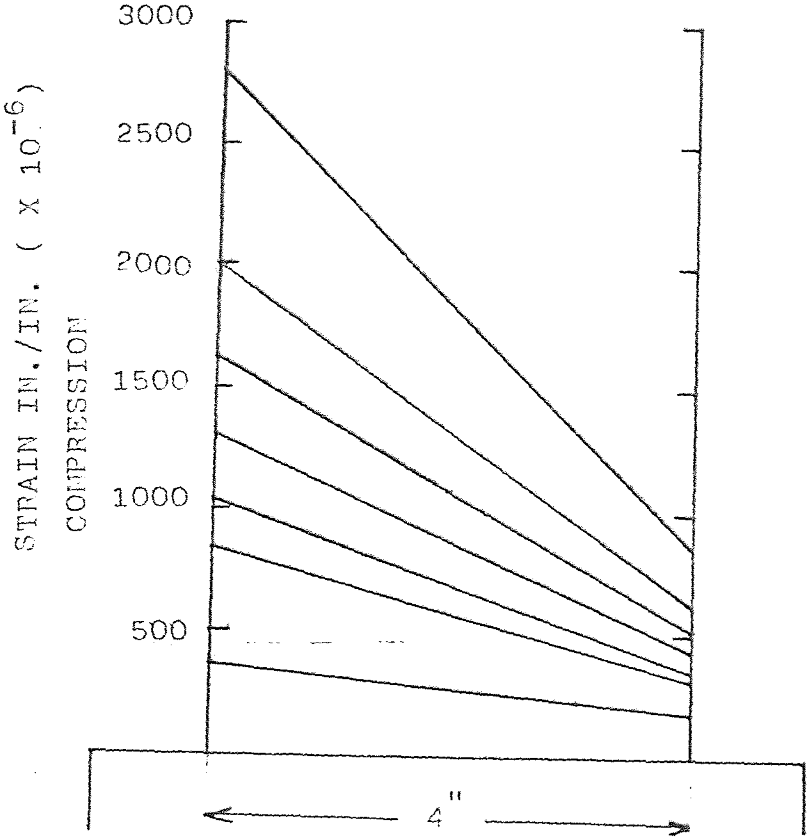

FIGURE 5.4.3.a STRAIN DISTRIBUTION LEADING TO Φ_Y
COLUMN #5

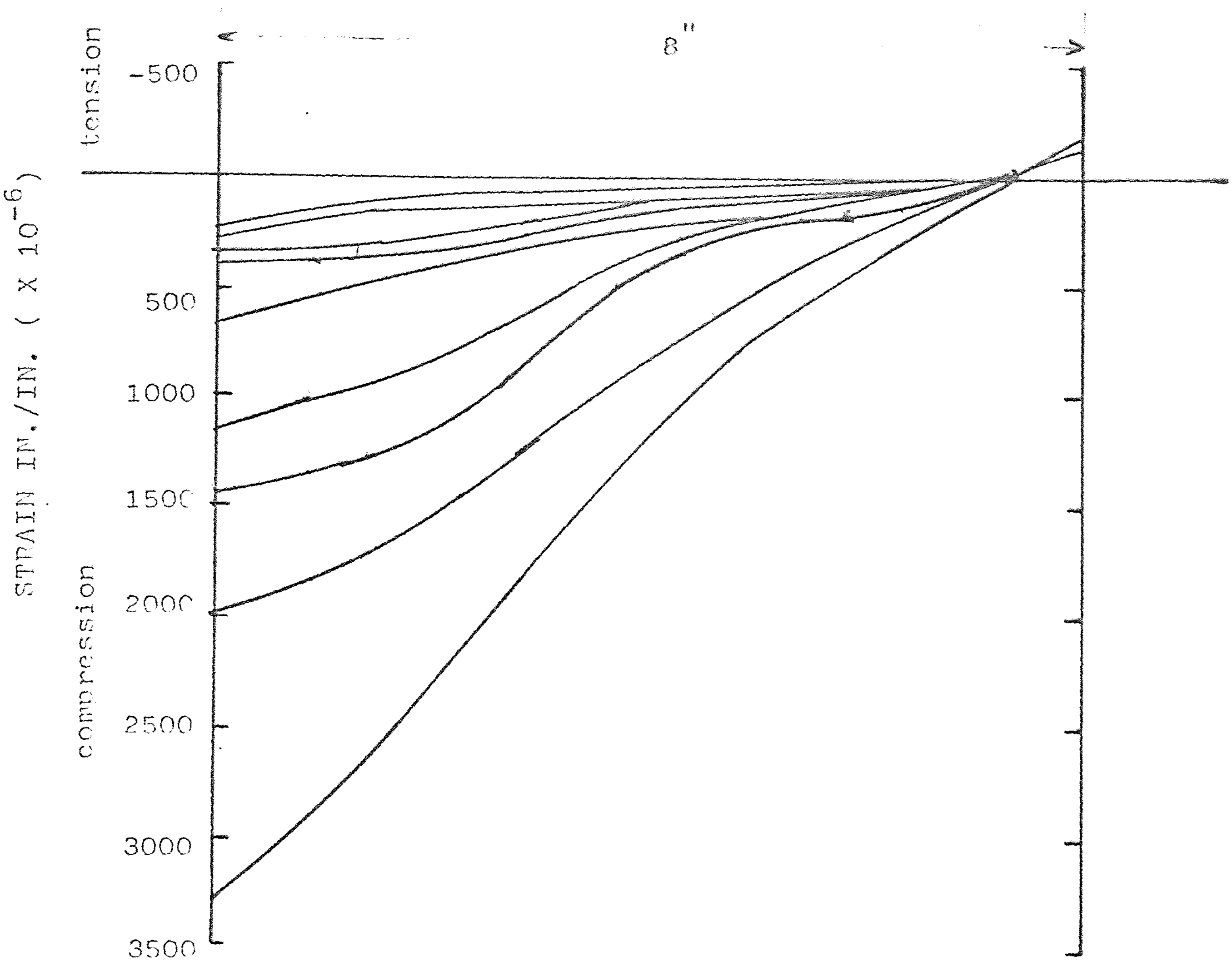

FIGURE 5.4.3.b STRAIN DISTRIBUTION LEADING TO ϕ_y
COLUMN #5

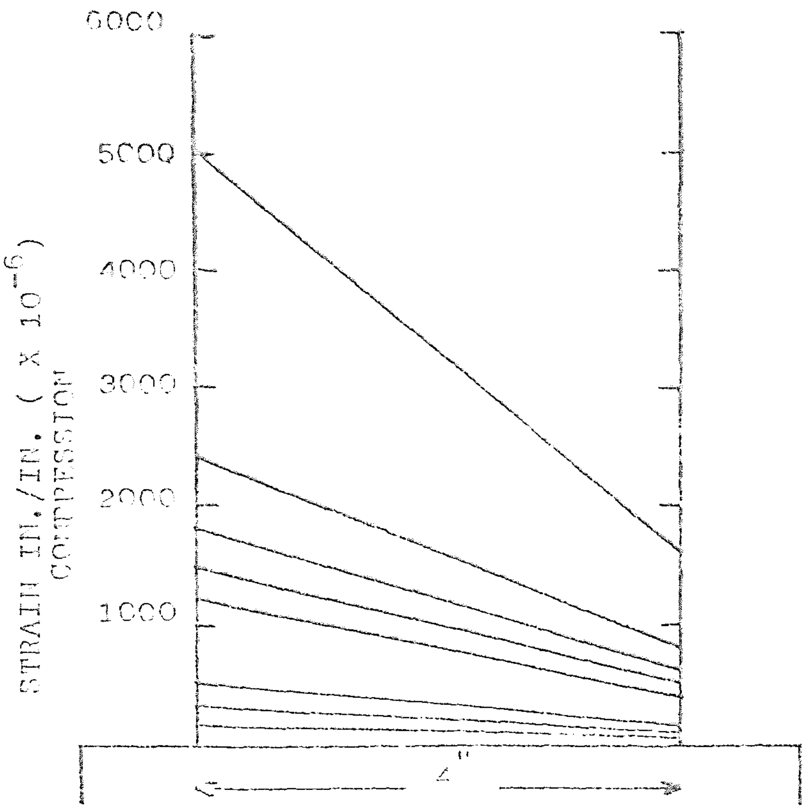

FIGURE 5.4.4.a STRAIN DISTRIBUTION LEADING TO ϕ_Y
COLUMN #6

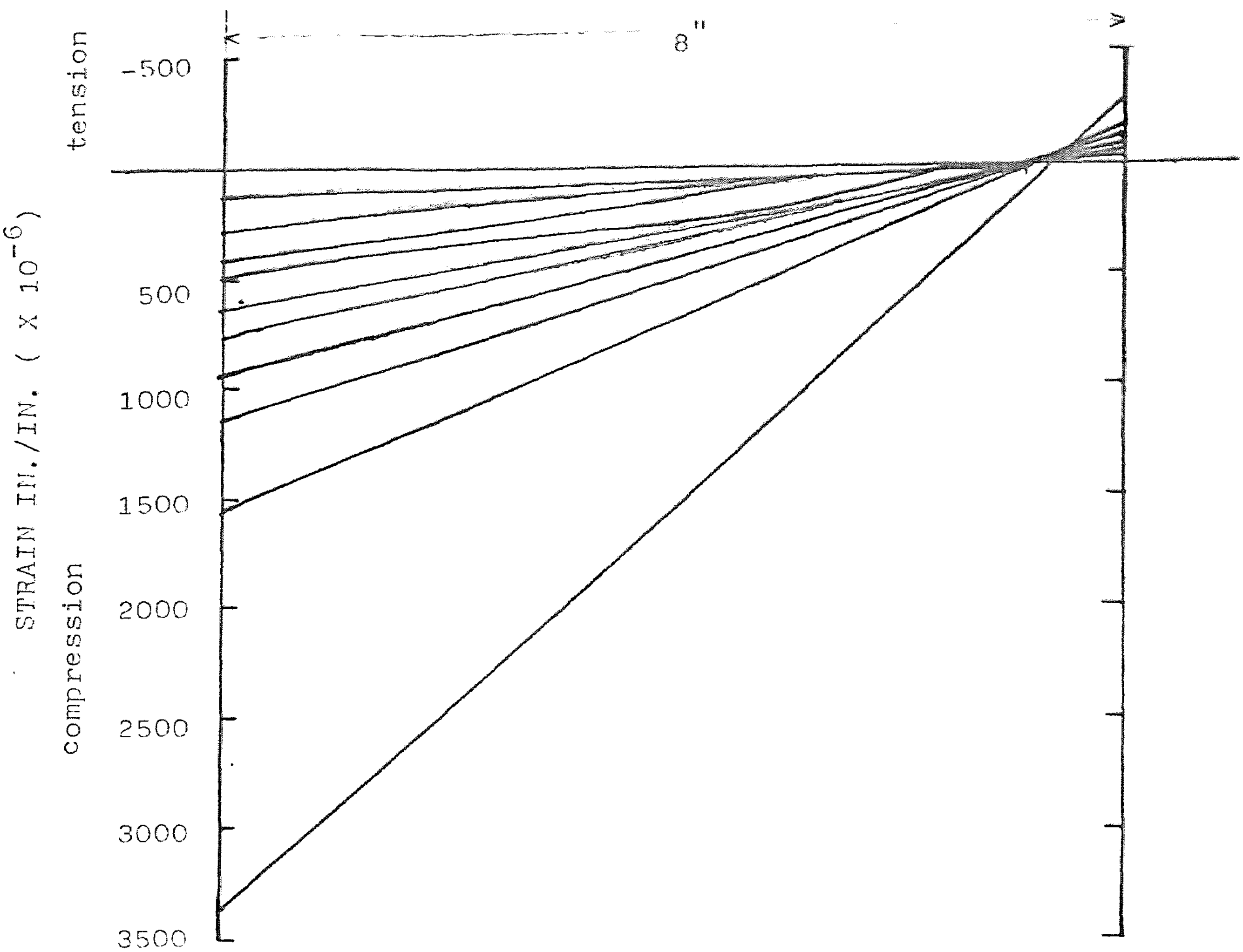

FIGURE 5.4.4.b STRAIN DISTRIBUTION LEADING TO ϕ_X
COLUMN #6

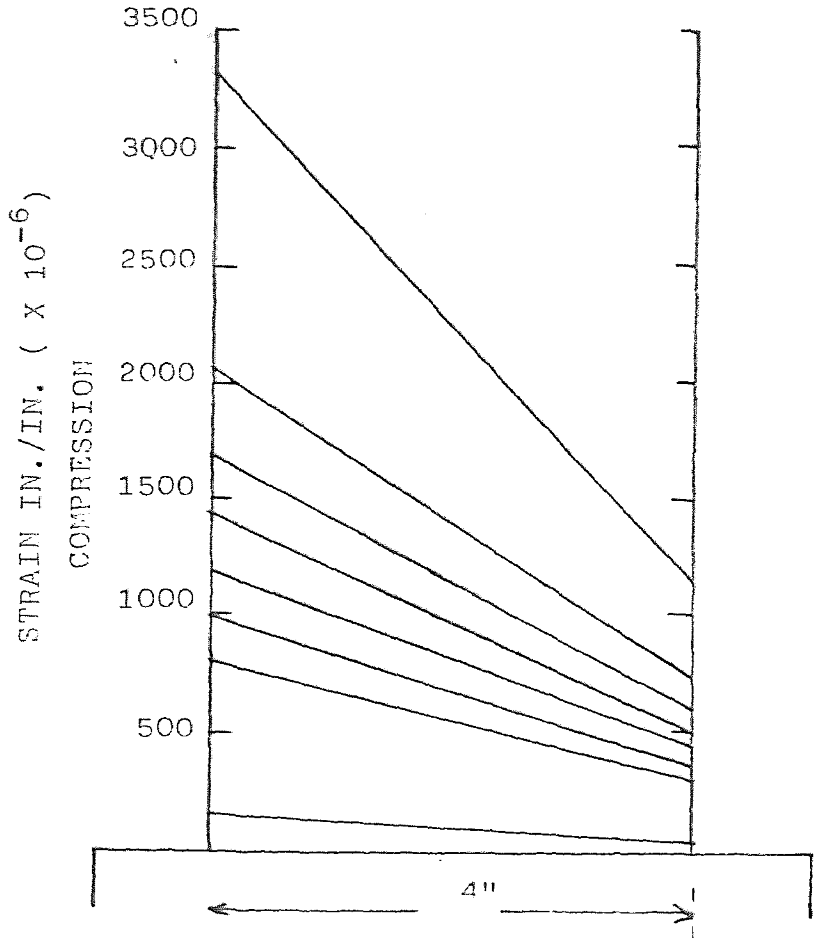

FIGURE 5.4.5.a STRAIN DISTRIBUTION LEADING TO Φ_Y
COLUMN #7

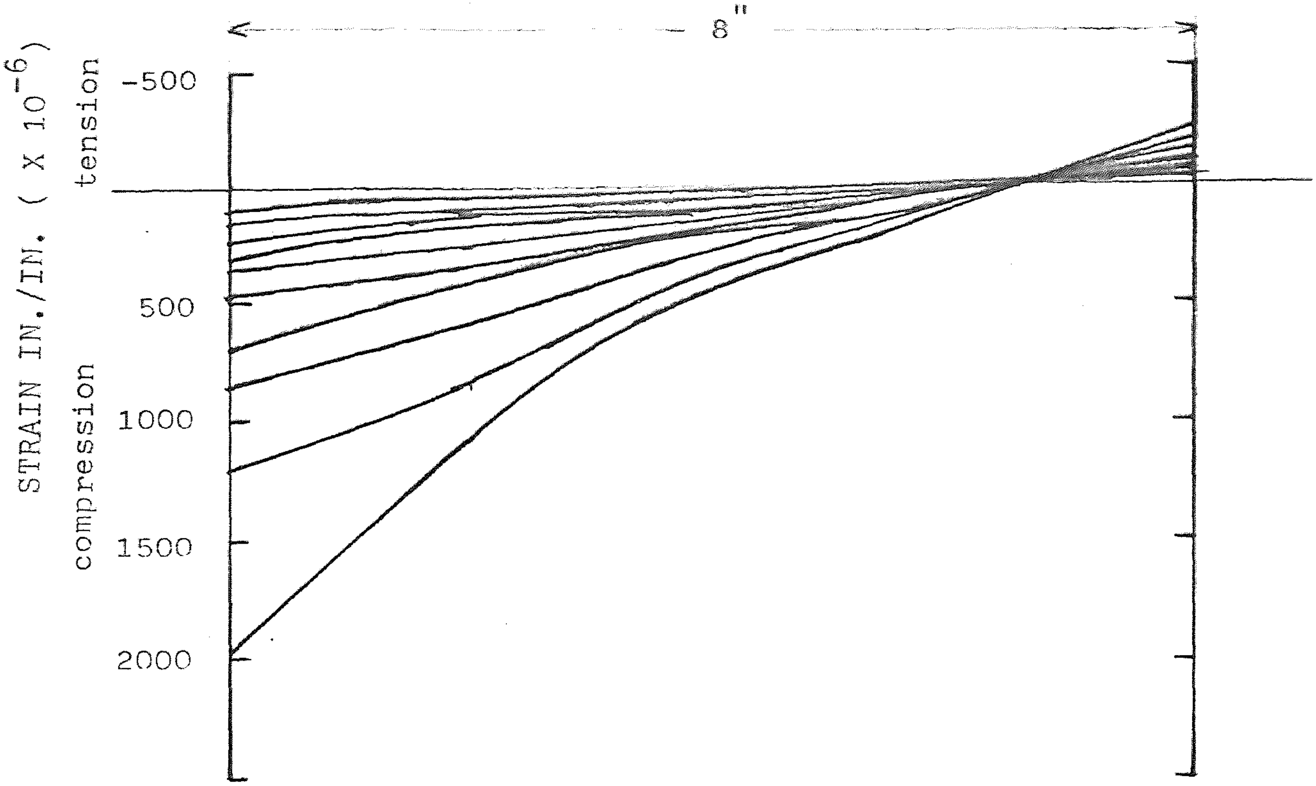

FIGURE 5.4.5.b STRAIN DISTRIBUTION LEADING TO ϕ_X
COLUMN #7

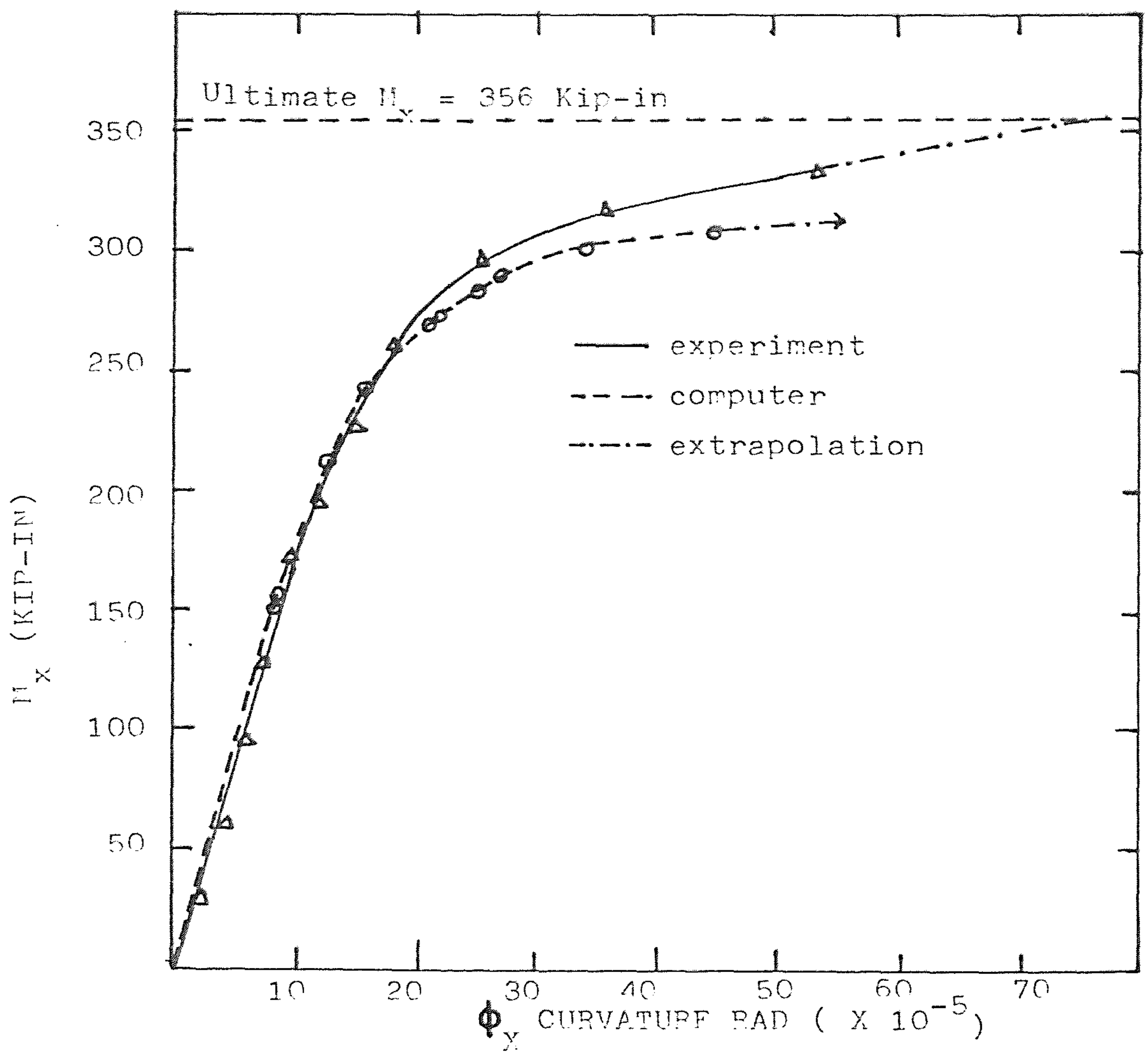

FIGURE 5.5.1.a M_x - Φ_x CURVE COLUMN #3

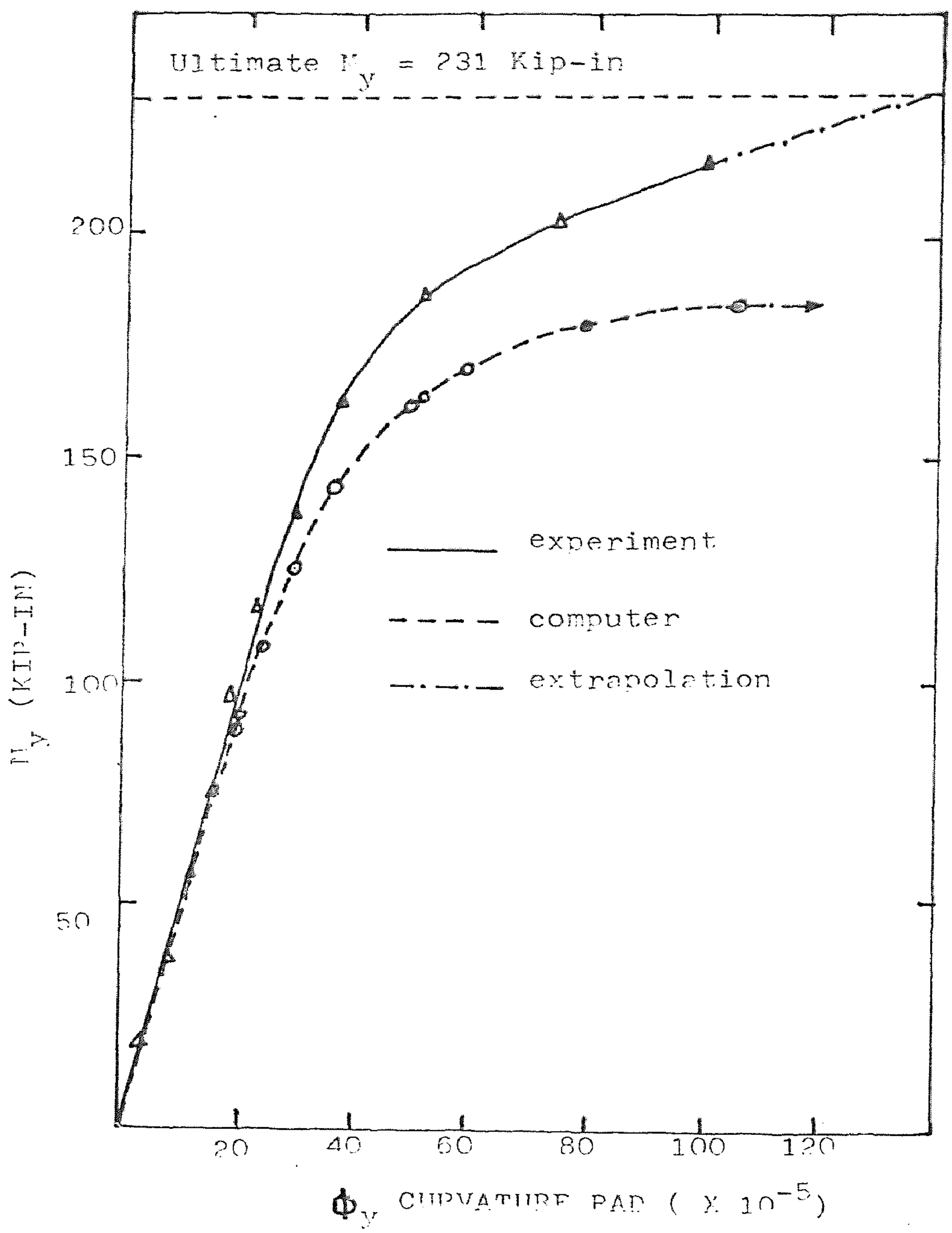

FIGURE 5.5.1.b M_y – Φ_y CURVE COLUMN #3

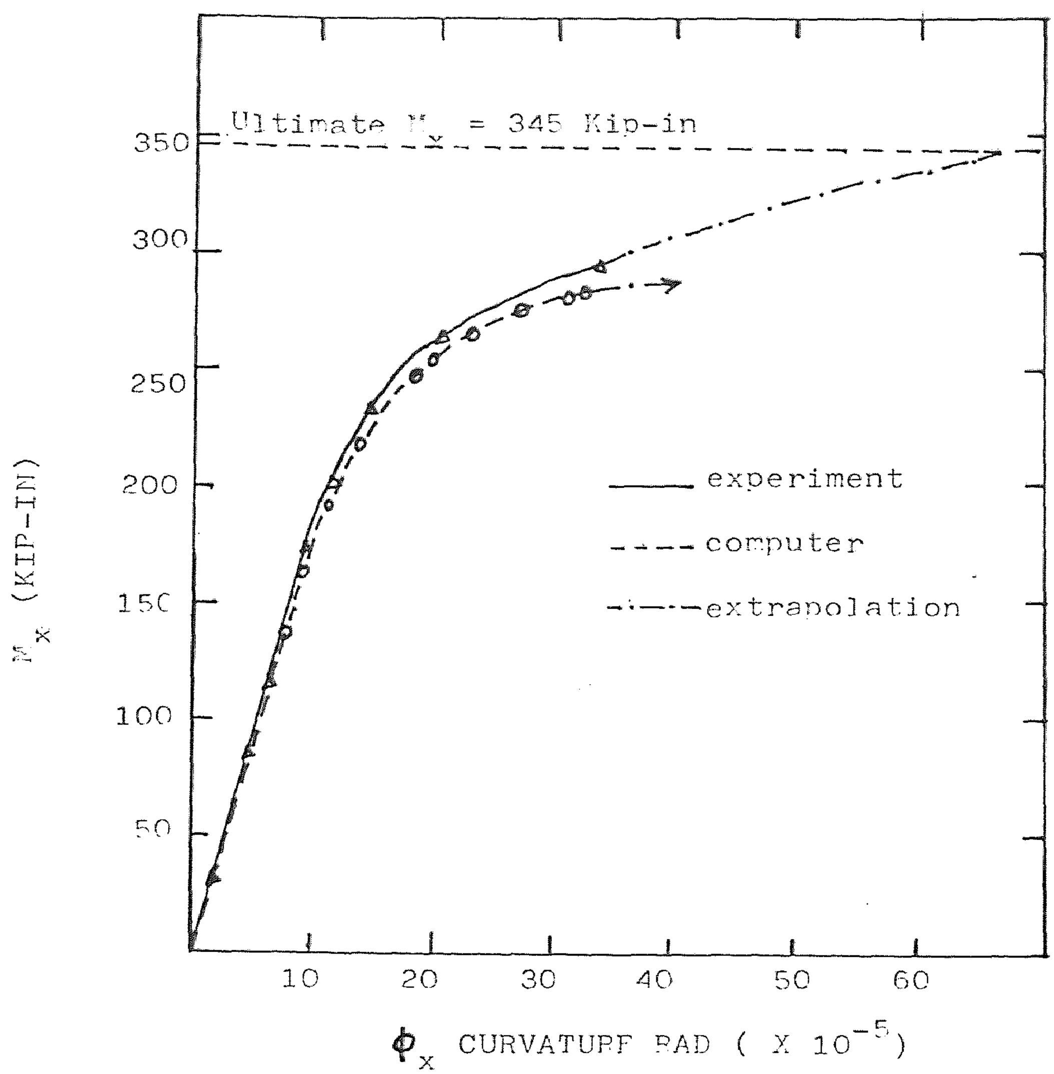

FIGURE 5.5.2.a M_x - ϕ_x curve column #4

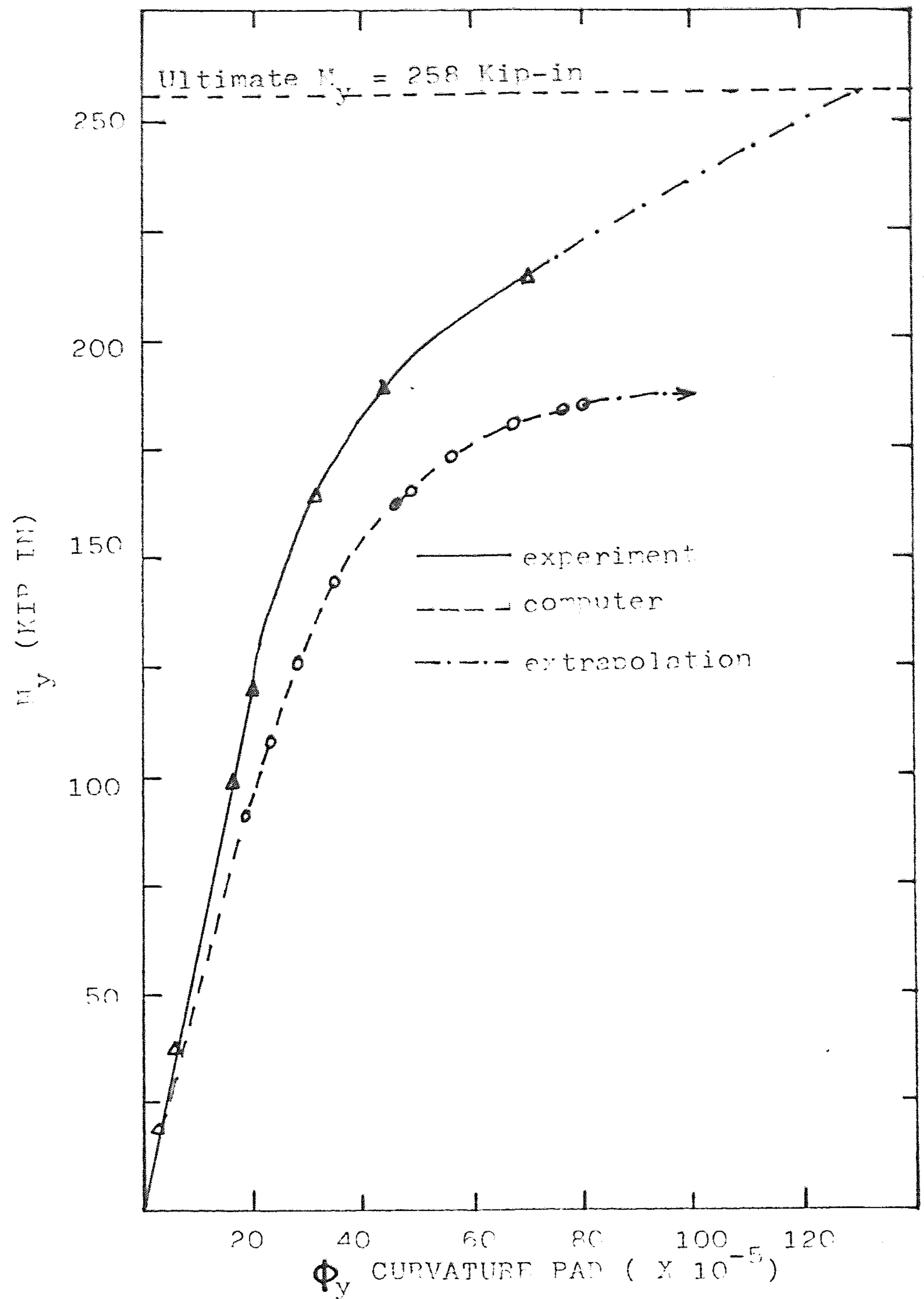

FIGURE 5.5.2.b M_y - Φ_y CURVE COLUMN #4

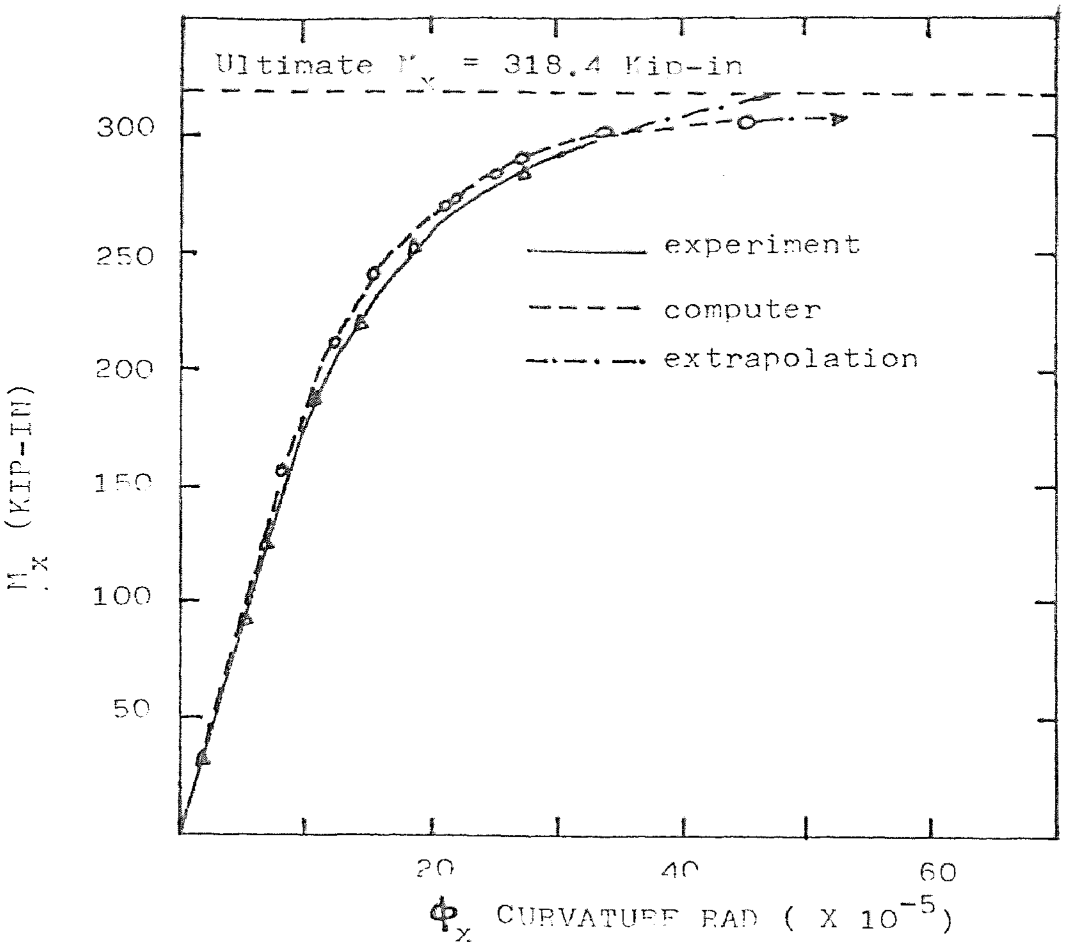

FIGURE 5.5.3.a M_x - ϕ_x CURVE COLUMN #5

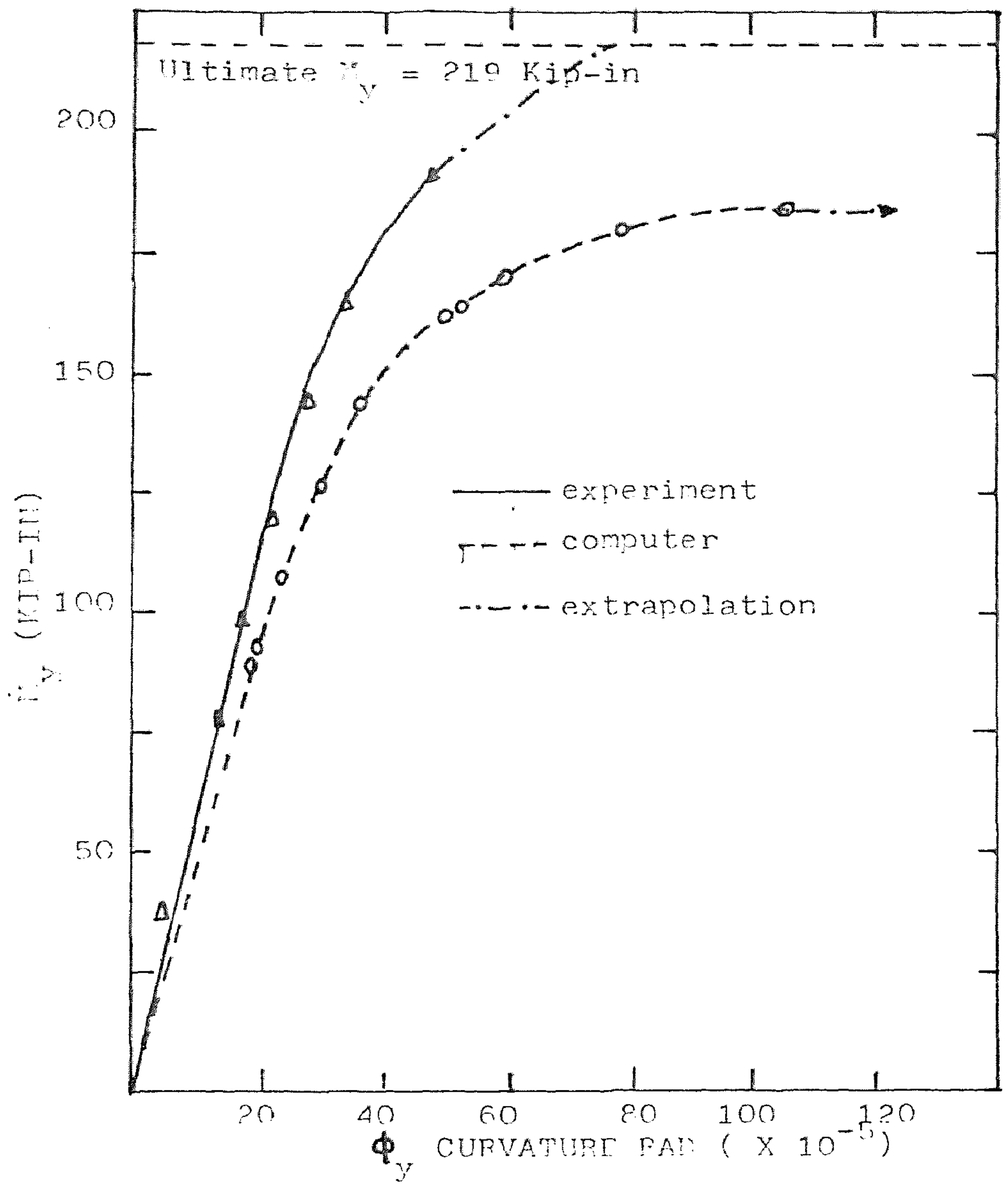

FIGURE 5.5.3.b M_y - Φ_y CURVE COLUMN #5

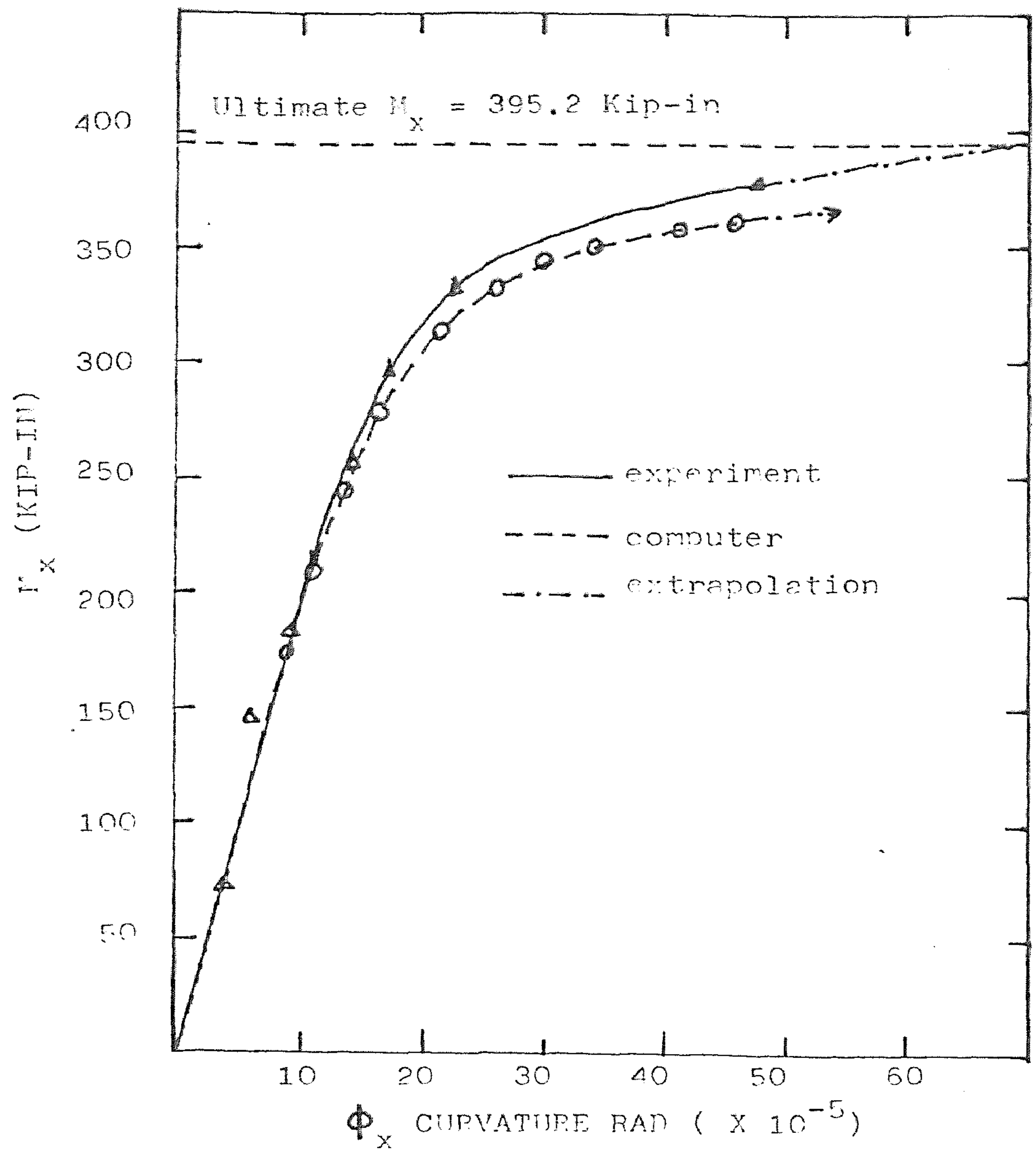

FIGURE 5.5.4.a M_x - Φ_x CURVE COLUMN #6

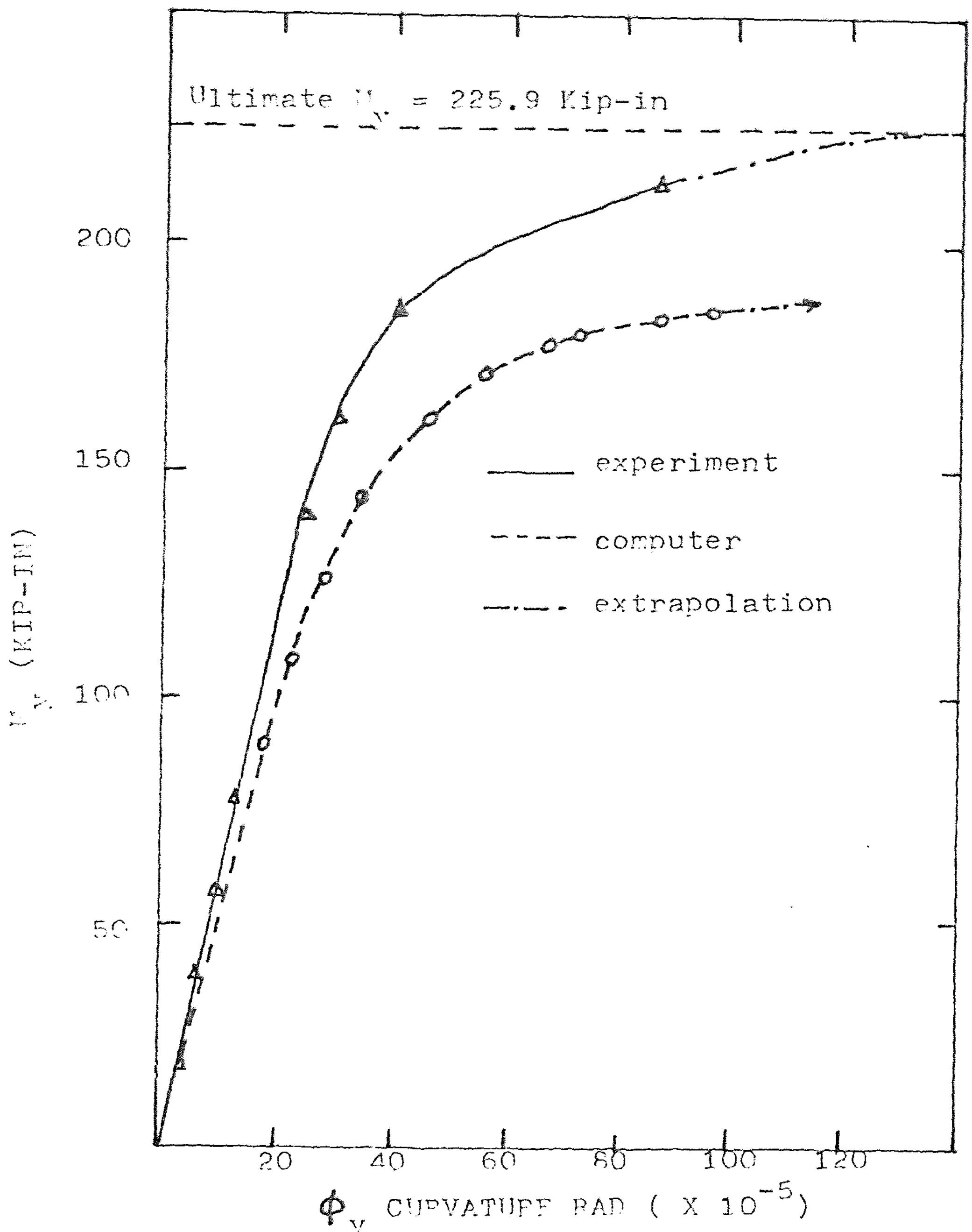

FIGURE 5.5.4.b M_y - ϕ_y CURVE COLUMN #6

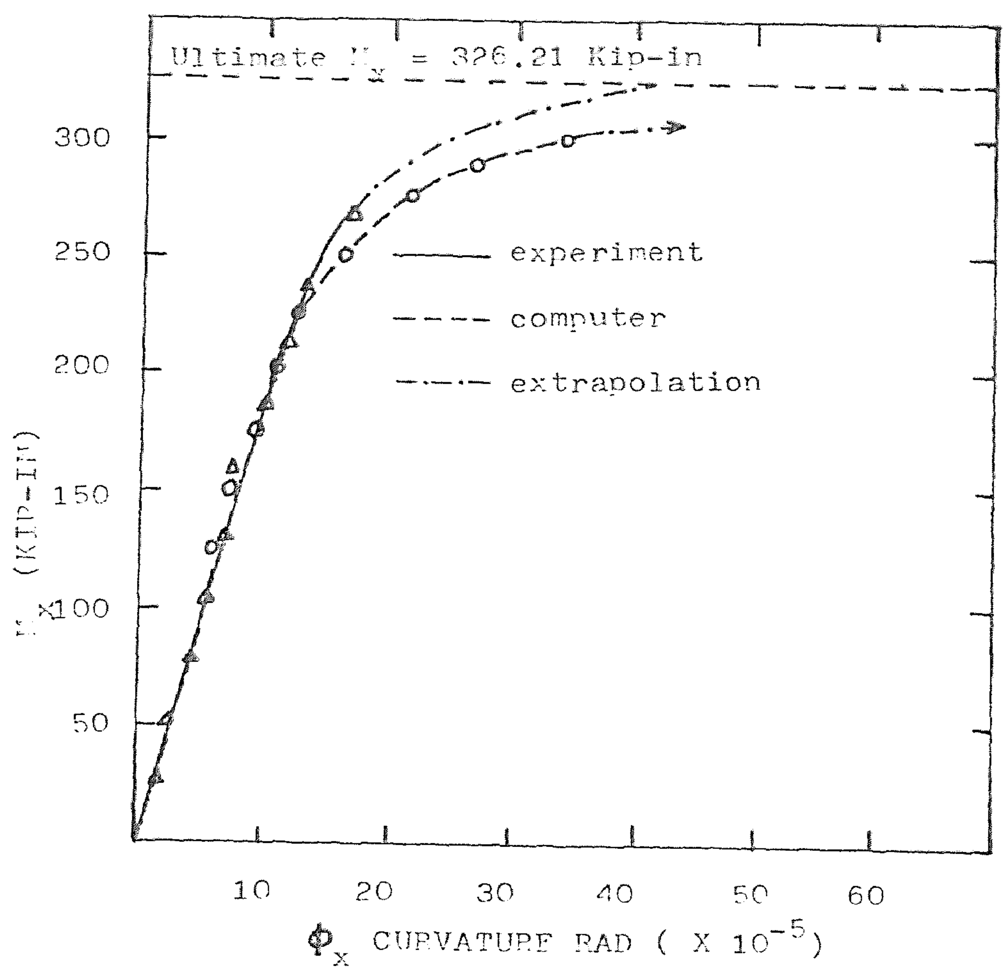

FIGURE 5.5.5.a M_x - Φ_x CURVE COLUMN #7

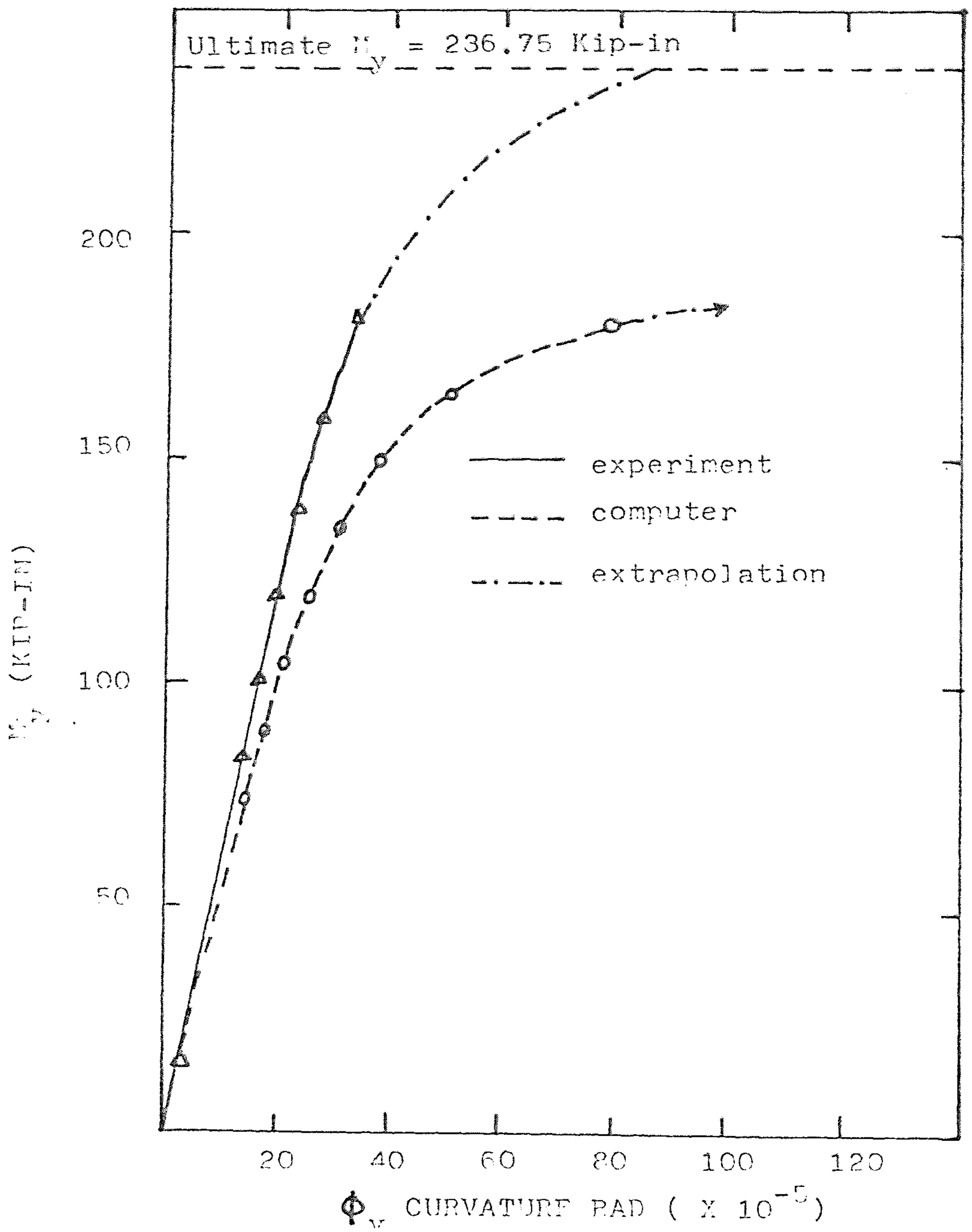

FIGURE 5.5.5.B M_y - Φ_y CURVE COLUMN #7

CHAPTER VI. DISCUSSION OF RESULTS AND CONCLUSIONS

There is excellent agreement between the experimental results and the computer analysis.

On looking at Table 5.5 it is evident that only in Column #4 the ultimate loads were away by about 15%; but nevertheless it was 15% toward the safer side. In the other columns the experimental values were to a maximum of 5% above the computer analysis.

In comparing the M_x-ϕ_x curves there was extremely good agreement except that the ultimate failure moments were higher and also the curvatures. The reason for this is that secondary moments were considered in the analysis of the experimental results but were not done so in the case of the computer analysis. The deflections were nevertheless not too large in the y direction.

In comparing the M_y-ϕ_y curves there was extremely good agreement for the first 70% of the load increments. As the load increased toward failure the deflections became much larger in this direction - ϕ_x - causing the secondary moment to be quite a large proportion of the ultimate moment. So the program has been more conservative in analyzing the moments and curvatures as failure is imminent. Nevertheless, in designing channel-shaped columns under combined biaxial bending and axial compression, the computer analysis can be used to determine the cross section and material properties. In other words, the mathematical model developed into a computer program has been experimentally verified as suitable for design of channel-shaped reinforced concrete columns under combined biaxial bending and axial compression. Also the material presented here could be used in developing design aids.

The load contour method has a general non-dimensional equation with α as a constant. α has been obtained as 1.75 for square or circular sections and 1.5 for rectangular sections. The results of this investigation could be used to develop the strength interaction diagrams and the failure surfaces that are needed in determining the value of α in equation 6.1, which is for a constant P_n:

$$\left\{\frac{M_{nx}}{M_{ox}}\right\}^{\alpha} + \left\{\frac{M_{ny}}{M_{oy}}\right\}^{\alpha} = 1 \qquad - \quad 6.1.$$

Where $M_{nx} = P_n e_y$; $M_{ny} = P_n e_x$

$M_{ox} = M_{nx}$ capacity at axial load P_n when M_{ny} is zero.

$M_{oy} = M_{ny}$ capacity at axial load P_n when M_{nx} is zero.

The inelastic behavior, which can be deduced from the ductility and deformation results of moment-curvature and moment-rotation curves for channel-shaped reinforced concrete columns has formed the basis of the redistribution of the moments and forces in a statically indeterminate structure, and these characteristics can also be found useful for the limit analysis and design of reinforced concrete structures.

APPENDIX 1 - LOAD STRAIN CURVES

The load strain curves are plotted here for a few steel reinforcement bars for each column. The column number and strain gauge number are specified for each diagram. The strains are in inch/inch ($x10^{-6}$) and the loads in kips. Here the loads are on the y-axis and strains on the x-axis. On the figures, "C" means compression and "T" means tension. The strain gauge number for each column is specified with reference to Figure 5.2.

The load strain curves could be used to determine the yield points for each column. For this the strain of the extreme steel bar in tension need be measured. Since very few strain gauges were used a proper use of the load-strain curves was not possible. The load strain curves could also be used to develop curvatures but once again enough measurements were not taken.

LOAD STRAIN CURVES

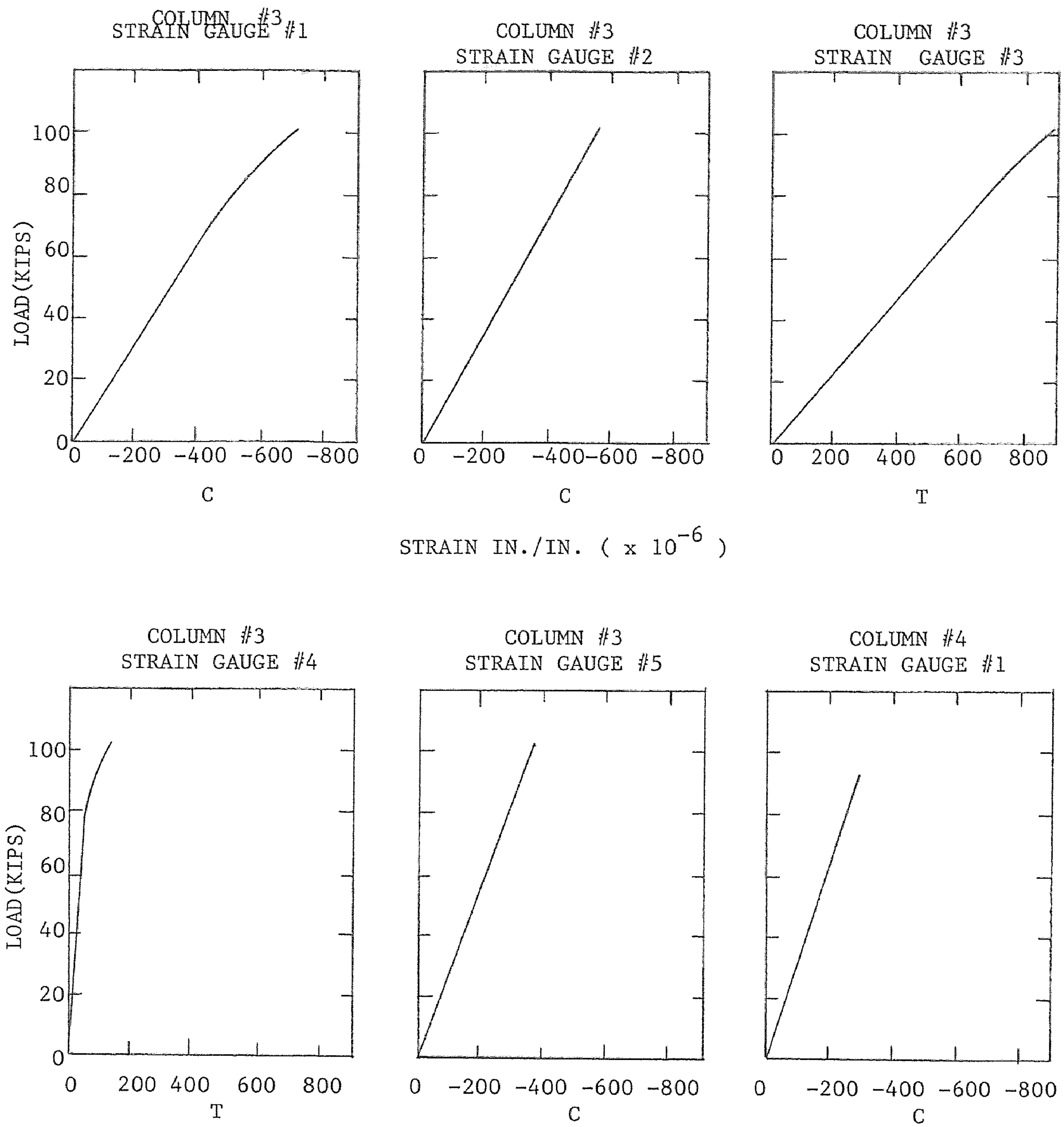

LOAD STRAIN CURVES - CONTINUED

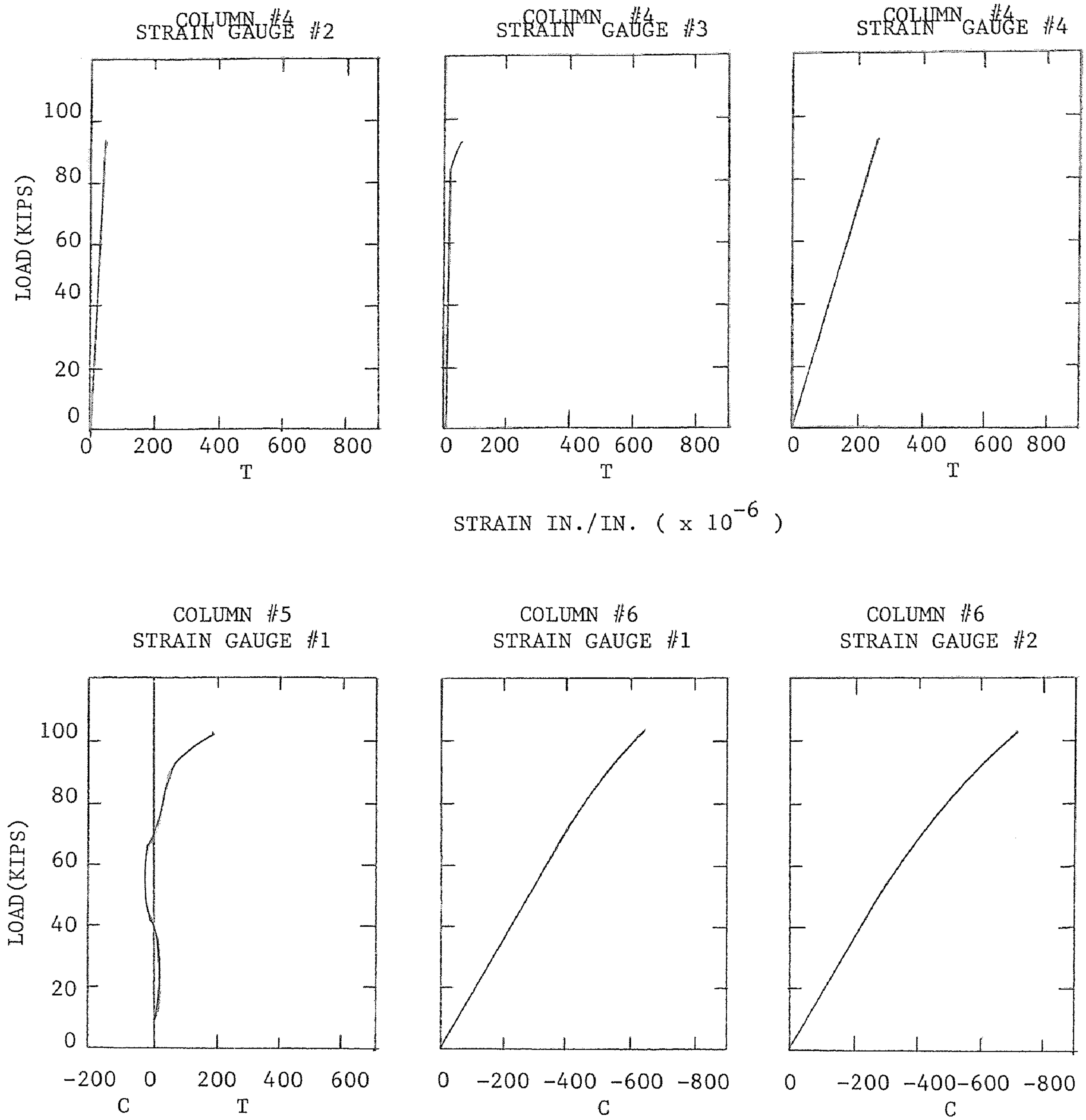

LOAD STRAIN CURVES - CONTINUED

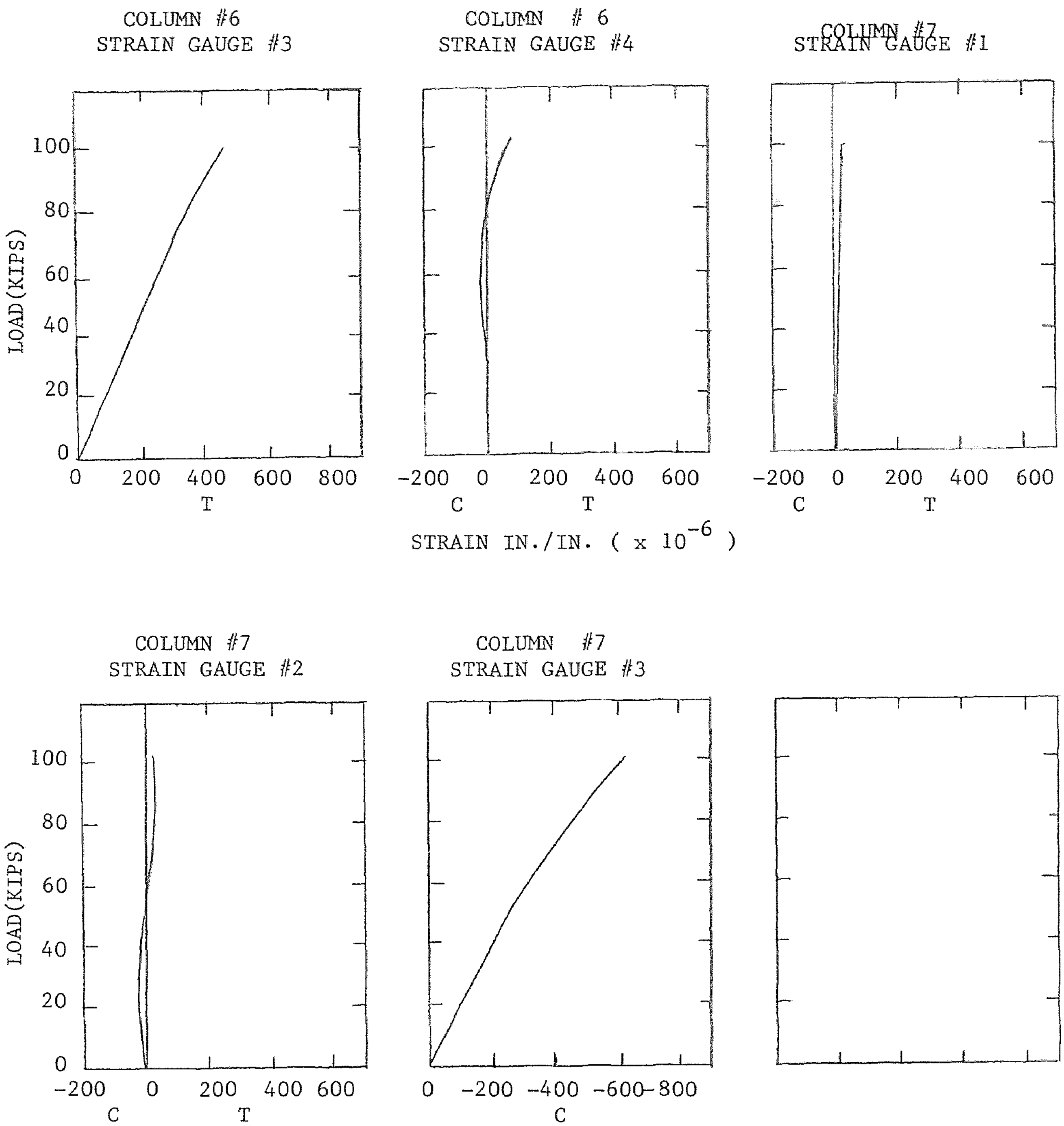

SELECTED BIBLIOGRAPHY

(1) Hsu, C.T.T., "Behavior of Structural Concrete Subjected to Biaxial Flexure and Axial Compression," Ph.D. Thesis, McGill University, August 1974.

(2) Fiorato, A.E., Oesterle, R.G., and Corley, W.G., "Importance of Reinforcement Details in Earthquake-Resistant Structural Walls," Proceedings of a Workshop on Earthquake-Resistant Reinforced Concrete Construction, University of California, July 11-15, 1977, vol. III, pp. 1430-51.

(3) Grasser, E. and Luise, D., "Bemessungstafeln für Stahlbeton-Querschnitte auf der Grundkage der neuen DIN1045." Werner-Verlag, Dusseldorf, 1972.

(4) Jiménez Montoya, A., Garcia-Mesequer, A. and Morán Cabré, F., "Hormigón Armado," 8th edition. Gustavo Gili, Barcelona, 1976. Two volumes.

(5) Anderson, A.R. and Moustafa, S.E., "Ultimate Strength of Prestressed Concrete Piles and Columns," J. ACI, vol. 67, No. 8, August, 1970, pp. 620-35.

(6) Brettle, H.J., "Ultimate Strength Design of Multi-Cell Rectangular Reinforced Concrete Piers," Publications No. 28-I, International Association for Bridges and Structures, Zurich, 1968, pp. 41-66.

(7) Marín, Joaquín, "Abacos, fórmulas y criterios para el Cálculo de Columnas en Edificios de Concreto Armado. Resumen de una Investigación UCV-BANAP." Boletin No. 61-62. IMME, Universidad Central de Venezuela, Jan-June, 1978, pp. 45-102.

(8) Marín, Joaquín, "Design Aids for L-Shaped Reinforced Concrete Columns." J.ACI

(9) Chen, W.F. and Atsuta, T., "Theory of Beam-Columns." McGraw-Hill, 1977, vol. 2.

(10) Jalil, W., Morisset, A. and Perchat, J., "Calcul du Beton Arme a l'Etat Limit Ultime." Eyrolles, Paris, 1976. Two volumes.

(11) Garfinkel, Germán, "Analysis of Footings Subjected to Biaxial Bending." J.ASCE, Proc. Paper No. 7329, ST6, June, 1970, pp. 1049-59.

(12) Menegotto, M. and Pinto, P.E., "Slender RC Compressed Members in Biaxial Bending." J.ASCE, vol. 103, No. ST3. March, 1977, pp. 587-605.

(13) Marín, Joaquín, "Resistencia y Ductilidad de Mures en forma de ce." Boletin No. 47. IMME, Universidad Central de Venezuela, July-Sept., 1974, pp. 3-22.

(14) Park, R. and Paulay, T., "Reinforced Concrete Structures." J. Wiley, 1975.

(15) Marín, J. and Martin, I., "Designing Columns with Non-Rectangular Cross Section," Preprint 3707, ASCE, Atlanta Convention, Oct. 1979, pp. 1-21.

(16) Herrera, G.H. and Ochoa, E.E., "Verificacion Experimental de un Diagrama de Interaccion de una Pantalla de Concreto Armado," Universidad Central de Venezuela, Caracas, March, 1976.

(17) Cranston, W.B. and Chatterji, A.K., "Computer Analysis of Reinforced Concrete Portal Frames with Fixed Feet." Technical Report TRA 444, Cement and Concrete Association, London, September 1970.

(18) Winter, G. and Nilson, A.H., "Design of Concrete Structures." McGraw-Hill, 1979.